ABSTRACT

Title of Thesis: COMPARISON OF IGNITION AND COMBUSTION CHARACTERISTICS OF WESTERN RED CEDAR AND ORIENTED STRAND BOARD EXPOSED TO FIREBRAND PILE DEPOSITION

Emily Lauderdale Dietz, Master of Science, 2022

Thesis Directed By: Dr. Stanislav I. Stoliarov, Professor, Department of Fire Protection Engineering

Some of the most devastating consequences of the increasing occurrence of large wildfires throughout the world are the acres of land burned and the number of structures lost. Firebrand exposure has been identified as one of the main mechanisms of how wildfires spread as well as an ignition source for structural components. A bench-scale experimental procedure was developed to study the ignition process of Western Red Cedar (WRC) and Oriented Strand Board (OSB), two common materials used in the construction of outdoor decks. To study the combustion process of these materials, they were loaded into a wind tunnel and exposed to a constant wind velocity of 1.4 m s^{-1}, 2.4 m s^{-1}, or 2.7 m s^{-1} and a glowing firebrand pile coverage density of either 0.06 g cm^{-2} or 0.16 g cm^{-2}. All tests were also conducted using Kaowool PM, an inert ceramic fiberboard, in order to quantify the heat feedback of the isolated firebrand pile as well as differentiate the contributions of WRC and OSB to the combustion process from that of the firebrand pile. Surface ignitions on the combustible materials were determined visually and characterized by time to

ignition after deposition, burn duration, and location of ignition events. Back surface temperature profiles were collected using an infrared camera. Results from gas analyzer measurements were used to compare the combustion characteristics of the WRC, OSB, and Kaowool PM under the same conditions through heat release rate (HRR) and modified combustion efficiency (MCE) profiles. Additional tests were conducted under a single airflow of 2.4 m s^{-1} and firebrand pile coverage density of 0.16 g cm^{-2} yet rotated the orientation of firebrand deposition onto the board by 90 degrees, doubling the leading edge length of the firebrand pile. A series of tests also varied the airflow in the tunnel for a comparison between the surface ignition characteristics and the temperature profiles of the firebrand pile between continuous and intermittent wind exposure for a 2.7 m s^{-1} airflow and a 0.16 g cm^{-2} firebrand pile coverage density. Results included a higher probability of ignition on WRC than OSB under all continuous wind conditions, higher peak temperatures achieved with an increasing airflow up to 2.4 m s^{-1}, and combination smoldering-flaming mode of combustion for the system, whether that be the firebrand pile alone or the firebrand pile deposited onto WRC or OSB. It was also found that changing the firebrand pile deposition orientation leading edge length by a factor of two doubled the number of surface ignitions observed on both WRC and OSB. Compared to the continuous wind condition, gusting the airflow velocity caused an increase in the number of ignitions by a factor of 14 on WRC and 19 on OSB, yet each saw a decrease in the burn duration by a factor of at least 4.

COMPARISON OF IGNITION AND COMBUSTION CHARACTERISTICS OF WESTERN RED CEDAR AND ORIENTED STRAND BOARD EXPOSED TO FIREBRAND PILE DEPOSITION

by

Emily Lauderdale Dietz

Thesis submitted to the Faculty of the Graduate School of the
University of Maryland, College Park, in partial fulfillment
of the requirements for the degree of
Master of Science
2022

Advisory Committee:
Professor Stanislav I. Stoliarov, Ph.D., Chair
Professor Peter Sunderland, Ph.D.
Professor Jim Milke, Ph.D.

Acknowledgements

I am incredibly grateful to the community around me that has supported me through this past year. First, to my parents, each of which who have pushed and encouraged me throughout my engineering career. I would not have joined this program without your motivation. To my friends, thank you for always being understanding of the late nights and workload demands. I am so glad we had one another to rely on, and even throw around some homework help here and there (or every assignment, but who's counting anymore).

I would also like to thank the faculty and staff of the FPE. To Dr. Stas, thank you for being my advisor this past year. Your dedication to each of your students is admirable, and your insight allowed this report to form a cohesive shape. To Dr. Sunderland, thank you for joining my committee, offering your expertise, and giving me helpful feedback during each of our weekly meetings. Dr. Milke, thank you for also joining this team, and even more so, for sitting down with my family and convincing me to join this incredible major 5 years ago. I would also like to thank Jacques de Beer, without whom this project would still be in preliminary testing. I really appreciate you taking the time to work with me each step of the way, patiently explaining every process. You have always gone the extra mile, selflessly ensuring that the work we produce is the best it can be.

Lastly, I am so grateful to Nicole Hollywood and the FPE Recruitment team. I would not have been able to work towards an MS without your support. I have learned and grown so much in the past year, and I could not have asked for a better person to work for. For the past 5 years, you have always put in the time and effort to help me along my path, no matter what shape that may take. I was lucky enough to find a major I love with FPE, and thank you for giving me the chance to share this major with as many people as we can.

Table of Contents

List of Tables

List of Figures

Chapter 1: Introduction

Section 1: Wildland Fires, the WUI, and Firebrands

Wildfires are largely uncontrollable events that often result in environmental damage, property loss, and human injury or death. They are an international phenomenon affecting millions of lives each year. Global changes associated with climate have resulted in increasingly severe wildfires in the western USA, Australia, Canada, Greece, Brazil, and Siberia [1 - 5]. A common theme between all countries is that the wildfires increasingly originate in what is now known as the Wildland Urban Interface (WUI), or "[a]reas where human development meets or intermingles with undeveloped wildland vegetative fuels" [6]. Essentially, this is the zone where manmade society meets unaltered nature. Unfortunately, developed areas contain many available combustible materials, resulting in wildfires being able to spread easily and develop quickly as opposed to when they are contained to undeveloped land. Thus, the aftermath of wildfires is only growing in severity each year; in the US alone, while there has not been a significant increase in the number of wildfire occurrences, there has been an upward trend in the amount of area burned and structures lost [1, 7], in part due to practices of controlled burning being restricted and even outlawed [8]. In the US, there are approximately 43.4 million structures within the WUI, a number that is growing by year [1]. Consequently, America's WUI continues to grow by approximately 2 million acres per year with no signs of a decline [6].

There are many concerns associated with the rise of wildfires. These include increases in fire season length, extreme fire weather, fuel aridity, and the severity of the areas burned [9]. Additionally, wildfires injure their local ecosystems, harming the biota in their regions that are often unable to regrow or return [10, 11]. Changes in the local climates result in hotter average temperatures and less precipitation per year [11]. These changes affect the likelihood of the initiation and spread of wildland fires, as the increased temperature and drier fuels create a better environment for the wildfires to flourish. In conjunction with the environmental effects, there is a large impact on the people that reside in these areas as well. In the US, between 2005 and 2020, wildfires have destroyed more than 89,000 structures in the WUI [6]. Of the structures lost, the most damaging wildfires have occurred in the last five years, accounting for 62% of the structures lost over the last 15 years [12]. This has an extraordinary economic impact as well. According to the EPA, wildfires in the USA inflict between $77.4 to $378.7 billion each year in damages [6]. Human communities are at risk, and therefore the means of spread of wildfires are an important characteristic to study in the hopes that these impacts can be minimized.

It has been found that there are three main methods of wildfire spread within the WUI: direct flame impingement, radiant heat exposure, and firebrand exposure [13]. Direct flame impingement causes subsequent ignitions by acting as a piloted ignition source for combustible materials. Radiant heat exposure describes the heat feedback process through radiation of wildfire fronts that pyrolyze and heat up nearby WUI structures or vegetation, which results in the combustion of nearby materials. Of the three, it has been determined that firebrand exposure is the ignition source of the majority of structures that burn in the WUI [14, 21]. Firebrands are small, sized on the order of centimeters, airborne embers comprised of solid structural or vegetative fuels. A main threat of firebrands is that they can be lofted in front of an existing wildfire and are able to travel vast distances, spreading the wildfire by acting as an ignition source for satellite wildfires. Firebrands can be solitary, but also often collect in piles, each of which proposes different challenges. They maintain elevated temperatures by smoldering for extended periods of time, produce minimal smoke, and with an oxidation source, can ignite nearby combustibles or themselves [15, 16]. Much of the existing research in the field is dedicated to understanding the generation, lifespan, and combustion behavior of firebrands. An additional vital area of study within the realm of wildfire events is to characterize how firebrands ignite adjacent materials, which is the focus of this study.

Section 2: Existing Firebrand Studies

Firebrand research has been of interest in the WUI field in recent years. These studies aim to characterize the physical appearance, including mass and shape, generation, transport, propensity to flaming ignition, and deposition orientation of firebrands and firebrand piles [17 - 20]. Understanding the combustion behavior, distribution, and lifespan of embers and firebrands is vital to constructing accurate predictive models and generalizing wildfire behavior in order to minimize the harmful effects listed above.

The timeline of ignition by firebrand has been categorized into three main processes: firebrand generation, transport, and the ignition of the target fuel [22]. The generation of firebrands occurs when already-burning fuels undergo thermal decompositions, resulting in the larger solid fuels breaking down into smaller portions. The resulting firebrands can be either flaming or glowing and characteristics are dependent on fuel type, morphology of the fuel, and the intensity of the original fire [22]. Then, the firebrands are transported by the fire plume or existing wind in the wildfire climate. The firebrands are light, and easily transported by the buoyant forces present, even up to distances of 9 km [23]. Then, when firebrands land on a target fuel, they maintain their elevated temperatures through the transport process and are able to cause spot fires [24, 25]. The conditions that cause ignition of a nearby fuel have not yet been fully characterized and serve as a motivation for this study. However, it is known that it is a combination of the conductive and radiative heat transfer originating with the firebrands that drive these ignitions, starting the aforementioned spot fires [24, 26]. Of course, this is highly dependent on the type of fuel present and the environmental conditions, including temperature, moisture content of the combustible, wind speed, and relative humidity.

There have been several studies that explore the generation and composition of firebrands alone [26 – 30], yet most relevant to these studies are those that relate to the ignition of solid fuels due to firebrand exposure. In regard to structural components acting as a source of fuel in the WUI, Manzello and Suzuki are large contributors to understanding firebrand deposition [31 - 33]. Manzello in particular focused on both a small and large scale using the NIST Dragon [31, 32]. In small-scale tests, they deposited glowing firebrands (between one and four total firebrands) in a cedar crevice. External airflows of 0.5 m s^{-1} and 1.0 m s^{-1} were applied. No ignition occurred [34]. On a larger scale, Manzello et al. [33] provides an extensive summary of large scale experiments in Japan's Building Research Institute Fire Research Wind Tunnel Facility using the full-scale NIST Dragon. These experiments determined vulnerabilities of siding, roofing, and other portions of full structures that are susceptible to firebrand attack. Santamaria et al. [27] conducted ignition tests on solid wood boards using a heat flux from a controlled source heater and piles of charcoal to simulate firebrands; however, charcoal was not found to simulate firebrands well. Heat fluxes from bark firebrands were taken on a vermiculate inert board and found to produce heat fluxes of up to 8 kW m^{-2}.

Early tests by Waterman and Takata were among the first experiments to explore the combustion characteristics of firebrands deposited onto common roofing and building fuels [36]. They found that ignition probability increased with increasing wind speed. An additional external heat flux was applied to act as an ignition source, an experimental necessity that inspired others to continue this research to encourage ignition by firebrands alone. Dowling conducted firebrand tests on bridge timbers and found that 7 g of firebrands were sufficient to produce ignition [28]. A later study found that firebrand coverage density was positively correlated with the firebrand pile heating rate, determined by quantifying the transient heat fluxes from the firebrand piles using water-cooled heat flux gauges (WC-HFG) and thin-skin thermopiles (TSC) [20]. In further experiments, four glowing firebrands were deposited into crevices made of either plywood or oriented strand board (OSB), both common building materials [30, 33]. Ignition was sensitive to angle – only tests at 60°or 90°ignited. Additionally, of tests at these angles, only tests with 2.4 m s^{-1} external airflow and dry recipient fuel ignited [33]. The authors expected that the fuels with higher moisture content (i.e. 11%) did not ignite due to the higher thermal inertia of these samples [33].

Section 3: Objectives and Motivation

As seen by the studies outline above, most of the firebrand studies focus on the combustion characteristics of the firebrands themselves rather than the ignition vulnerability of WUI materials. Instead, they rely on observational data alone to determine susceptibility to ignition by firebrand exposure [14]. There is a technical gap to be filled to inform about the quantifying ignition criteria and thermal response profiles of WUI decking materials exposed to varying wind flows. These series of tests were conducted in order to better inform about the nature of firebrand piles deposited onto common WUI materials, Western Red Cedar (WRC) and Oriented Strand Board (OSB) and how they may contribute to subsequent ignitions during a wildfire. Because so many of the existing studies require invasive forms of measurements, such as thermocouples (TC), WC-HFG, and TSC, that disrupt the heat transfer of the firebrands and the decking material itself, a less intrusive method of data collection was desired.

In particular, this body of work intends to expand upon the insight gained by the studies conducted in [37]. An alternative to intrusive temperature measurements, such as TCs, was introduced in the form of infrared (IR) thermal imaging to capture the thermal profiles of the substrates, placed 0.4 m away from the back surface of each sample tested. This method was used in [37] and maintained for this study as well because of its ability to capture the back surface temperature of the substrate without altering the experimental conditions. WRC was chosen for [37] because while it receives attention in large-scale studies, there is little existing data about this material on the bench-scale. The flat deposition of the firebrand piles onto this material allowed for a look into the primary driving forces for surface ignitions of WRC, uncomplicated by reradiation effects or other fuels present that would be introduced with more complex configurations.

There were three main ways that this study aims to expand that of [37]: introducing an additional decking material, OSB, a preliminary look at the effects of changing the firebrand pile orientation, and a preliminary look into varying the wind flow during a test. OSB has a similar composition to WRC, though nearly twice the density, seen alongside other thermophysical properties of each material in Table 1. Thus, all results considering differences between the ignition and combustion behavior of WRC and OSB explores the impact of material density on substrate susceptibility to firebrand deposition. Three phases of testing were conducted in order to learn more about each material under the specified conditions. Phase 1 completely mimics [37] with the addition of introducing OSB and completing a further set of tests at 2.7 m s^{-1} based on the results of [37], which considered airflows only up to 2.4 m s^{-1}. Phase 2 introduces an adjustment to the orientation of how firebrands are deposited onto each test substrate, yet only under one specific set of conditions relating to firebrand pile size and air flow direction in the wind tunnel on both types of materials. Both Phase 1 and 2 expose the boards to continuous airflow throughout the entire test duration. In contrast, Phase 3 aims to reflect the wind gusts present during a wildfire by introducing intermittent airflow, again conducted on both WRC and OSB under only one airflow velocity and firebrand pile size.

Table 1. Thermophysical Properties of Each Substrate

	Density (kg m^{-3})	Heat Capacity (J g^{-1} K^{-1})	Thermal Conductivity (W m^{-1} K^{-1})
Kaowool PM[a]	256[38]	1.07[38]	0.049 +1.5 × 10^{-5} T + 1 × 10^{-7} T^2 (T in °C) [38]
WRC[b]	368[39]	1.7[40]	0.11[39]
OSB[c]	670[45]	1.599[44]	0.118[44]

[a] *All properties of Kaowool PM correspond to the dried samples.*
[b] *The density of WRC corresponds to the dried sample. Heat capacity and thermal conductivity of WRC correspond to samples of 15% moisture content.*
[c] *All properties of OSB correspond to samples of 10% moisture content.*

All three phases test three materials: WRC, OSB, and a thermal insult, Kaowool PM, a ceramic fiberboard that does not get involved in combustion. Outlined in Chapter 2, the experimental setup for each is explained, including the wind tunnel used to introduce airflow and how the samples were mounted as well as the instrumentation used for measurements. This chapter also further outlines each substrate and the firebrands chosen for this study as well as the experimental procedure for each phase. Additionally, for each of the phases, there was common information collected for each test. This includes a look into the surface ignitions that do or do not occur during each test, determined visually through video analysis and quantified by the time to ignition after firebrand pile deposition, burn duration, and overall probability of ignition under each condition. Furthermore, IR thermal imaging was conducted in order to determine the temperature profiles of the back surface of each material. The temperature profiles found using non-invasive means could then be used in an inverse heat transfer analysis to quantify incident–heat flux profiles, also generally found using intrusive methods like WC–HFGs or TSCs, from the firebrands to the deposited surface. Finally, the composition of the gaseous outputs of each test were collected in order to generate heat release rate (HRR) curves and possibly determine the mode of combustion present, whether that be flaming or smoldering, through the modified combustion efficiency (MCE). All measurements were collected simultaneously to give a comprehensive overview of the combustion process, no matter the firebrand pile size, orientation, or velocity of the airflow through the wind tunnel. The methods of analysis are seen in Chapter 3, while the results and discussion are found in Chapter 4. Here, the combustion behavior of WRC is compared to that of OSB and is broken up by phase of testing. Finally, conclusions from the analysis and recommendations for future work are found in Chapter 5.

Chapter 2: Experimental Methodology

Section 2.1 Instrumentation and Setup

Subsection 2.1.1 Wind Tunnel

All experiments were conducted within a bench-scale wind tunnel apparatus. A rendering of the setup used is seen in Figure 1. As shown, there are three main sections of the apparatus: the contraction cone, the test section, and the exhaust.

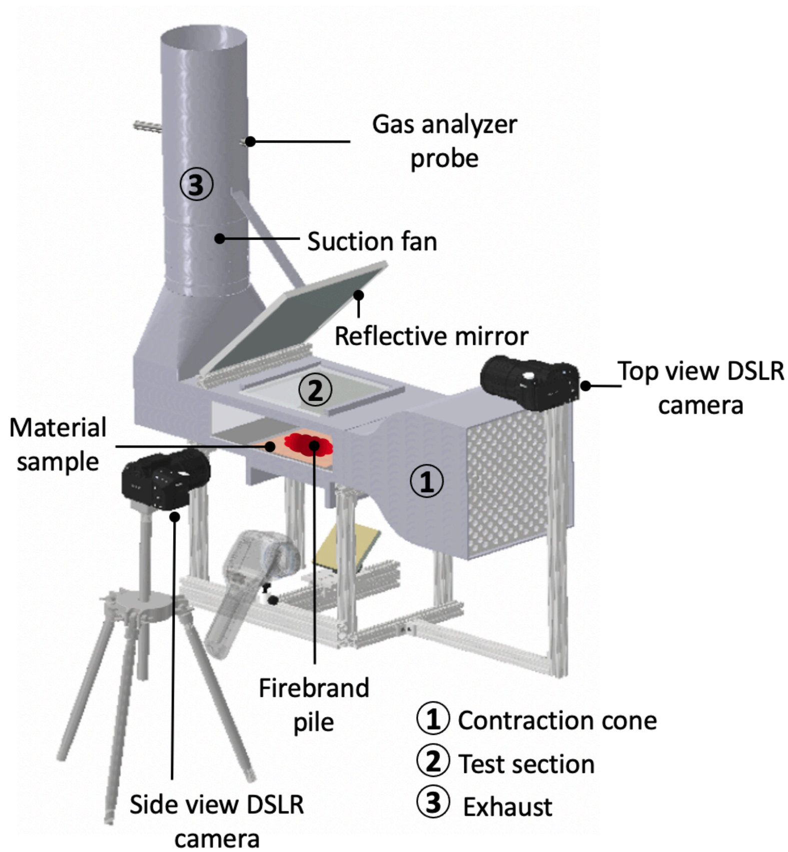

Fig. 1. A CAD drawing of the experimental wind tunnel setup.

The contraction cone serves to pull in and laminarize air flow to the test section through the use of a reducer and honeycomb mesh. All components of the cone are constructed of stainless steel. The larger opening of the contraction cone, consisting of honeycomb mesh, is 26 cm wide by 27 cm tall. It reduces in height to only 10 cm while maintaining the horizontal dimension.

The test section is where the samples were loaded and where the firebrand piles were deposited. This section is 37 cm long, 26 cm wide, and 10 cm tall. Here, as confirmed by [37], the air flow was developed and uniform. This section also housed the removable sample holder, an 18.5 cm by 18.5 cm aluminum frame that slid into an opening in the bottom of the tunnel. The depth of the holder could be adjusted to accommodate the varying thickness of the test materials. The frame also allowed for infrared temperature readings as described in Section 2.3.1. Directly above the bottom opening is a 20 cm by 20 cm top opening to allow for firebrand deposition after the sample had been loaded. The deposition process is described in Section 2.4. Finally, there is a 20 cm by 6 cm borosilicate glass opening on the side of the tunnel to allow for video recording during a test while the tunnel is sealed.

The exhaust portion of the tunnel follows downstream of the test section. There is a 90-degree bend in the tunnel which connects to a 6-in diameter exhaust duct. Here, a TerraBloom DBF6 high-temperature suction fan is located to generate the desired air flow through the apparatus. The air velocity for each test condition was set using a Hydrofarm Active Air Fan Speed Adjuster. The fan has the capability to generate air speeds from 0.5 – 3 m s^{-1}, capturing the range of wind speeds studied in [30, 33, 34]. 23 cm upstream of the fan located a gas sampling probe, a 23 cm stainless steel seamless tube of 1.6 cm outer diameter and with a wall thickness of 1.7 mm. This probe contained 72 1 mm holes, spaced at 2 mm apart, centered within the exhaust duct and facing opposite to the exhaust flow. The protruding end of the probe and both insertion holes in the duct were sealed with a –65 °C to 343 °C rated RTV Silicone gasket maker. This probe was then connected to the gas analyzer system using 150–cm long 6.4 mm diameter Coilhose

Pneumatics NC0435 red nylon tubing. Before entering the gas analyzer system, the exhaust fumes passed through a 316 L stainless–steel Headline Filters Model 126 soot filter. Once filtered, a 8 LPM supply vacuum pump carried the flow through two rows of Drierite to remove any moisture, and finally delivered it to the gas analyzer system.

Subsection 2.1.2 Gas Analyzer

The gas analyzer quantifies the amount of CO and CO_2 produced during a test, used to characterize the total heat release rate (HRR), the substrate versus the firebrand pile contribution to heat release rate, and the modified combustion efficiency (MCE) of each condition as discussed in Sections 3.3.

The model used was a California Analytical Instruments (CAI) ZPA Non–Dispersive Infrared (NDIR) Gas Analyzer, connected to the vacuum pump as described above. A needle valve purged most of the flow, allowing only 1.5 LPM of what was sampled to pass through the NDIR system. To determine the composition of the sampled gas, this system utilizes infrared absorption characteristic of the present gases. An infrared bean is passed through a cell of known length containing the exhaust gases. The attenuated beam is then introduced to the front chamber of the two–chamber infrared microflow detector. The voltage output measurements from this analyzer for both the CO and CO_2 volumetric percentage concentrations were obtained with a National Instruments 27NI–9215 analog voltage output module between 0 – 10 Volts at a frequency of 10 Hz and processed via a LabVIEW script.

Subsection 2.1.3 Cameras

In addition to the gas analyzer measurements, the ignition events and decomposition of the firebrand piles were captured on three cameras. There were two DSLR cameras, one to capture the side profile of the firebrand pile and one to capture the top-down view. The side camera was a Nikon D7100, and the top profile camera was a Sony Alpha SLT–A55V. In order to capture this top view, the camera was mounted to T-slot aluminum framing above the contraction cone, aimed at a mirror angled above the test section. Because the borosilicate glass used to close the top opening of the tunnel during a test is clear, this camera and mirror setup made it possible to visually observe the pile without interference during a test. There was also a FLIR E95 thermal imaging camera, capable of measuring infrared (IR) radiation intensity to capture the temperature of the back surface of each substrate after firebrand deposition, detailed in Section 3.1. This was used in conjunction with a gold mirror, also secured in place by T-slot aluminum framing, placed directly below the sample, able to redirect the camera's view to the substrate's back surface. All camera positions are shown in Figure 1, and a closer look of the FLIR camera setup is seen in Figure 2.

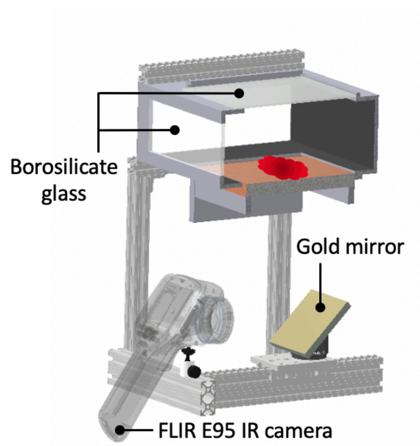

Fig. 2. A CAD drawing of the IR setup within the test section of the wind tunnel.

Section 2.2 Materials

Subsection 2.2.1 Firebrand Choice and Preparation

The same shape, size, and material of firebrands were used in all trials to minimize the experimental variables present. Cylindrical birchwood dowels of length 25.4 mm and diameter 6.35 mm were chosen for all trials as they were easily accessible and were found to produce appropriate peak substrate heating rates and durations [20, 30, 41]. This is representative of firebrands generated during wildfire events [20].

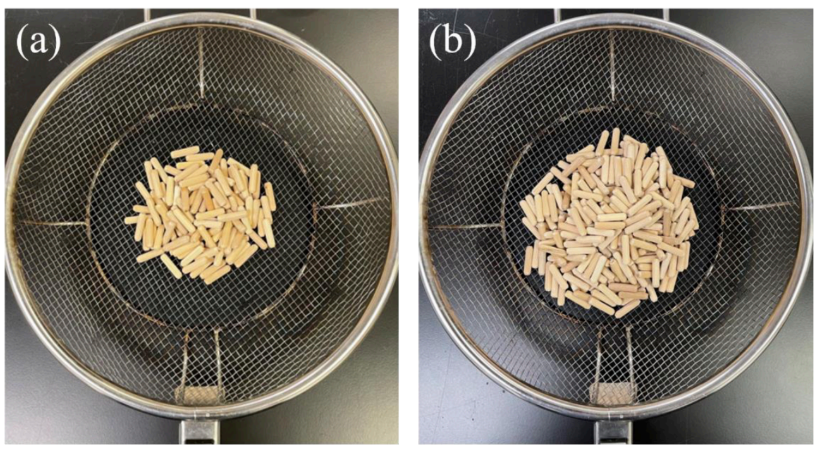

Fig. 3. Unburned dowels used in this study, which result in the 0.06 g cm^{-2} (a) and 0.16 g cm^{-2} (b) firebrand pile coverage densities.

The firebrands were also prepared the same way for all experiments. First, they were dried in a Quincy Lab, Inc. Mechanical Convention Oven at 103 ± 2 °C, per ASTM Standard D4442, for 24 hours [42]. About 1400 g of dowels were prepared at a time, or enough to a fill a one-gallon bag, where they were placed once removed from the oven. Three silica gel desiccant packets were placed in the bag as well to regulate the amount of moisture absorbed by the prepared dowels. Afterwards, they were ready for experimental use.

The experiments involve two firebrand pile coverage densities: 0.06 cm^{-2} and 0.16 cm^{-2}. This corresponded to 3 g or 8 g, respectively, of glowing firebrands deposited onto the board, funneled to land onto the center of the sample in what is hereinafter referred to as the firebrand deposition area. The firebrands were prepared to reach a glowing state because this is what most commonly occurs in a WUI fire scenario [31]. The two pile sizes represent the extremes of firebrand behavior with respect to a deposition area; the 3 g pile was found to be the minimum mass of firebrands that would envelop the deposition area, and the 8 g pile corresponded to the largest firebrand pile before a measured decrease in the peak heat flux onto the substrate as determined by [37]. A 3 g prepared pile required 48 g and an 8 g prepared pile required 112 g of unburnt dowels. This was first found by [37] and confirmed for this study. The correct mass of dowels for each respective trial were placed into a wire mesh pan and exposed to an ignited propane burner at a flow rate of 1.83 ± 0.06 SLPM for 40 s. The dowels would engage in flaming combustion due to this exposure and were kept in place until there were no visible flames, at which point they were considered glowing. For the 3 g firebrand pile mass, the complete glowing state occurred around 140 ± 15 s after ignition of the propane burner, and the same for the 8 g piles occurred around 220 ± 30 s after ignition of the propane burner. At this stage, they were deposited through the tunnel onto the substrate, beginning the experiment.

Subsection 2.2.2 Inert Substrate Choice and Preparation

In all testing conditions, the firebrand piles were deposited on an inert substance that would not contribute to the combustion process. This method isolated the burning conditions of the pile itself, allowing the possibility to characterize the firebrands without any effects from the combustible substrates. Kaowool PM, a ceramic fiber board, from Morgan Advanced Materials was chosen as the inert substrate used. The material has a thickness of 3.175 mm, which allows the assumption that heat transfer through the board is one-dimensional and that the back surface temperatures approximate the effects of heat flux from the firebrand pile to the material surface with respect to time due to its thinness. Additionally, this is the same substrate that was chosen for [37] study, and the experiments in this study aim to recreate those experiments exactly.

A goal of this study was to characterize the thermal feedback from the firebrand piles onto all substrates, which required all Kaowool PM tests to include IR measurements of the back surface temperature. First, the Kaowool PM pieces were cut into 18 cm by 14 cm samples for Phases 1 and 3 and 18 cm by 18 cm samples for Phase 2 tests. Then, for Phases 1 and 3, a 98 cm^2 portion of the back surface of the material was sprayed with a MedTherm optical black coating of known broadband emissivity of 0.94. The 98 cm^2 area included the entire deposition area of the firebrands, extended 1 cm on the shorter sides and 4 cm on the leading edge to ensure completeness of temperature measurements. Here, the leading edge refers to the periphery of the firebrand pile that is both closest to and perpendicular to the airflow inlet. The preparation of the MedTherm coating is shown on the back surfaces in Figure 4. In order to identify where the deposition area on the top of the sample was when captured by the IR camera, metal tape was used to outline this on the back surface. This is seen in Figure 4. Due to its reflective nature, the zone was clearly identifiable during analysis. For Phase 2, the coated area was instead 126 cm^2, the larger size necessary because these for a different deposition orientation. The differences between the two sample sizes and firebrand pile orientations used between tests is shown in Figure 5.

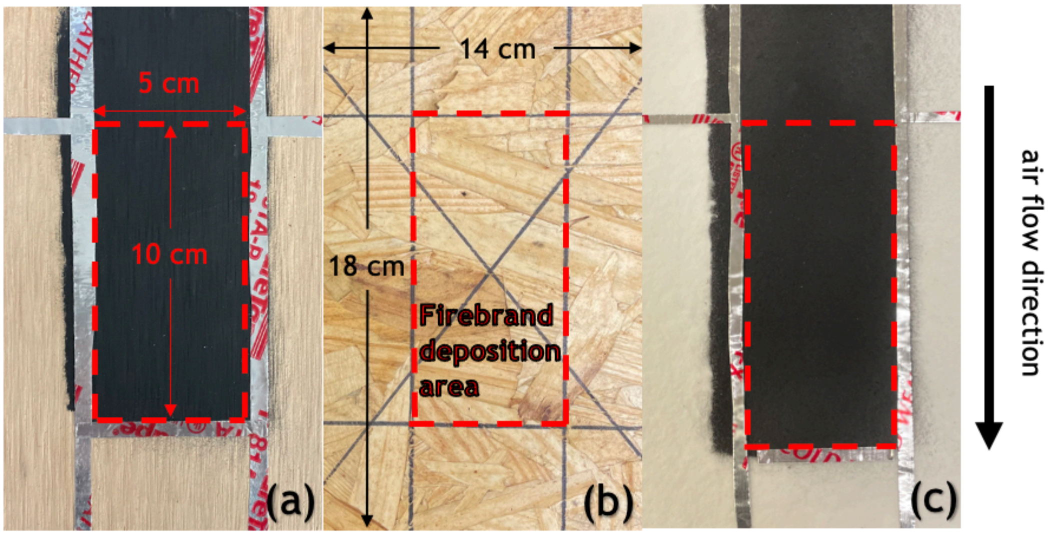

Fig. 4. Prepared back surface of WRC (a), front surface of OSB (b), and back surface of Kaowool PM (c) samples. The red dashed line indicates the firebrand pile deposition area. This orientation was used for Phases 1 and 3.

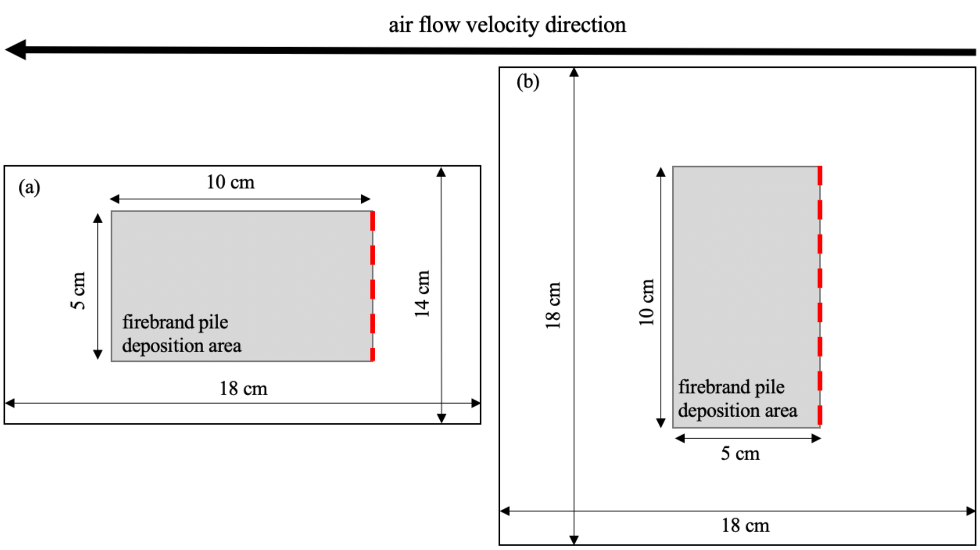

Fig. 5. Phases 1 and 3 (a) and Phase 2 (b) dimensions and orientations of the sample and firebrand pile deposition area. The red dashed line indicates the position of the leading edge of the pile.

Subsection 2.2.3 Combustible Substrate Choice and Preparation

The two combustible materials used in all experiments were 19.05 mm thick WRC boards and 12.7 mm thick OSB. Their thermophysical properties can be found in Table 1. WRC is a lightweight commercial softwood. It has a low thermal conductivity, seen in Table 1, meaning that applied heat to the material remains mostly concentrated to the area of exposure rather than equally distributed throughout the material. Its low density is owed in part to large cell cavities that contain air which in part contribute to its thermal insulation properties [39]. In contrast, OSB is the result of the amalgamation of small diameter poplar and aspen trees, mixed with waterproof resin and bonded through an industrial process involving high levels of heat and pressure [46]. It is often used in "floor, roof and wall sheathing in light-frame wood construction" [46]. Notably, it has nearly twice the density of WRC, though a similar heat capacity and thermal conductivity.

As discussed in Section 1.2, both are common decking materials used in wildland fire-prone areas, yet are dissimilar enough in density to vary in combustion behavior when exposed to the same radiant conditions. For the back surface temperature measurements, only conducted on either combustible for the Phase 1 tests, both boards were prepped the same as Kaowool PM. Each board had a visible "rough" and "smooth" side; the MedTherm coating was applied to the rough side for both. For the WRC, sandpaper was applied before the Medtherm coating to ensure that the back surface area had a smoother surface to analyze, intentioned to have more accurate readings from the FLIR camera during analysis. This step was not necessary for OSB. In addition to the IR preparation, done only for Phase 1, each wood sample was placed in a desiccator with Drierite for at least 48 hours before a test to lower the moisture content to 22 ± 2 %. They were not oven dried as it was expected that this is not representative of the boards in the WUI [31].

Section 2.3 Instrumentation Calibration

Subsection 2.3.1 Gas Analyzer

Two distinct calibration curves for CO and CO_2 were necessary to convert the gas analyzer output in voltages to the volumetric fractions (in %) necessary for subsequent calculations, outlined in Section 3.3. Preliminary testing determined that the CO and CO_2 volumetric concentrations were in the range of 0.01 – 0.4 vol.% for CO_2 and 0.001 – 0.04 vol.% for CO, which then became the focus of this calibration. To obtain the desired curves, 3 SLPM flow of known concentrations of CO, CO_2, and N_2 were passed through a 1 L plastic chamber using red nylon tube attaching the suction pump and the gas sampling probe detailed in Section 2.1. The tube was several meters long to ensure proper mixing of the gases before entering the chamber and sampling probe. The flow, initially 8.0% CO_2, 0.8% CO, and 91.2% N_2 by volume, was controlled by an Alicat Scientific MC–500SCCM–D/5M mass flow controller. This was then diluted by a flow of 100% N_2 controlled by an Alicat Scientific MC–10SLPM–D/5M mass flow controller to obtain the concentrations from each canister that would result in the desired values of volumetric concentrations for each gas. To obtain each curve, the test first ran a baseline of 100% N_2 to purge the system, then introduced CO and CO_2 for 90 s to obtain an average value of the voltage output. This was done for 12 distinct measurements that captured the desired volumetric concentration output range. All tests were recorded LabVIEW. This calibration was performed three times over the course of experimental testing to determine if there was any systemic shift in the gas analyzer equipment. An average of the three curves was used to process all data collected during testing. These curves are shown in Figure 6.

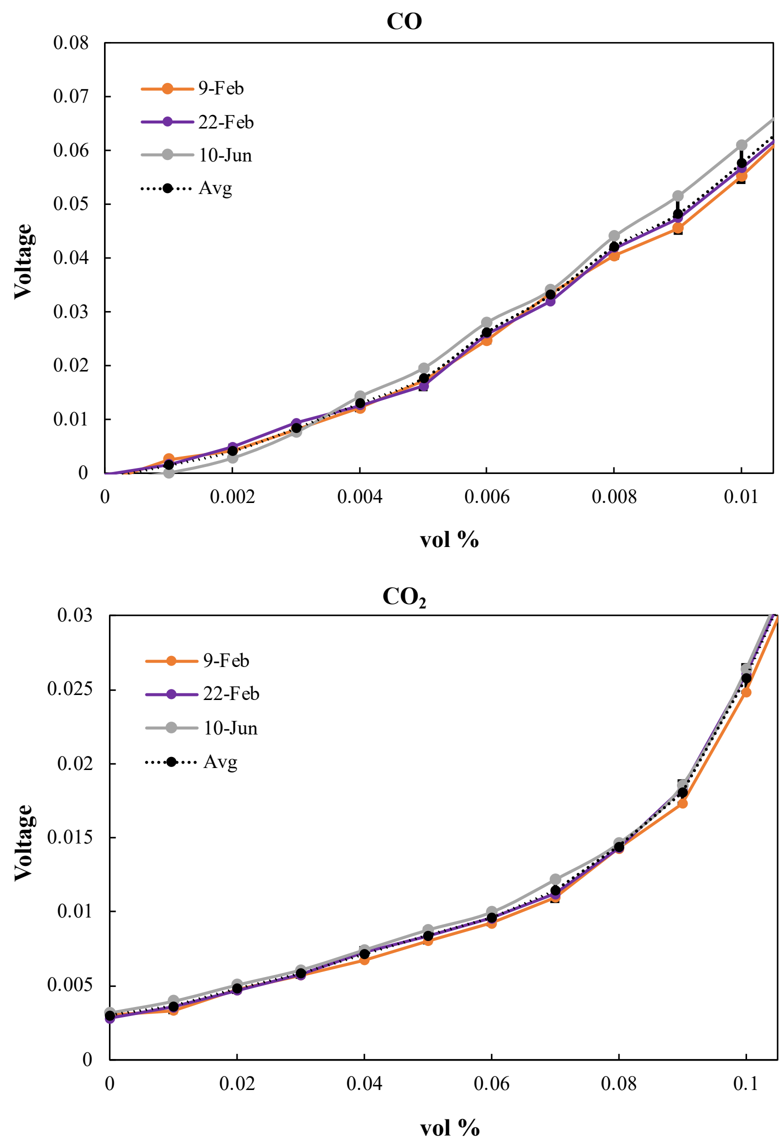

Fig. 6. The calibration curves for CO and CO_2 to convert from the voltage output of the CAI ZPA NDIR gas analyzer system into volumetric concentrations to be used in calculations.

The MedTherm high temperature optical black coating has a known value for average absorbance of 0.95, but to achieve the most accurate temperature readings, the emissivity of the coating applied to each surface was found. Each value was determined by comparing the readings of a 0.127 mm bead diameter K-type thermocouple and inputting the FLIR camera analysis with varying emissivities, set to expected values of the surface: 0.90 – 0.95 in intervals of 0.1. Experimentally, coated samples were mounted in a radiant cone heater and exposed to 85 kW m^{-2} of incident radiant heat flux, intended to be representative of the firebrand piles of these experiments. The thermocouple was mounted on the same side as the coated surface, and only a 2.5 cm square opening was exposed to the heater; the remainder of the sample and the thermocouple wires were covered with Kaowool PM insulation to limit the exposure of the wires. The thermocouple was then connected to a NI–9213 C Series Temperature Input Module (± 78 mV), which interpreted the voltages from the thermocouple at a frequency of 6 Hz and was collected using LabVIEW. The IR analysis set up exactly mimicked that of the wind tunnel, using the same FLIR E95 camera and gold mirror at the 0.4 m distance. Once mounted, the radiant heater, set to a heat flux of 85 kW m^{-2} was covered by a shutter until the heater reached a steady value of 300 °C. Then, the shutter was opened, exposing the sample for 165 s.

Calibration tests were conducted twice per material. For analysis, four spot measurements surrounding the thermocouple bead in FLIR Tools were used to determine the temperature at the surface of the bead, understanding that the bead itself would block the IR camera and thus measurements could not be taken in the exact same spot on the sample. A more complete outline of the analysis capable by FLIR Tools is detailed in Section 3.1. These four spot measurements, corresponding to 36 temperature measurements by pixels, were averaged to determine the temperature profile with respect to time of the substrate. A FLIR profile was compared to the temperature profile produced by the thermocouple during the same test, the emissivity on FLIR altered until the two profiles well-aligned. When the two matched, the value input into FLIR was then taken as the emissivity of the surface. The two emissivities of the two tests conducted for each material were considered. This resulted in emissivities of 0.94, 0.92, and 0.91 for Kaowool PM, WRC, and OSB, respectively.

Section 2.4 Experimental Procedures

An overall test matrix can be found in Table 2. This set of experiments was split into three phases, each with distinct goals and procedures. Table 2 shows the number of tests conducted per material for each of the three phases, resulting in a total of 189 tests included in this report.

Table 2. Overall Testing Matrix Per Material (WRC, OSB, or Kaowool PM)

		Continuous Forced Flow Velocity (m s^{-1})			Intermittent Forced Flow Velocity (m s^{-1})
	Firebrand Pile Coverage Density (g cm^{-2})	1.4	2.4	2.7	2.7
Phase 1	0.06	9 tests	9 tests	-	-
	0.16	9 tests	9 tests	9 tests	-
Phase 2[a]	0.16	-	9 tests	-	-
Phase 3	0.16	-	-	-	9 tests

[a] Phase 2 introduced a 90° difference in orientation of the firebrand pile deposition from Phases 1 and 3. See Section 2.4.2 for details.

Subsection 2.4.1 Phase 1

As stated earlier, the first phase of testing intended to recreate all of the WRC tests conducted in [37] using OSB instead to note the differences in combustion behavior between substrates. This included a total of 45 tests: 9 trials for each condition, those consisting of 0.06 g cm^{-2} and 0.16 g cm^{-2} firebrand coverage densities deposited on the substrate at air flow velocities within the wind tunnel set to 1.4 m s^{-1} and 2.4 m s^{-1}, and just the 0.16 g cm^{-2} firebrand coverage density at 2.7 m s^{-1}. The measurements taken during these trials included the gas flow analyzer outputs, the back surface temperature of the substrate, and the DSLR camera videos.

The relative humidity and temperature of the testing environment were recorded for all test days. Additionally, the gas analyzer system was span calibrated at the beginning of each test day as well using gases of known compositions. This included first running a 100 vol.% N_2 canister to zero out the NDIR sensors, and then introducing an 8.0 vol.% CO_2, 0.8 vol.% CO canister to begin each testing day with the same sensor readings. This was set before any voltage readings were recorded from the analyzer. After this was established, the 14 cm x 18 cm sample was placed in the test section of the wind tunnel in the sample holder described in Section 2.1 and secured with metal tape to ensure any air pulled into the enclosure was through the contraction cone as well as ensure that any gaseous combustion products were captured by the exhaust hood. All three cameras were placed into their respective locations, shown in Figure 1, and focused. The wind velocity was set to the desired testing condition using the air flow velocity controller. This measurement was confirmed using an Omega HHF–SD1 Hot Wire Anemometer that was inserted into the test chamber at an elevation of 3 cm above the substrate. In order to not disturb the flow through the tunnel, the top opening was sealed using a piece of hardboard with a hole drilled in the center for the anemometer. Once this reading was set, the hardboard was removed and the deposition funnel was placed atop the sample, aligned with the markings shown on the front side of Figure 4.

Once all measurement systems were set, the test could begin. The firebrands were measured and prepared as according to Section 2.2.1. The gas analyzer measurements were taken simultaneously as the firebrands were placed unto the propane burner, and this was when the timer began. 110 s after the firebrands were placed, both DSLR camera videos were initiated. 20 s later, or 130 s after the timer started, the FLIR camera recording was initiated. Once the firebrands were entirely in a glowing state, they were deposited onto the substrate using the previously described funnel. For context, for the 0.06 g cm^{-2} pile coverage densities, deposition occurred around 120 s after the firebrands were placed on the burner, and for the 0.16 g cm^{-2} pile coverage densities, this occurred at around 240 s. The top mirror was placed, and the borosilicate glass covering was slid into the top opening, designating the beginning of the test (time t = 0 s) for purposes of analysis. The tests continued for a total of 1100 s after the gas analyzer system was initiated, capturing about 860 s after the borosilicate glass seals the tunnel. This was deemed enough time so that no further surface ignitions occurred and that there was minimal involvement in combustion from the board sample or the firebrand pile. On occasion, the 0.16 g cm^{-2} firebrand piles did burn through the OSB boards due to their smaller thickness, at which point these tests were terminated.

Subsection 2.4.2 Phase 2

The second phase of testing examined the changes in burning characteristics when the firebrand pile was deposited onto the substrate at a 90 degree difference in orientation. In these scenarios, the leading edge of the pile was double the length as it was in the first phase, changing from 5 cm to 10 cm. This is shown in Figure 5. This phase consisted of 27 tests: 9 trials for each Kaowool PM, WRC, and OSB with a 0.16 g cm^{-1} firebrand pile coverage density and the wind velocity set to 2.4 m s^{-1}. This condition was chosen because it resulted in the greatest number of surface ignitions observed for both the WRC and the OSB at the original pile orientation as determined by preliminary testing. The measurements here included the gas analyzer outputs for all tests on all three materials, the video recordings from both DSLR cameras and the IR back surface temperature readings for the Kaowool PM tests, and the DSLR camera readings, no IR, for the tests conducted on either wood.

The testing procedure follows very closely to that of Phase 1, outlined in the previous section. The gas analyzer was span-calibrated, the wind velocity set, and the firebrands prepared in the same exact ways. For the OSB and WRC samples, no back surface temperature measurements were taken, so the FLIR camera was not used in these tests. In contrast to Section 2.4.1, the samples were 18 cm by 18 cm squares, still an appropriate size for the sample holder, and any air gaps around the sample were sealed with metal tape. The deposition tunnel was then aligned with markings on the sample, drawn to ensure that the funnel was centered on the substrate. Because the area of deposition was the same, and the difference came from altering the orientation of the firebrand pile, the same tunnel was used in all three phases. For Phase 2, the tunnel itself was turned 90 degree during deposition to achieve the desired orientation within the wind tunnel. The timing of the camera recordings and the duration of the tests remained the same.

Subsection 2.4.3 Phase 3

The third and final phase of testing focused on the effects of alternating turning the forced flow in the tunnel on and off in order to mimic gusts of wind during wildfire events. The main focus of this phase is to characterize the surface ignitions of the WRC and OSB as well as examine the thermal profile of the firebrand pile using the inert substrate. This phase also consisted of 27 tests: 9 trials for each Kaowool PM, WRC, and OSB with a 0.16 g cm^{-1} firebrand pile coverage density and the maximum wind velocity, 2.7 m s^{-1}. After some preliminary testing and analyzing the previous phases, these conditions were the most conducive to observing surface ignitions of the materials. The measurements taken consisted of the video recordings from both DSLR cameras and the IR back surface temperature readings for the Kaowool PM tests, and the DSLR camera readings, no IR, for the tests conducted on either wood.

The gas analyzer was not used for this phase. Instead, the initial procedure exactly mimics Phase 1 in that the samples were mounted, the wind flow velocity determined, the cameras placed, and the firebrands prepared and deposited all in the same ways. The difference here comes from the exposure to forced flow within the tunnel. As a note, turning off the forced flow consisted of unplugging the air flow controller so not to disrupt its setting, which had been previously calibrated, and to ensure that the set wind flow velocity was consistent for the entire test duration. After the tunnel was sealed, the air flow velocity within the tunnel of 2.7 m s^{-1} was maintained for 60 s. After this 60 s, the forced flow was turned off for 10 s, and then turned back on for 20 s. This 30 s cycle, which does not include the initial 60 s exposure, continued for a total of 14 times. The entire experimental duration after which the tunnel was sealed lasted for 480 s.

Chapter 3: Data Analysis Process

Section 3.1 Surface Ignition Characteristics

All surface ignitions of WRC and OSB were determined visually using the two DSLR cameras. These events were characterized by a flame that is anchored by the combustible target substrate; ignitions of the firebrand piles alone were not included for this analysis. An ignition of the firebrand pile was fainter in color than one of the combustible, the flame itself would not reach the material surface but instead would be located on the top surface or side of the firebrand pile, and typically were unable to sustain as long as a surface ignition. These distinguishable differences between flames are seen in Figure 7.

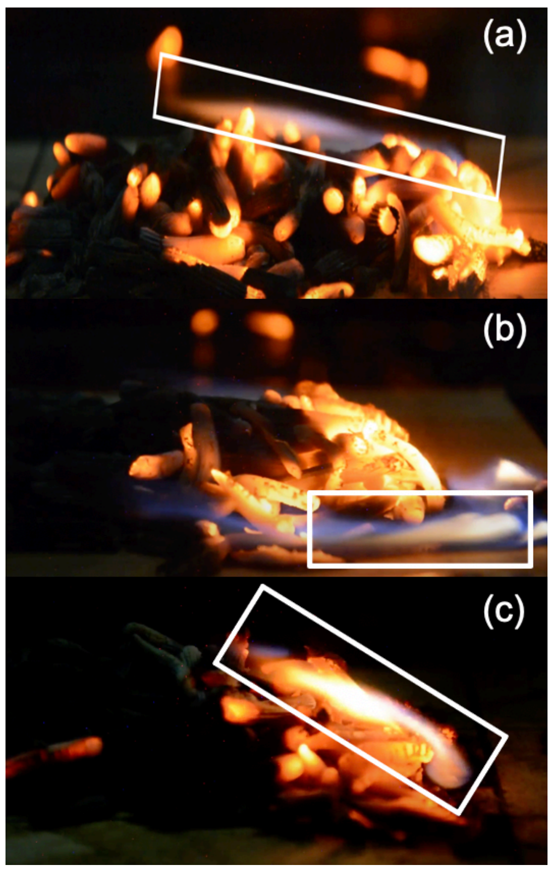

Fig. 7. Firebrand pile ignition on Kaowool PM (a) and surface ignitions on WRC (b) and OSB (c). White boxes indicate the location of the flame. Each photo was taken from the side facing DSLR camera during a 0.16 g cm^{-2}, 2.4 m s^{-1} test.

For all conditions and phases, the burn duration and location of the flame were identified for each ignition event. For Phases 1 and 2, the time of ignition with respect to the time of firebrand pile deposition was also found. The uncertainties of the time to ignition and the burn duration were taken as two standard deviations of the mean. In these phases, it was overwhelmingly common for only one ignition event to occur over the duration of a test for both WRC and OSB. Thus, the probability of ignition under a given condition was determined by dividing the number of tests in which an ignition did occur by the nine tests conducted for each condition. These are seen in Sections 4.1.1 and 4.2.1. In contrast, Phase 3 observed multiple ignition events over the course of a single test with the introduction of intermittent airflow, seen in Section 4.3.1, and so the mean number of ignitions per test was taken with two standard variations of the mean. As stated, burn duration and combustion location were also noted for all Phase 3 tests. Additionally, it was also seen whether ignitions and extinctions occurred when the forced flow through the wind tunnel was on or off. An example of the distinction between the two is shown in Figure 8.

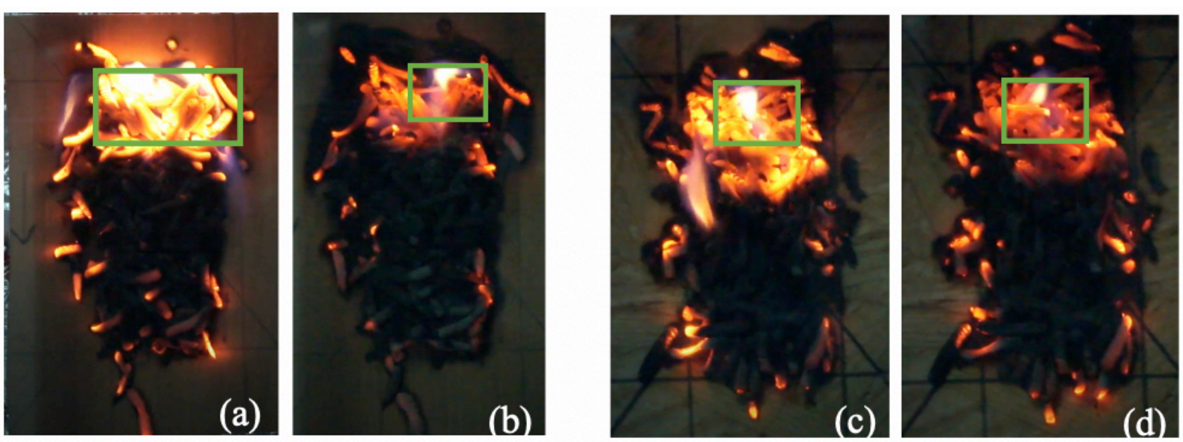

Fig. 8. Phase 3 surface ignitions on WRC with the forced flow on (a) or off (b) and OSB with the forced flow on (c) or off (d). Ignition locations are highlighted in green.

Section 3.2 Back Surface Temperature Measurements

The back surface temperature measurements were performed using the IR camera and the FLIR Tools software. For all tests in all phases, the inert substrate temperature profile was found in order to isolate the thermal behavior of the standalone firebrand piles under a given condition. The method used on the combustible substrates has the same approach as outlined below, yet was only conducted for Phase 1.

The method used had a three-zone approach to the deposition area: the preleading, leading, and middle zones, seen in Figure 9. The deposition area had dimensions of 5 cm by 10 cm; the leading edge was 5 cm long in Phases 1 and 3, and 10 cm long in Phase 2. For Phase 1, all three analysis zones were 4 cm in length. The preleading zone was 1.5 cm in width, with 0.5 cm extending into the firebrand pile and 1 cm capturing the length just in front of the leading edge of the firebrand pile. The middle and leading zones were each 3 cm in width. For Phase 2, only the preleading zone was considered as this is where the majority of the surface ignitions were located. It was 8 cm in length to capture the larger leading edge of the pile and 1.5 cm in width, matching the Phase 1 placement. Phase 3 also only considered the preleading zone, again because this is where the majority of ignitions occurred, and had the exact same dimensions and placement as the preleading zone of Phase 1. The dimensions and locations of each zone are identified in Figure 9.

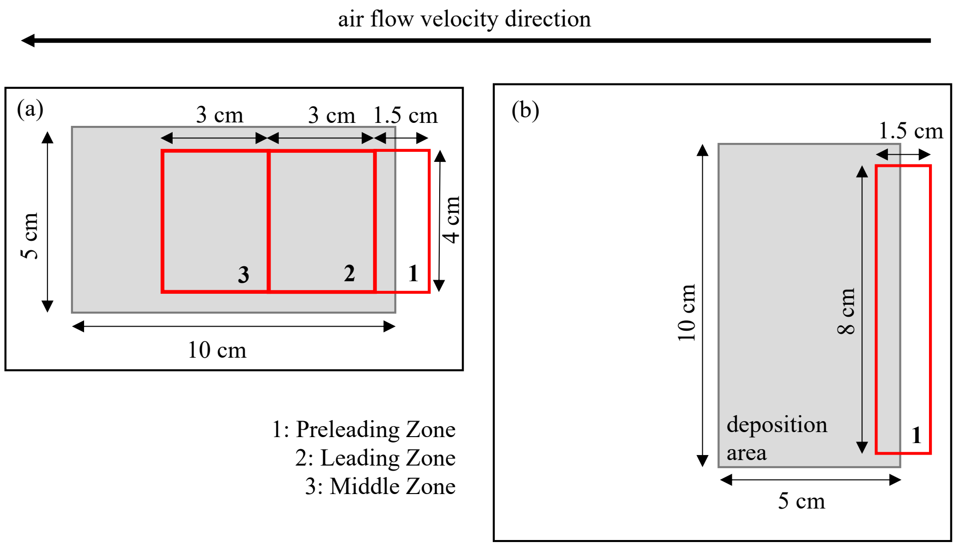

Fig. 9. The preleading, leading, and middle zones used in the FLIR analysis to determine back surface temperatures in Phases 1 and 3 (a) and Phase 2 (b). The shaded area represents the deposition area of the firebrands on the top surface of the material. Drawing is not to scale.

The videos taken with the FLIR camera were input into FLIR Tools software for analysis. A length of 0.4 m, the distance from the camera to the gold mirror, was accounted for as well as the emissivity of the MedTherm coating for each respective substrate, identified in Section 2.3.1. In the middle and leading zones, 30 spot measurements were placed randomly, yet not overlapping, in order to capture the evolution of the thermal profile of the region with respect to time. For the preleading zone, only 24 spot measurements could fit without overlapping in the zone. Each spot contains 9 pixels corresponding to 9 temperature measurements that are averaged within FLIR Tools and create a profile for the spot by recording one temperature every 0.033 s. Each of the spot measurements were then averaged to create a single representative profile for each zone. This was conducted for every test and averaged, shown with two standard variations, for the analysis in Chapter 4. The same procedure was followed no matter the substrate material.

Section 3.3 Gas Analyzer Measurements

Subsection 3.3.1 Determining HRR

The heat release rate at any given time during the test duration could be found using the gas analyzer system outputs. As previously mentioned, the volumetric concentrations of CO and CO_2 in the combustion products were collected using probes in the exhaust section of the wind tunnel. These were reported as voltages by the apparatus. Using the calibration curves outlined in Section 2.3.1, the voltages were converted into volumetric percentages to be used in further calculations. A baseline reading of the ambient CO and CO_2 volumetric percentages were taken prior to firebrand pile deposition for each test. These baselines were averaged over 50 s and subtracted from each subsequent measurement. The profiles were smoothed using a third order Savitsky-Golay filter every 3 s. This was then used to find the mass productions rates of CO and CO_2, $\dot{m}_{CO}^{e}$ and $\dot{m}_{CO_2}^{e}$,

$$\dot{m}_{CO}^{e} = \rho_{CO}\dot{V}(\phi_{CO}^{e} - \phi_{CO}^{a}) \tag{1}$$

$$\dot{m}_{CO_2}^{e} = \rho_{CO_2}\dot{V}(\phi_{CO_2}^{e} - \phi_{CO_2}^{a}), \tag{2}$$

in which ρ_i is the gas density at 25 °C, $\dot{V}$ is the volumetric flowrate of air across the inlet of the test section and the forced flow velocity specific to each test, ϕ_i^e is the experimentally-determined volumetric percentage, and ϕ_i^a is the averaged baseline volumetric percentage, all with regard to each specific gas. $\dot{V}$ volumetric flowrate through the test section, computed as the product of the test section cross-sectional area (0.26 m × 0.1 m) and the set flow velocity, and was assumed constant throughout the test duration, corroborated by [37]. The gas densities used can be found in Table 3.

Table 3. Properties of Gases, Taken at 25°C, Used to Find Mass Production Rates and HRR. All values found from [47].

	Density (kg m^{-3})	Heat of Combustion (kJ g^{-1})
CO	1.15	11.1 ± 2
CO_2	1.81	13.1 ± 1.5

The mass production rates of CO and CO_2 were then implemented into the following correlation for HRR for each time step, stemming from carbon dioxide calorimetry,

$$HRR = \frac{\Delta H_{c,CO_2}\dot{m}^e_{CO_2} + \Delta H_{c,CO}\dot{m}^e_{CO}}{A_{pile}}, \quad (3)$$

where $\Delta H_{c,i}$ is the known heat of combustion of each gas, found in Table 3, and A_{pile} is the area of the firebrand pile deposition area, or 0.005 m^2. Both firebrand pile coverage densities fully covered this deposition area at the start of each test. This profile was found for each test of a given condition though only the averages with variation are shown in Chapter 4. This methodology for HRR was the same for Phases 1 and 2. Because this quantity relies on the forced flow velocity through the contraction cone in the wind tunnel, assumed constant, HRR was not determined for the intermittent air flow conditions in Phase 3.

Subsection 3.3.2 Determining Combustible Contribution to HRR

In Phases 1 and 2, which included gas analyzer measurements, the contribution of the combustible board to the total HRR profile was also found. This was taken by subtracting the average HRR profiles of each combustible board from the corresponding HRR profile of the Kaowool PM at each condition. It is assumed that the firebrand pile decomposes the same way with the same mass and exposed to the same air flow velocity no matter the substrate they are deposited on. Thus, subtracting the two profiles allows for analysis into how the board itself gets involved in combustion; if the contribution to HRR is negative, the board acts as a heat sink, and the portion of the energy produced during the decomposition of the firebrands used to heat and/or gasify the substrate is more than the energy produced from the combustion of the board. When the contribution is positive, it indicates that the board combustion is sufficiently intense to compensate the slight reduction in the heat release from firebrands associated with the heat losses to the combustible board.

Subsection 3.3.3 Determining MCE

Lastly, the MCE profiles with respect to the test duration of WRC and OSB were found from the volumetric percentages of CO and CO_2 using

$$\mathrm{MCE} = \frac{\left(\phi_{CO_2}^{e} - \phi_{CO_2}^{a}\right)}{\left(\phi_{CO_2}^{e} - \phi_{CO_2}^{a}\right) + \left(\phi_{CO}^{e} - \phi_{CO}^{a}\right)} \,. \tag{4}$$

This quality describes the propensity of combustion towards flaming or smoldering. The MCE indicates that flaming combustion dominates when reporting values greater than 0.9, and is within the smoldering regime when MCE values are within 0.65 and 0.80 [43]. There is some disagreement in the literature, and some suggest that an MCE value of 0.9 indicates that combustion is dominated by neither process, but instead shares an equal contribution from both smoldering and flaming [43]. WRC and OSB are solid polymers and thus are expected to result in a combination of smoldering and flaming combustion.

Chapter 4: Results and Discussion

Section 4.1: Phase 1

Subsection 4.1.1: Surface Ignition Characterization

Phase 1 examined the probability, location, burn duration, and time of ignition for the surface ignition events on both WRC and OSB under the five conditions in this phase. Figure 10 shows the ignition probability, taken as the probability of a surface ignition occurring under the outlined condition. For all tests, only one ignition event occurred per test when ignition did occur, so the probability shown is the number of tests with an ignition over the number of tests performed for each condition, or nine. As shown in Figure 11, WRC has a greater tendency towards ignition across all conditions. Notably, OSB conditions of the 0.06 g cm^{-2} firebrand pile coverage density did not result in any ignitions, while WRC had at least one ignition event no matter the condition. The location of these ignitions mostly occurred in the preleading zone, identified in Figure 11. Though there is smoldering of the combustible in the leading and middle zones, there does not appear to be sufficient oxygen in these locations to sustain flaming combustion due to the presence of the firebrands themselves. Thus, the ignitions occur where there is enough oxygen flow and radiative feedback from the firebrand pile to pyrolyze the virgin substrate: the preleading zone. This occurred consistently between materials and all airflows and firebrand pile coverage densities when a surface ignition did occur, shown by Figure 11.

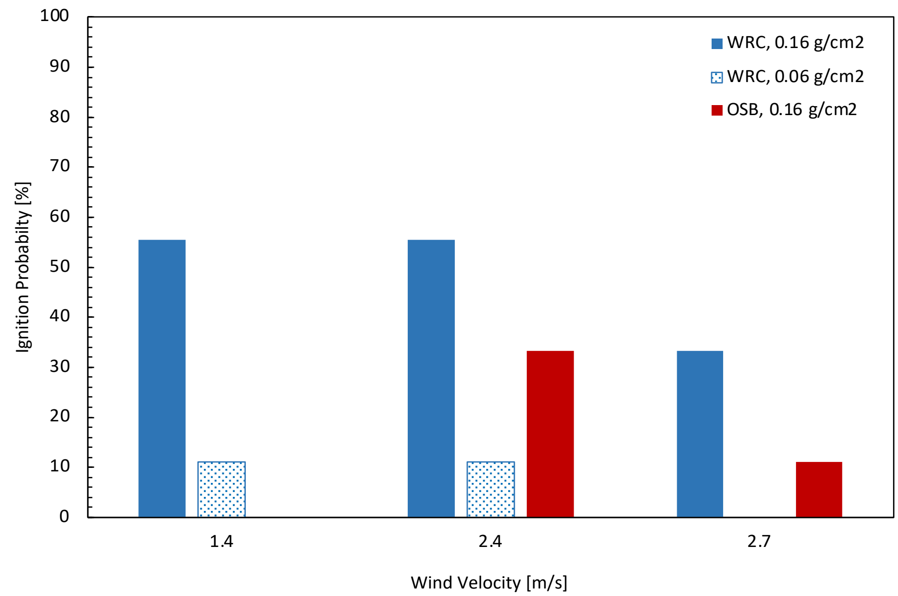

Fig. 10. Phase 1 ignition probability, taken as the number of ignitions that occurred over the course of 9 tests, for WRC and OSB under all 5 testing conditions. Absence of any bars indicates that there were no ignition incidents under that condition.

The conditions with the highest number of ignitions were the larger firebrand pile deposited on WRC at 1.4 m s^{-1} and 2.4 m s^{-1}, each resulting in five ignitions out of the nine tests conducted. All of the rest of the conditions on either material had three or less ignition events; this is important context to the burn duration and time to ignition of the surface ignitions detailed in Figure 10, especially in regard to the large variations shown as two standard deviations of the mean. The larger firebrand pile size on WRC was the only configuration that had multiple ignitions at various wind speeds. Here, the burn duration decreases with an increasing forced air flow. At the only condition where WRC and OSB each had multiple ignitions, the larger firebrand pile at 2.4 m s^{-1}, the two materials have comparable burn times, though OSB required more time to achieve flaming ignition. This is likely due to the much higher density of OSB, which is nearly twice that of WRC, necessitating a longer time of exposure to the radiation from the firebrand pile to pyrolyze enough combustible gases to flame. In all other conditions, if ignition did occur, there was only one event out of nine, which is not sufficient to qualitatively determine clear trends between the two materials due to the inherent randomness of each ignition event as demonstrated by the large variations present in the conditions that resulted in more than one ignition.

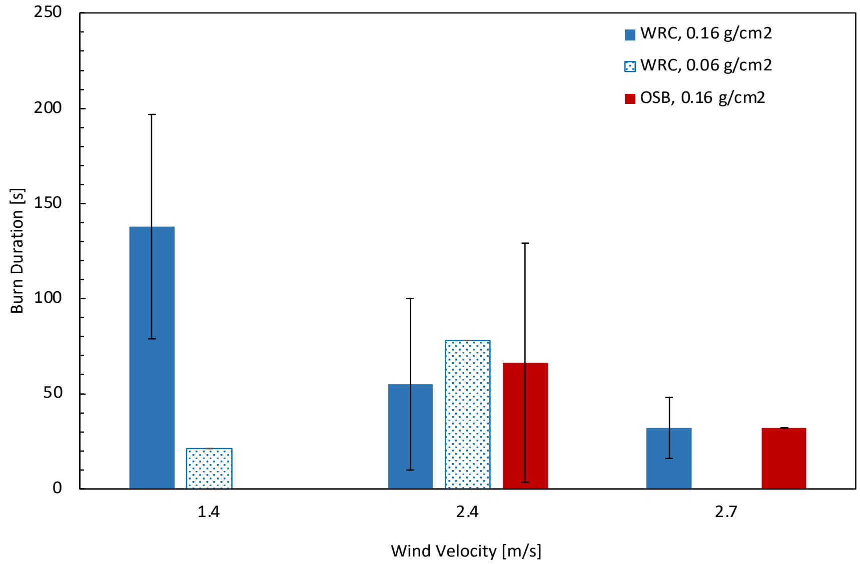

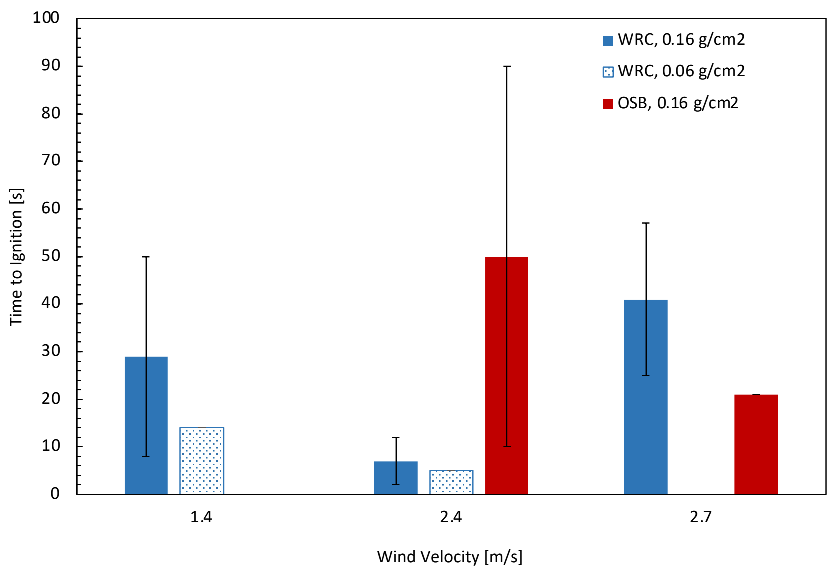

Fig. 11. Phase 1 burn duration and time to ignition of surface ignition occurrences, shown as the average of all ignitions that occurred over the course of 9 tests for each condition, for WRC and OSB under all 5 testing conditions. Error bars shown as two standard deviations of the mean. Absence of any bars indicates that there were no ignition incidents under that condition.

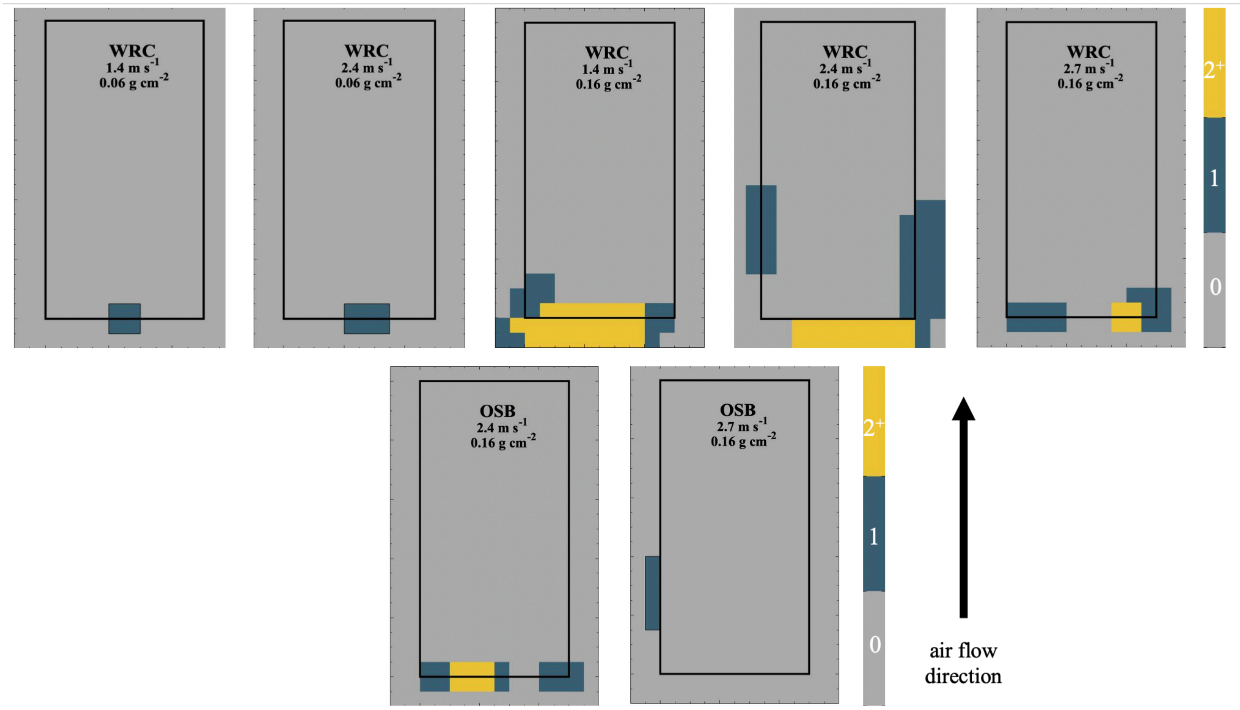

Fig. 12. Surface ignition locations on WRC and OSB for Phase 1. Grey indicates that no surface ignitions were observed in that location, blue shading indicates that exactly one ignition event was located in that area, and yellow shading indicates that two or more surface ignitions were located in that area. The solid line indicates the location of the firebrand deposition area. Note the direction of airflow through the wind tunnel.

Subsection 4.1.2: Back Surface Temperature Measurements

As detailed in an earlier section, three-zone back surface temperature measurements were conducted on each substrate at each of the five conditions. These profiles are shown in Figures 13-15.

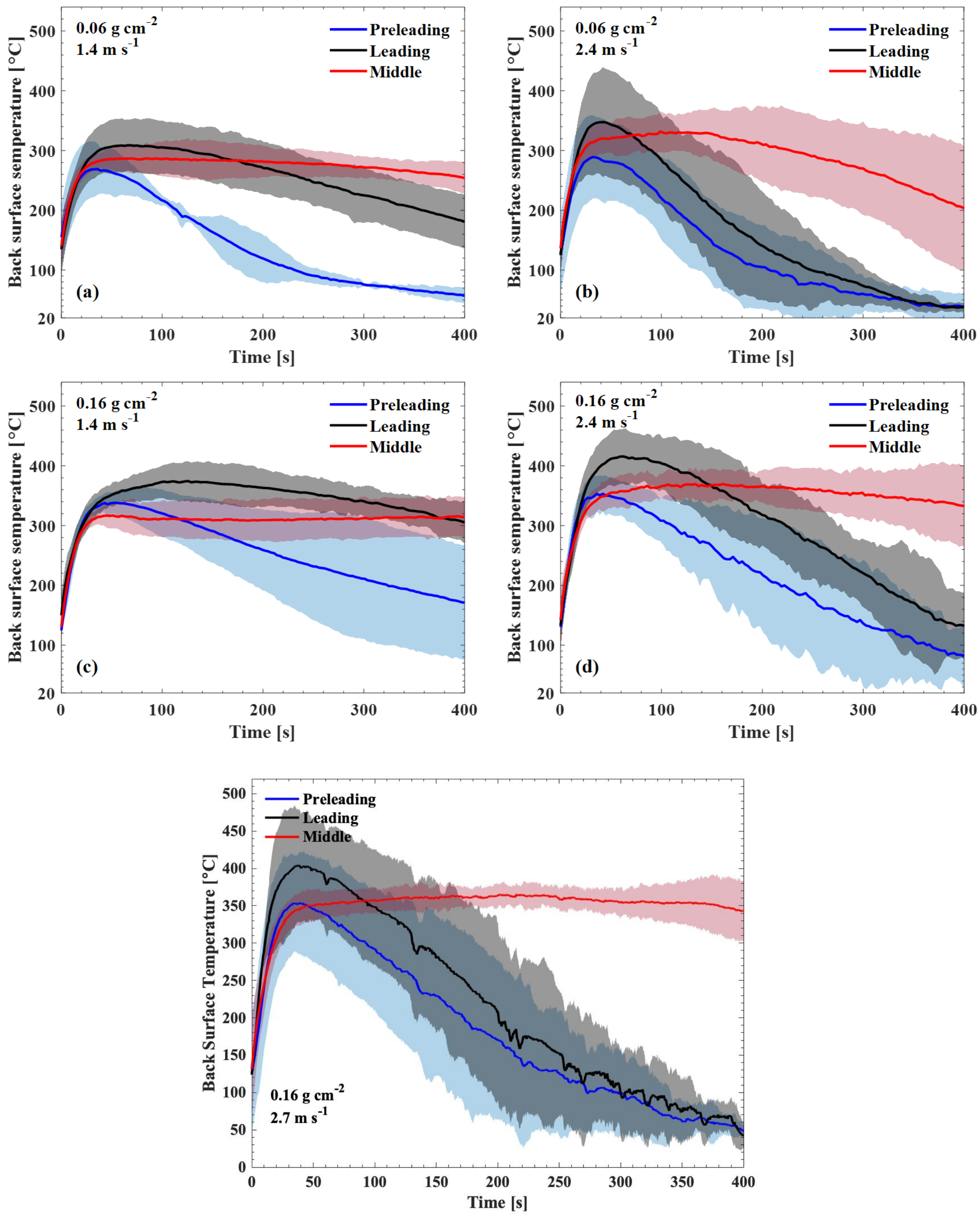

Fig. 13. Back surface temperature measurement profiles for each of the zones identified in Fig. 6 for the Phase 1 Kaowool PM tests. The shaded area represents variation, or two standard deviations.

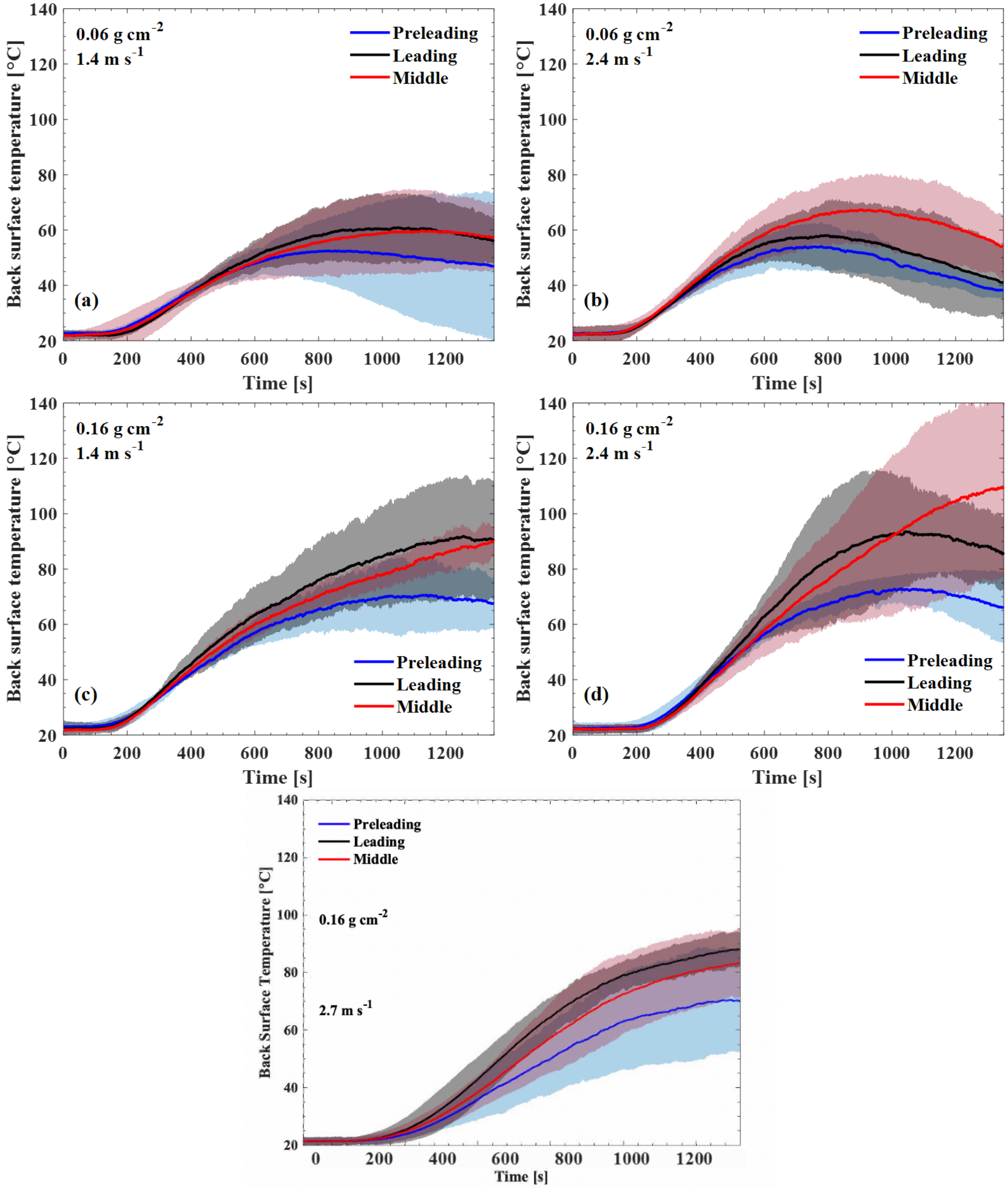

Fig. 14. Back surface temperature measurement profiles for each of the zones identified in Fig. 6 for the Phase 1 WRC tests. The shaded area represents variation, or two standard deviations.

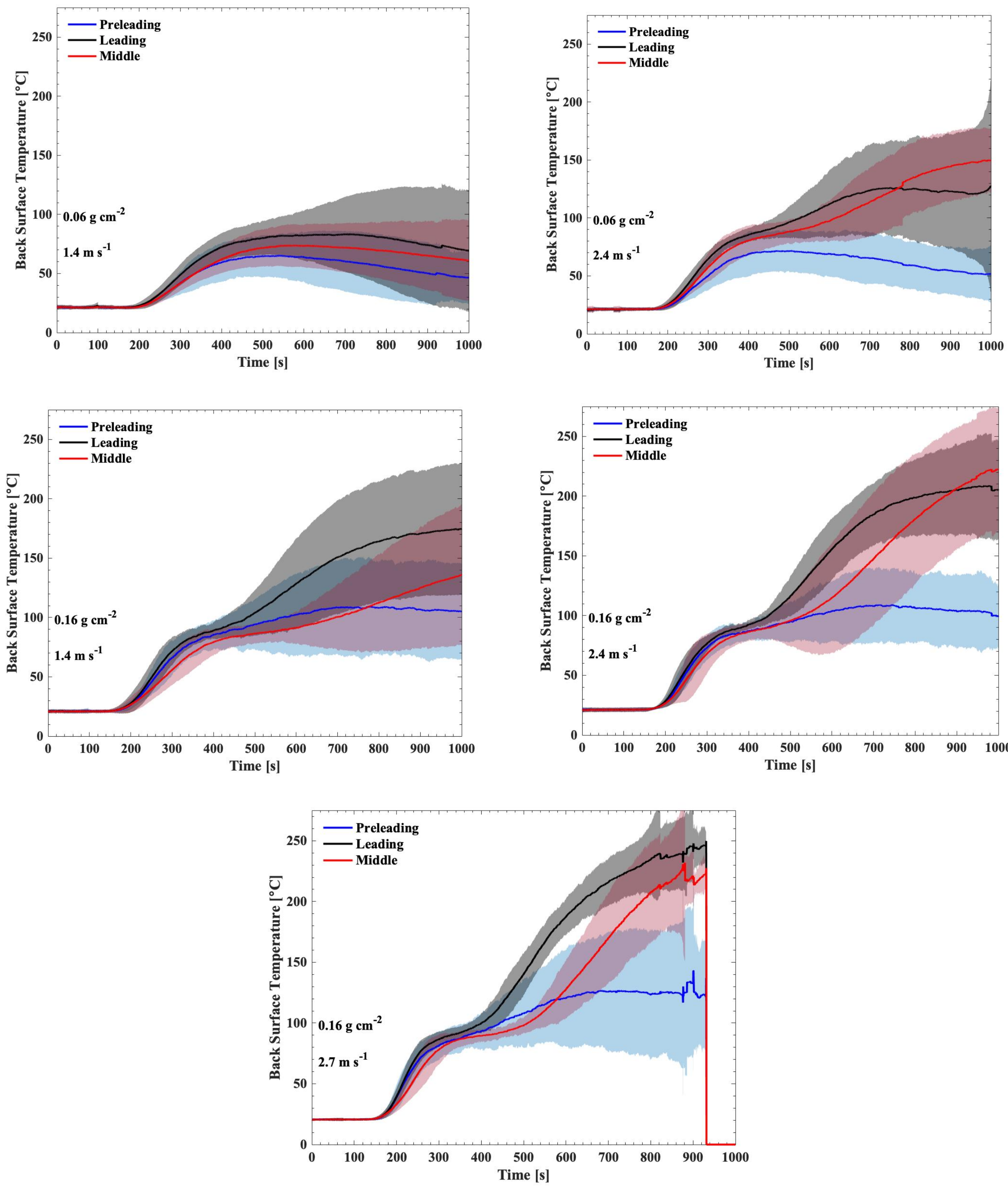

Fig. 15. Back surface temperature measurement profiles for each of the zones identified in Fig. 6 for the Phase 1 OSB tests. The shaded area represents variation, or two standard deviations.

The duration shown on the x-axis of each figure was chosen to capture the behavior of the piles in time; the Kaowool PM profiles saw an almost immediate rise in temperature, as the samples were relatively thin, while the WRC and OSB boards were denser and physically thicker, and thus saw a delay in the initial rise is temperature at the back surface. As a reminder, the leading and middle zones were completely covered by firebrands in all scenarios, and the preleading zone had 0.5 cm overlap with the firebrand pile and measured 1 cm in front of it.

There were certain trends present for all three materials. In all cases, the highest temperatures were measured in the leading zone, which was directly exposed to the forced air flow throughout the test's duration, and thus consistently oxidized the firebrands in this zone. Additionally, temperatures in all zones increased with an increasing firebrand pile size exposed to the same velocity. The temperatures of all zones between profiles of the same firebrand pile size increased until 2.4 m s^{-1}, after which there is a slight decrease. This is attributed to the fact that an increased flow increases the convective cooling applied to the firebrand pile. This effect competes with the increased firebrand pile burning rate that is present with an increased airflow, which would lead to higher temperature measurements.

The Kaowool PM and WRC profiles all have the same general trend: a rise in temperature followed by a decrease. The rise of Kaowool PM is much steeper than that of WRC due to the thinness of the board being able to capture the increase in firebrand burning intensity right at the onset of forced flow exposure, and both experience gradual declining profiles as the firebrand piles are consumed. OSB, while there is a delay in which after deposition the back surface of the board takes to heat up, it rises more quickly than WRC, likely due to its thinner dimensions. Interestingly, after the initial temperature increase on OSB, there follows a subsequent rise in all but the 1.4 m s^{-1} with the 0.06 g cm^{-2} firebrand pile coverage density. The inconsistent behavior at the end of the higher airflow OSB tests was observed because several of these boards developed holes that burned through the substrate, affecting the measurements able to be read by the IR camera.

Looking at the initial rises in temperature, the temperatures correlating to surface ignition events, the initial heating rates in °C s^{-1} were calculated by finding the first instance that the temperature at the back surface reached 30 °C and finding the rise in temperature over time for the next 80 s, a period of time that was within the linear region of the rise in temperature for all zones under all conditions. An example of this correlation is shown in Figure 16 for the average profile of the preleading zone of the 0.16 g cm^{-2} firebrand pile at 2.4 m s^{-1}, though the same procedure was conducted for all zones under all conditions. The results from the linear correlations describe the initial heating rates for each zone, seen in Figures 17 and 18.

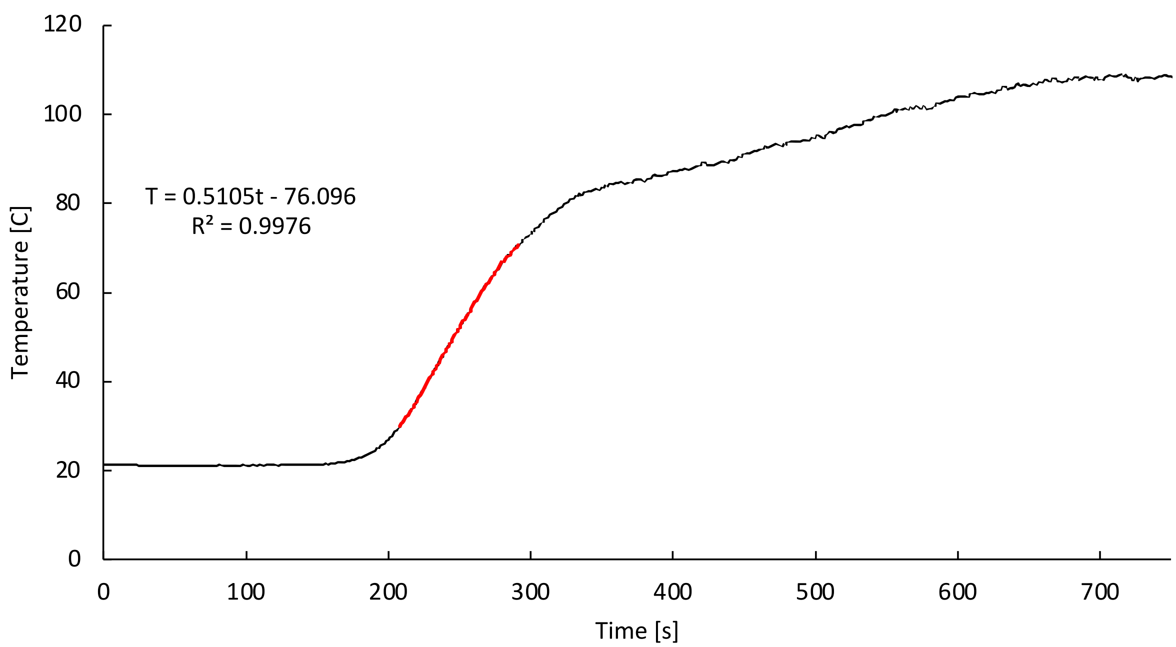

Fig. 16. Average profile of the preleading zone of a 0.16 g cm^{-2}, 2.4 m s^{-1} test on OSB. The red shows the initial rise in temperature, used to determine the average heating rate for this condition. The equation and R^2 value shown correspond to the red line.

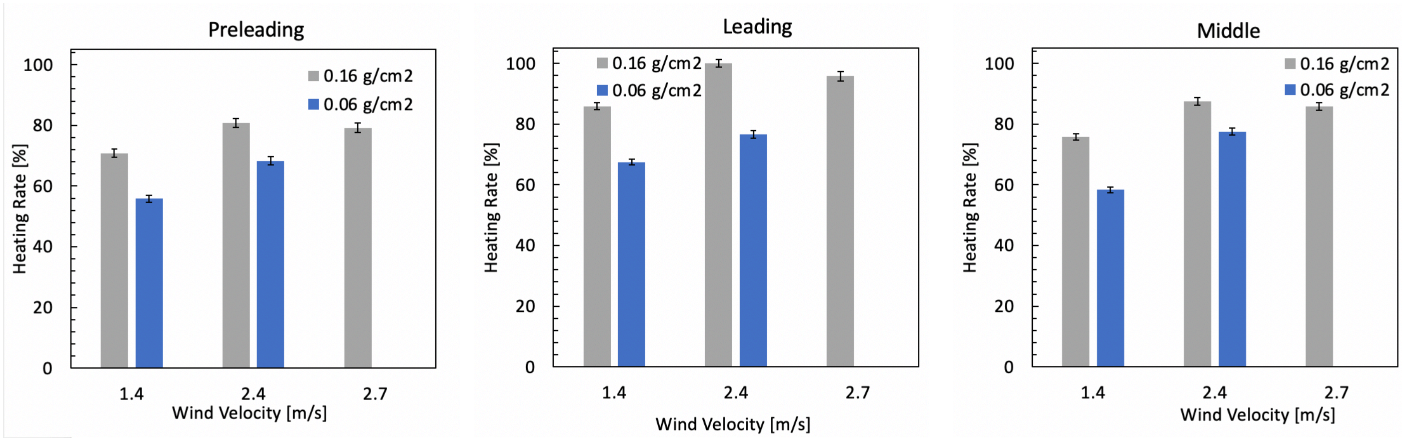

Fig. 17. Heating rates for each of the zones identified in Fig. 6 for the Phase 1 WRC tests, depicted as the average of 9 tests per condition and normalized by the maximum value. The error bars shown are two standard deviations of the mean.

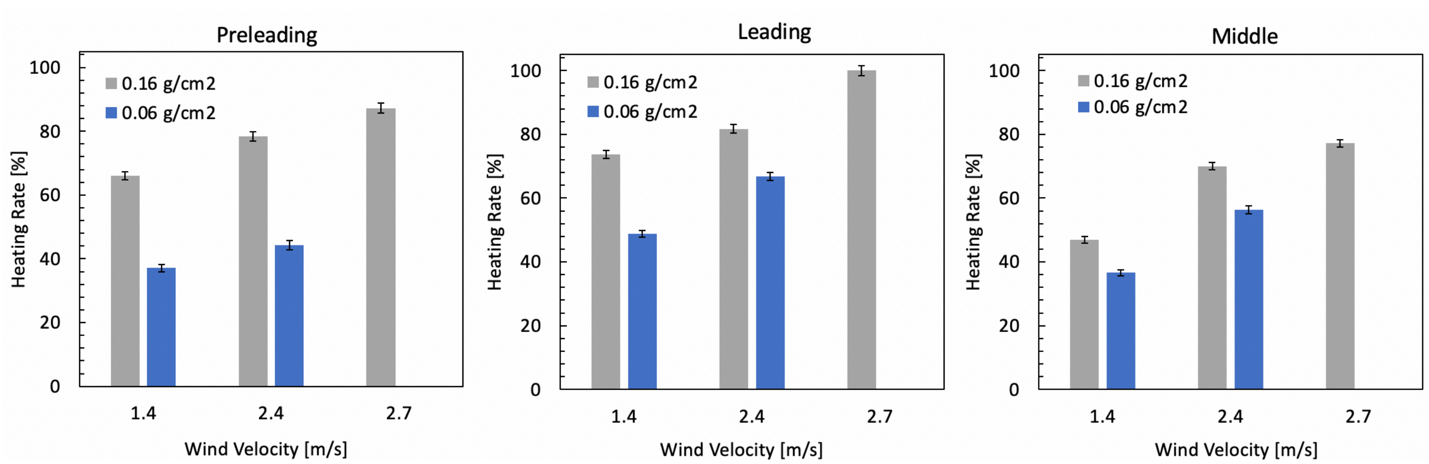

Fig. 18. Heating rates for each of the zones identified in Fig. 6 for the Phase 1 OSB tests, depicted as the average of 9 tests per condition and normalized by the maximum value. The error bars shown are two standard deviations of the mean.

The samples of WRC and OSB used have different thicknesses, and such the heating rates found from the back surface temperature readings during the initial temperature rise after firebrand deposition would not be a one-to-one comparison. Instead, all measurements of heating rate, found in °C s^{-1} from the profiles such as the one shown in Figure 16, were normalized by the greatest heating rate found per material, shown as 100% on Figures 17 and 18. For WRC, this value was greatest for the leading zone under the 2.4 m s^{-1} airflow and 0.16 g cm^{-2} firebrand pile coverage density. For OSB, this was instead for the leading zone under the 2.7 m s^{-1} airflow and 0.16 g cm^{-2} firebrand pile coverage density. For both materials, the leading zones had higher heating rates than the other two zones no matter the testing condition. This is the zone directly underneath the firebrand pile.

Subsection 4.1.3: Gas Analyzer Measurements

The first quantity examined using the CO and CO_2 volumetric percentage outputs from the gas analyzer is the total heat release rate profiles of each substrate under each condition. These are shown in Figure 19. The profiles from the tests conducted on Kaowool PM are discussed as the burning characteristics of the isolated firebrand pile for the inert substrate is assumed to not contribute to combustion for all conditions.

There were certain trends present in the total HRR profiles between conditions no matter the material. With the same firebrand pile coverage density, HRR increased with an increasing wind velocity until 2.4 m s^{-1}, after which there was a decrease due to the effects of convective cooling introduced with subsequent greater values of velocity. Additionally, at the same air flow velocity, there is a greater HRR profile with an increasing firebrand pile coverage density. They all follow the same shape; there is an initial peak soon after firebrand pile deposition followed by a gradual decrease. This rapid increase is likely caused by an increase in the burning intensity of the firebrand piles when first exposed to the forced flow through the tunnel, and subsequent decrease as the firebrands decompose, forming ash as they do so, further inhibiting the combustion process and decreasing the HRR, as seen in Figure 19

The peak HRR of each material under each condition is shown in Figure 20. Here, the value reported is the average of the 4 s surrounding the peak temperature reading, and the variation is two standard deviations of the values within this time range. For the 0.06 g cm^{-2} firebrand pile coverage densities, the peak of the firebrand piles on Kaowool PM are the largest, followed by WRC then OSB for both wind velocities conducted. For the larger piles, Kaowool PM has the highest peak for the two lower wind velocity, but this trend changes for the 2.7 m s^{-1} profile in which OSB and WRC are comparable and both above the inert substrate.

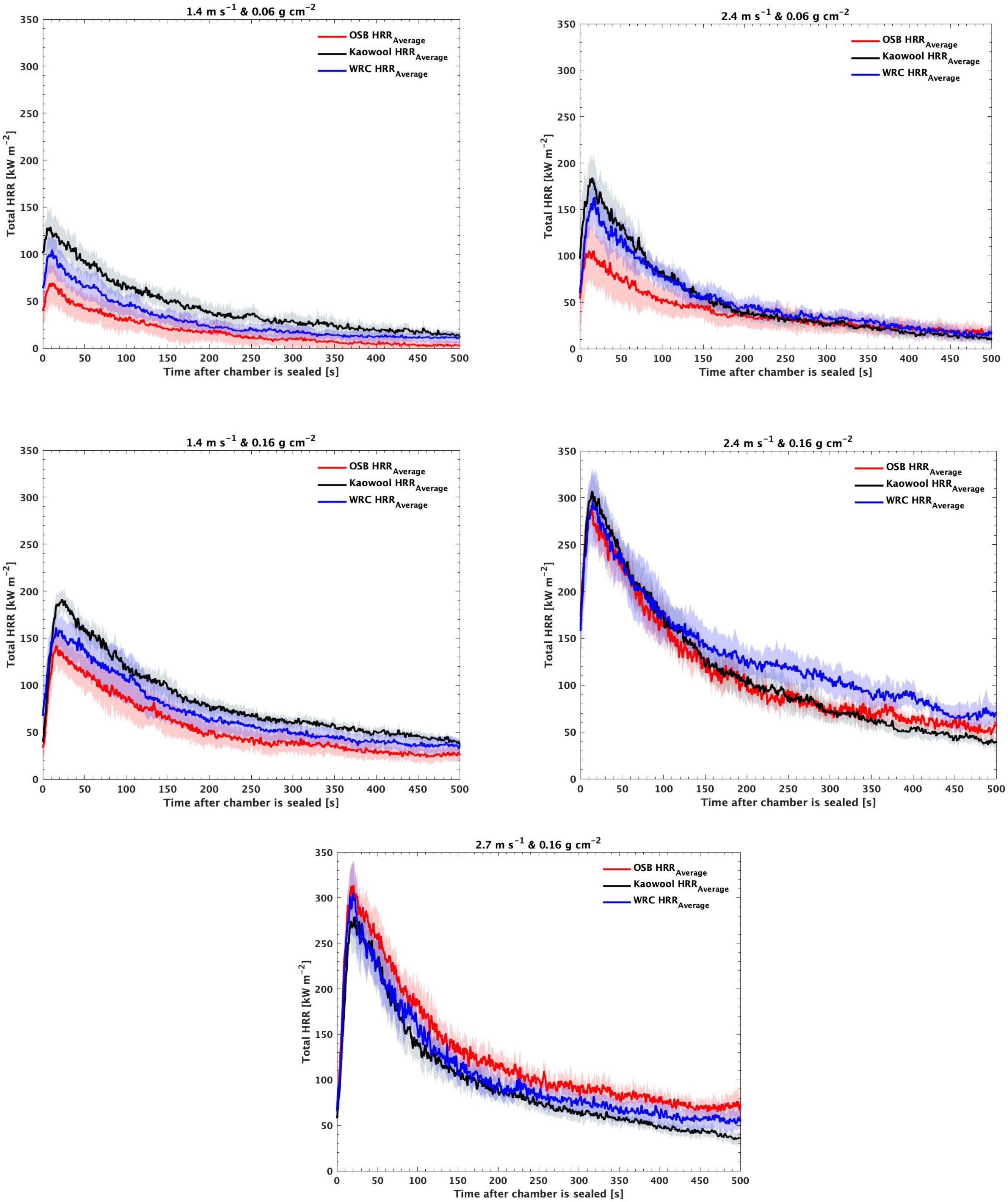

Fig. 19. The average total HRR profiles for all three materials under all five conditions for Phase 1. Each profile is the average of 9 tests. The variation shown in the shaded regions are two standard deviations.

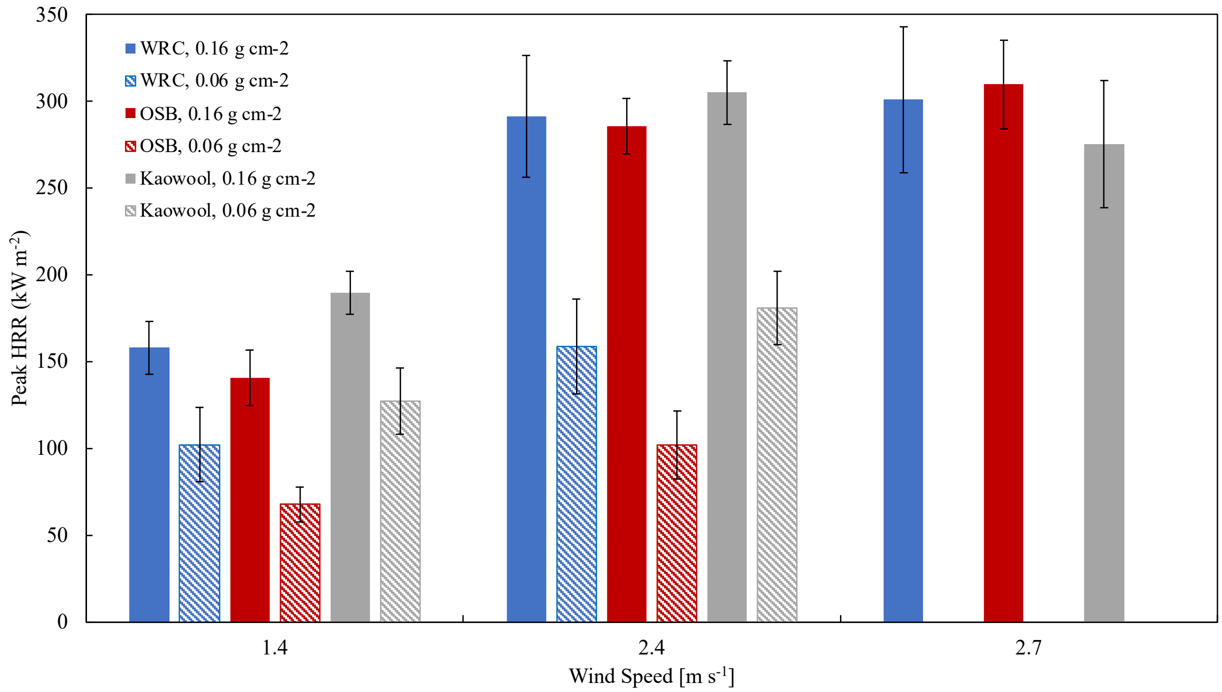

Fig. 20. The average peak HRR for all three materials under all five conditions for Phase 1. Each quantity is the average of 9 tests. The variation was taken as two standard deviations of the mean.

The contribution of each board to the total HRR profiles were also considered and shown in Figure 21 These were found by examining the difference between the HRR behavior of the firebrand pile and that of each of the combustible boards. Thus, when the profile becomes positive, it indicates that the board itself is involved in combustion and contributing to HRR at sufficiently high level to compensate for a reduction in the rate of firebrand burning caused by heat losses to the board. The variations shown, two standard deviations, are larger for WRC due to the number of surface ignitions on this material. The ignitions had a large impact on HRR, and did not also occur in the same timeframe after deposition, shown in the time to ignition graph of Figure 10. For each profile, the initial value is negative or near zero. This shows that the boards initially act as a heat sink brought on by the higher thermal inertia of either material compared to Kaowool PM, resulting in heat losses from the pile. For all profiles except the 2.7 m s^{-1} case, these profiles trend upward with time. Only the 2.4 m s^{-1} and the 2.7 m s^{-1} conditions result in positive values from either WRC or OSB. Furthermore, the 2.7 m s^{-1} profiles have an initial rise in contribution, and then maintain a semi-steady positive value for the rest of the duration shown. Overall, the order of magnitude of the contribution of either board is significantly lower than the overall HRR profile throughout the test duration, even when it is positive. Furthermore, WRC contribution to HRR is slightly - within uncertainties - but somewhat systematically higher than that of OSB. Shown in Figures 17 and 18, the OSB initial heating rates continue to rise as the airflow increases, reaching a maximum at 2.7 m s^{-1}. In contrast, the WRC initial heating rate reaches a peak at 2.4 m s^{-1} and decreases with an increasing airflow. This could in part explain the discrepancy between the 2.7 m s^{-1} testing condition and why the trends between WRC and OSB that are consistent between the 1.4 m s^{-1} and 2.4 m s^{-1} airflow velocity tests differ at this airflow.

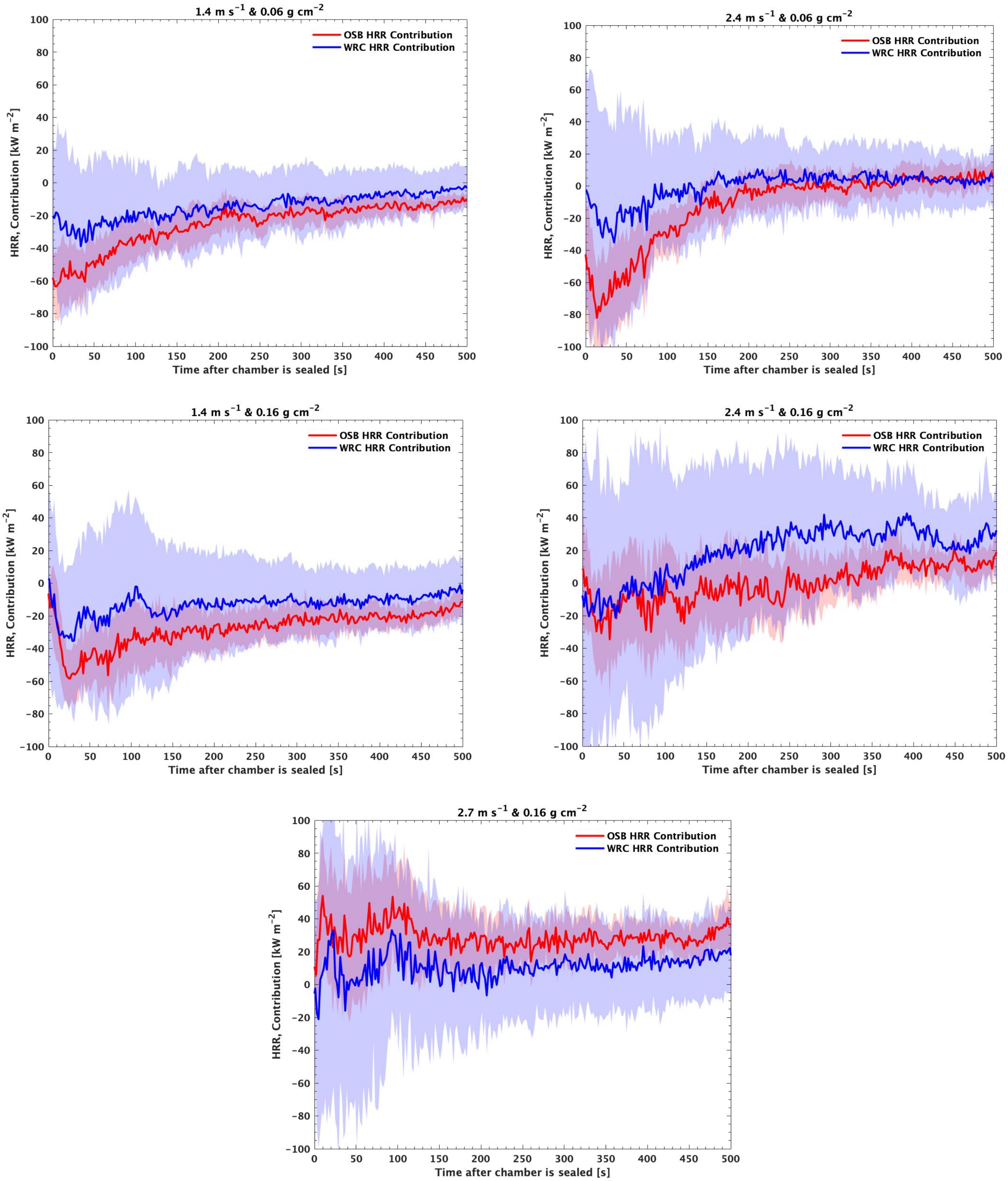

Fig. 21. The average board contribution to HRR profiles for WRC and OSB under all five conditions for Phase 1. Each profile is the average of 9 tests. The variation shown in the shaded regions are two standard deviations of the mean.

The final quality considered from the gas analyzer outputs of Phase 1 is the MCE of each material, shown in Figure 22. The Kaowool PM mean MCE profiles were found to be effectively constant for the duration of the tests indicating no change in the mode of combustion, all containing an MCE of 0.81 ± 0.02. Because the MCE values differed little with time on Kaowool PM, an average value for each set of conditions was calculated using the first 400 s of the corresponding mean MCE profile. At the beginning of all tests, the values are consistently within the in-between regime of flaming and smoldering combustion for all materials because they are neither greater than 0.9 nor between 0.65-0.8. For the larger piles, the same is also true; there appears to be hybrid combustion. Throughout these tests, the MCEs trend downward regardless of wind velocity. Additionally, the MCE of the boards are reliably below that of the firebrands on Kaowool PM, where even when isolated, they are neither decidedly flaming nor smoldering combustion. Thus, this decrease denotes the involvement of the substrate in combustion, and so it can be said that the presence of combustible lignocellulosic substrate shifts overall combustion toward smoldering. The magnitude of the shift does not appear to depend on the exact properties of this lignocellulosic substrate because the same trends occur for both WRC and OSB. As such, the involvement of the boards in combustion is corroborated by the contribution to HRR profiles that show about then the boards begin to combust. Finally, as seen in Figure 22, increasing wind speed or pile coverage density slightly increases this shift.

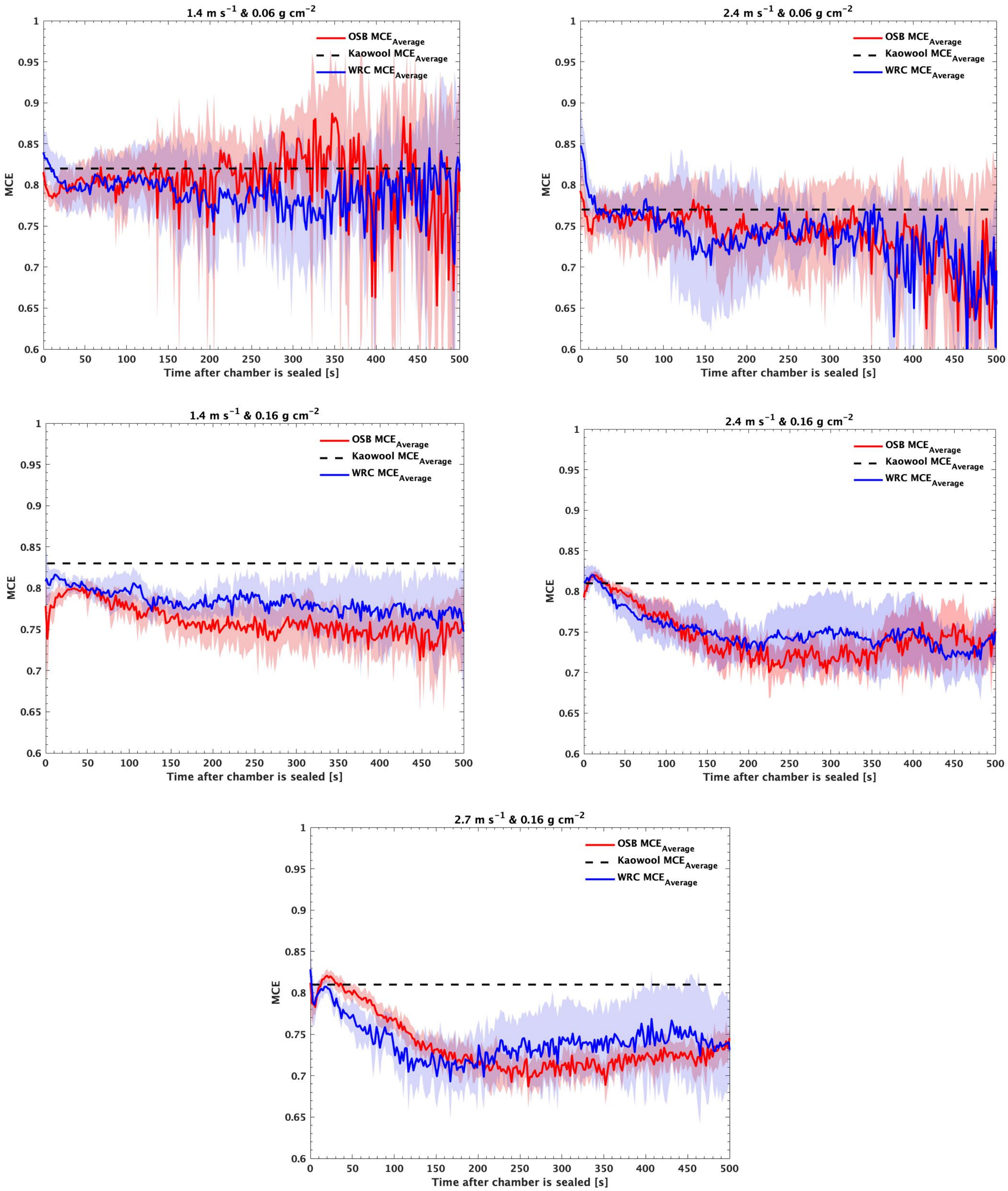

Fig. 22. The average MCE profiles for all three materials under all five conditions for Phase 1. Each profile is the average of 9 tests. The variation shown in the shaded regions are two standard deviations of the mean.

Section 4.2: Phase 2

Subsection 4.1.1: Surface Ignition Characterization

For both materials, the change in orientation of the firebrand pile resulted in an increased percentage of surface ignitions compared to the 5 cm leading edge case. As stated in Section 2.4.2, only the 2.4 m s^{-1} wind velocity with a 0.16 g cm^{-2} firebrand pile coverage density was considered for these tests. Similar to Phase 1, the probability, location, burn duration, and time of ignition for the surface ignition events on both WRC and OSB under this condition were examined and summarized in Figures 23-25. Here, they are compared to the same test conditions, yet smaller leading edge size, from Phase 1.

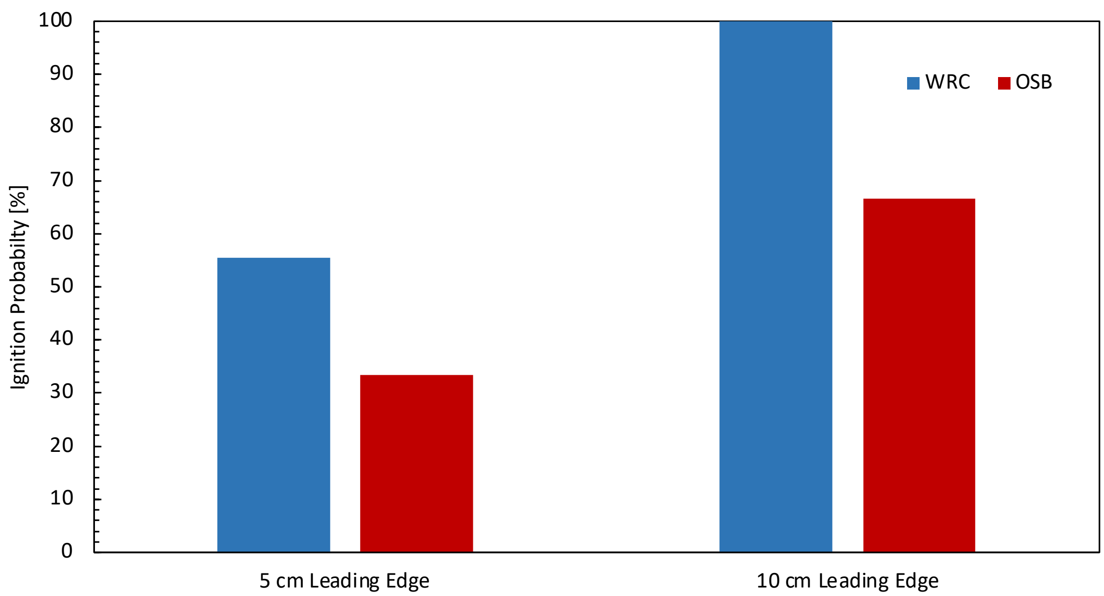

Fig. 23. Phase 2 ignition probability, taken as the number of ignitions that occurred over the course of 9 tests, for WRC and OSB, compared to Phase 1 ignition probability seen in Figure 11. All tests were conducted using an airflow velocity of 2.4 m s^{-1} and a firebrand pile coverage density of 0.16 g cm^{-2}.

For both woods, the ignition probability significantly increased from the Phase 1 tests. Similar to Phase 1, the overwhelming majority of tests had only one ignition event occurred per test when there was a surface ignition observed. There was one case of a reignition event with a WRC sample, in which there were two distinct surface ignitions during the same test. In order to keep the comparison between the two woods consistent, for all figures in this section, only the first ignition event was considered when discussing the ignition probability, location of ignitions, average burn duration, and average time to ignition. This being said, WRC saw an ignition event for every test of the 9. OSB increased from having an ignition in 3 out of 9 tests to 6, or a 50% increase. This suggests that the orientation of the pile has a significant impact on the probability of surface ignitions occurring, no matter the substrate. This is likely due to the increased area of the board that receives the greatest magnitude of heat feedback from the firebrand pile to the surface because the leading edge length of the pile is twice that of the previous testing conditions. Simply put, there is a greater area of the board in which ignition may occur, and thus the ignition probability increases. Additionally, OSB still has a lower probability of ignition than WRC under the same conditions. Though the ignition probability increased for both materials, the location of ignitions remained similar, shown in Figure 24. All ignitions originated in the preleading zone, though some followed the shape of the firebrand pile and the flames present were able to anchor to the side of the pile as well. This is the zone that receives the greatest radiative effects from the firebrand pile and is inhibited by the presence of the firebrands themselves, and thus able to pyrolyze and still receive sufficient airflow to maintain flaming combustion.

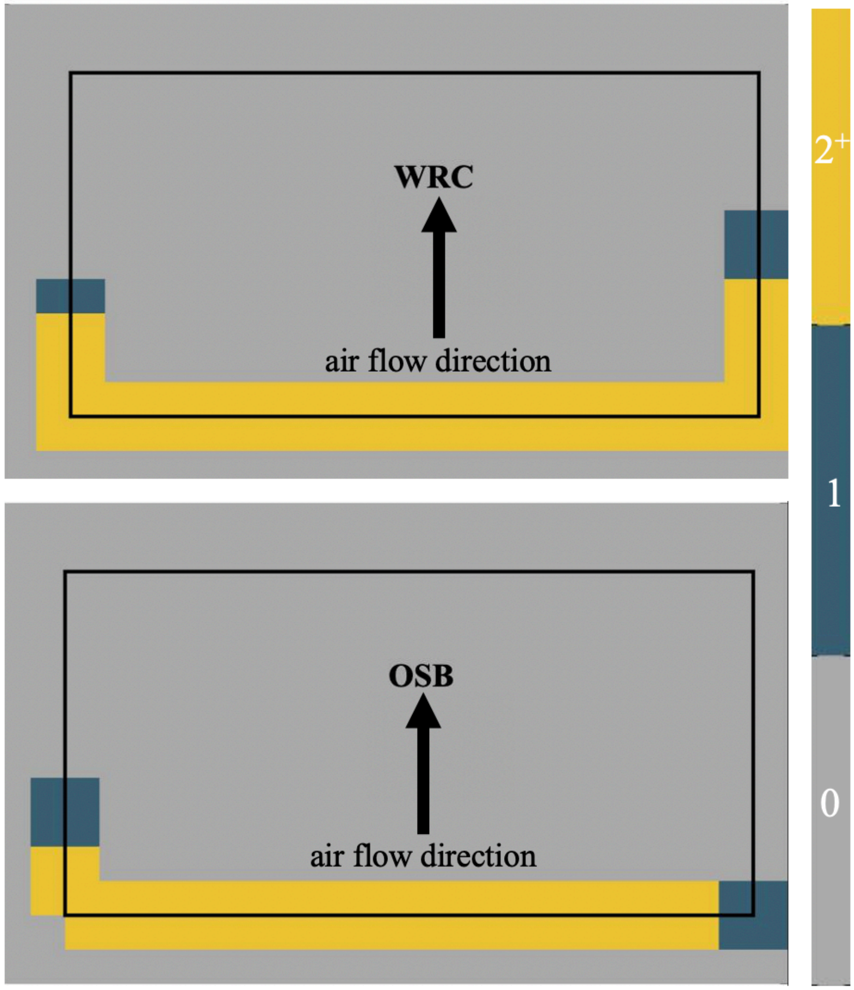

Fig. 24. Surface ignition locations on WRC and OSB for Phase 2, which had an airflow velocity of 2.4 m s^{-1} and a firebrand pile coverage density of 0.16 g cm^{-2}. Grey indicates that no surface ignitions were observed in that location, blue shading indicates that exactly one ignition event was located in that area, and yellow shading indicates that two or more surface ignitions were located in that area. The solid line indicates the location of the firebrand deposition area. Note the direction of airflow through the wind tunnel.

Seen in Figure 25, there may be a difference in the burn duration of these ignition events based on the length of the leading edge of the pile for WRC; the mean duration on average is longer but within the error bars shown. Between leading edge lengths for the same material, there is a slightly longer duration for WRC, but OSB is completely within its variation, shown for all bars as two standard deviations of the mean. Similarly, the difference in leading edge lengths does not seem to have a significant impact on the time to ignition of the substrate, and most occur within the first minute after deposition. Consistently between the leading edge lengths, WRC ignites sooner than OSB, likely due to the thermal response parameter of each material, tied to the fact that OSB has nearly double the density of WRC. Overall, the ignition events are stochastic, and there is a relatively low number of ignitions per condition and substrate to compare, leading to large variations in all quantities discussed.

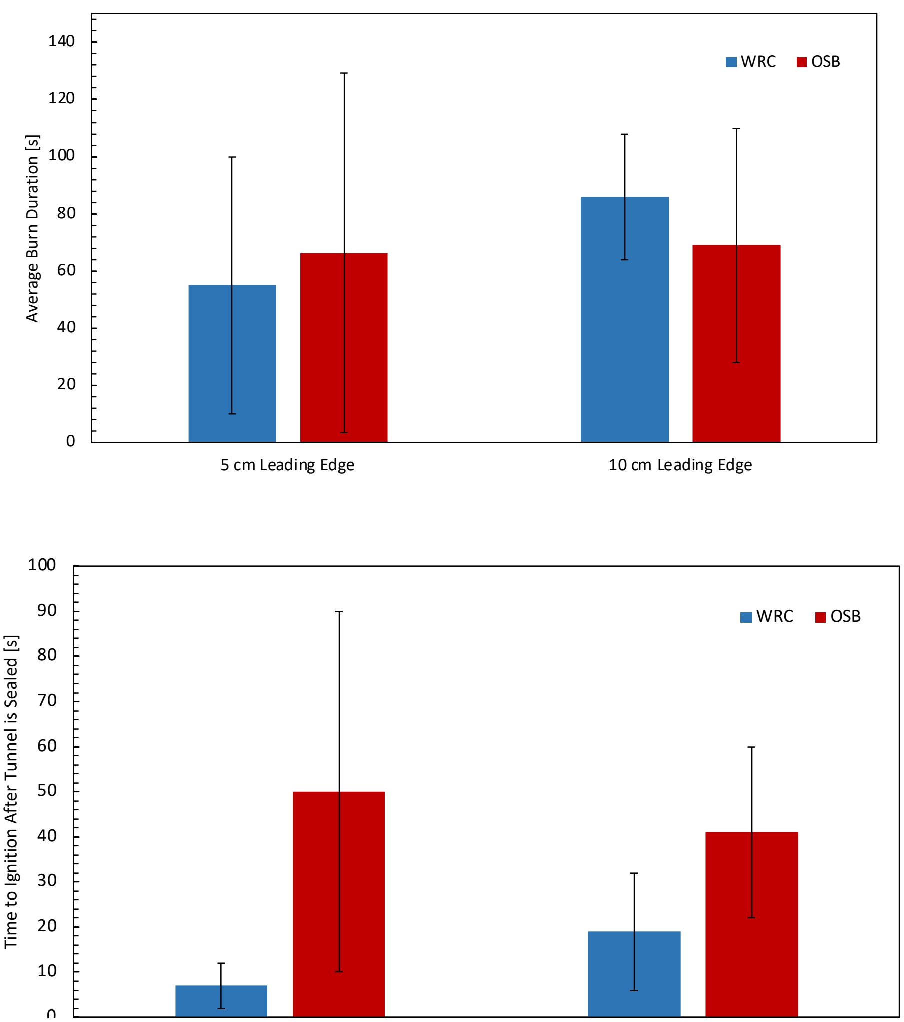

Fig. 25. Phase 2 burn duration and time to ignition for WRC and OSB, reported as the mean value of each ignition occurrence across 9 tests, compared to Phase 1 quantities seen in Figure 10. The errors bars shown are two standard deviations of the mean.

Subsection 4.1.2: Back Surface Temperature Measurements

The temperature of the back surface was taken only for the inert substrate. This was done to determine any changes in behavior in the decomposition process of the firebrand pile due to the change in orientation. As the majority of surface ignitions occurred in the preleading zone for both materials, this was the only zone analyzed for this phase of testing. As seen in Figure 26, there is a change in mean temperature behavior between the two lengths of the leading edge. The initial heating rates are comparable, as is the time of the peak temperature value with respect to the time of deposition. Here, there is an increase in the peak value achieved. This is attributed to the fact that there are more firebrands available to oxidize at the leading edge, the interface of the pile and the forced flow. This leads to an increase in the radiation effects at the surface of the material, which results in higher temperatures being read at the back surface. Additionally, there appears to be a slightly increased downward trend of the 10 cm pile temperatures in this zone over time, likely due to the increased rate of oxidation causing the firebrand pile to decompose faster and thus the leading edge of the pile to exit this zone comparatively sooner. However, it is of note that the two profiles are within one another's variation, shown as two standard deviations.

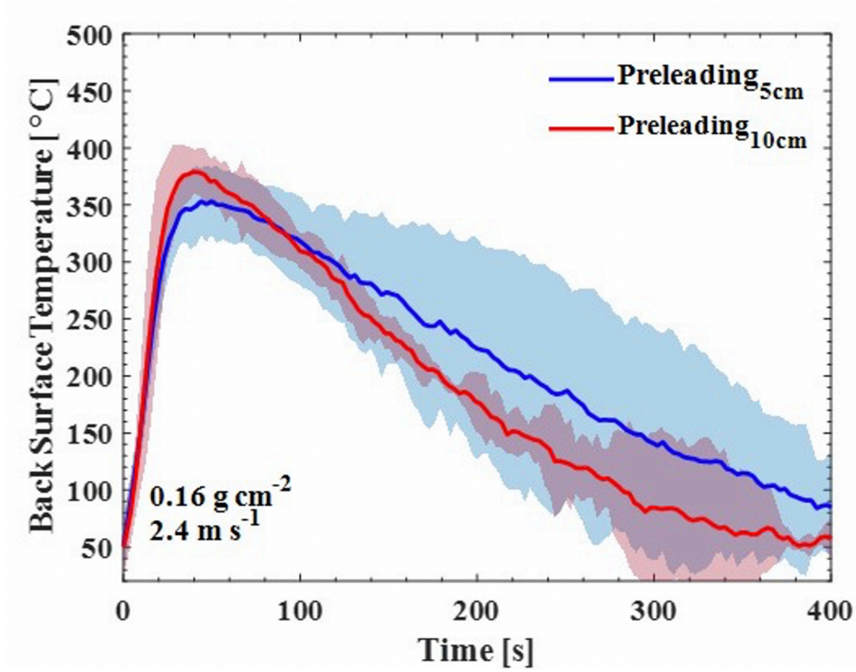

Fig. 26. Back surface temperature measurement profiles in the preleading zone, identified in Fig. 6, for the Phase 1 and Phase 2 Kaowool PM tests. The shaded area represents variation, or two standard deviations.

Subsection 4.1.3: Gas Analyzer Measurements

The first gas measurement analyzed was the HRR over the test duration. The time at which the peak values occur are within the same timeframe as the smaller leading edge length, which logically follows as the same trends appeared in the back surface temperature measurements. These peaks are seen in Figures 27 and 28. Consistently across the materials, the peak values increased with the new orientation. Whereas Kaowool PM had the greatest peak HRR value in Phase 1, WRC does in Phase 2.

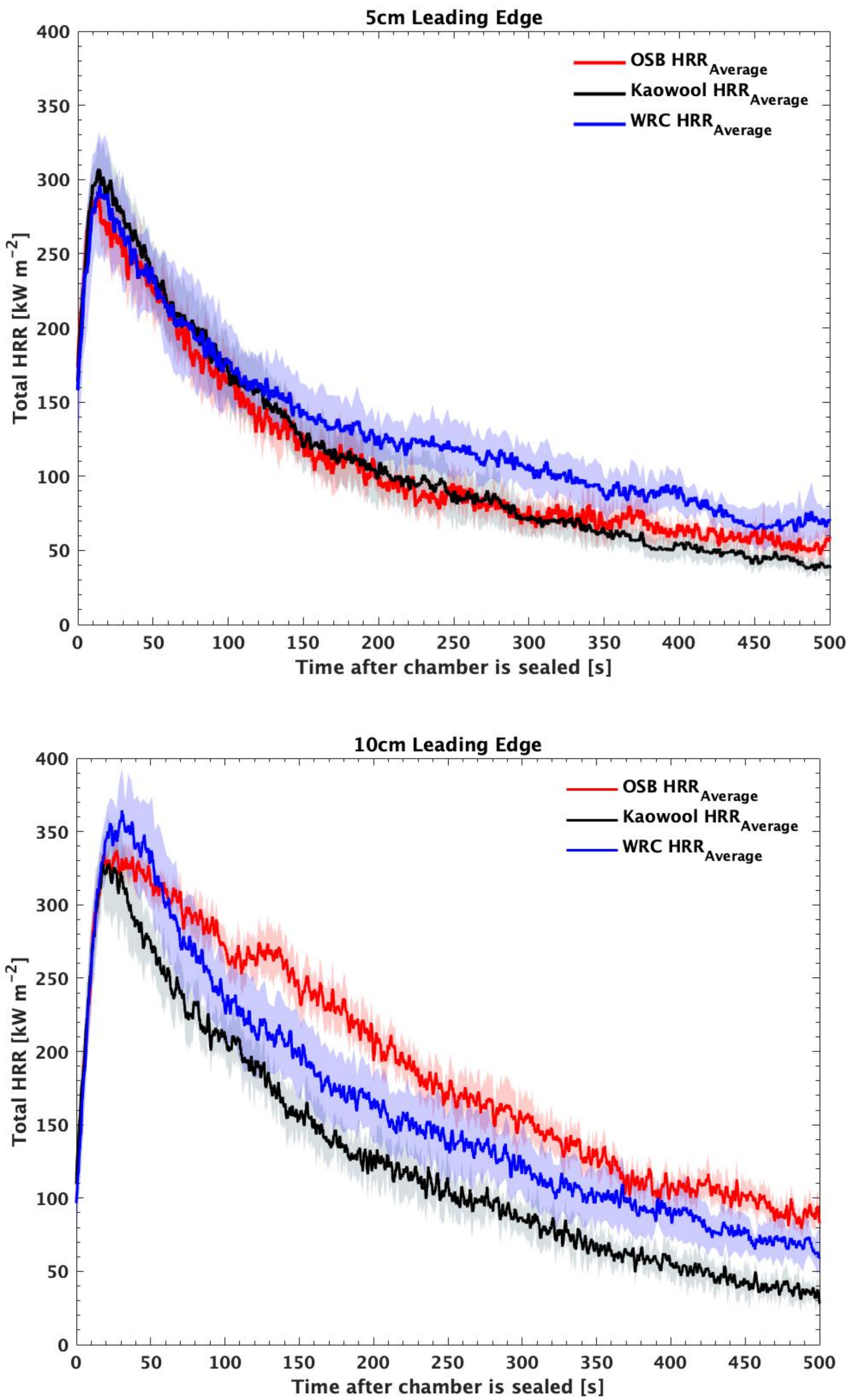

Fig. 27. The average total HRR profiles for all three materials for Phases 1 and 2. Each profile is the average of 9 tests. The variation shown in the shaded regions are two standard deviations.

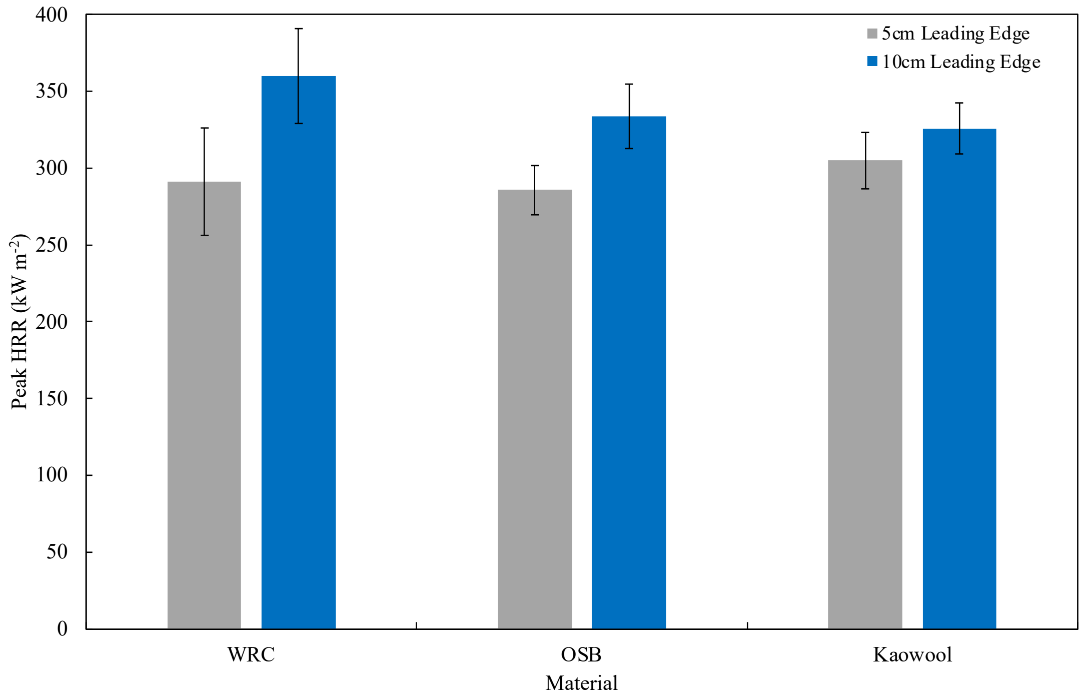

Fig. 28. A comparison of the average peak HRR for all three materials between Phases 1 and 2. Each quantity is the average of 9 tests. The variation was taken as two standard deviations of the mean.

Seen in Figure 28, not only are the peak values reached for the Phase 2 tests greater than that of Phase 1, the profiles over the test duration maintain this trend. Shown in Figure 27 by the increased temperature profile, there is an increased area of the board that receives a strong heat feedback from the pile, allowing for a greater involvement from the combustibles under the same wind tunnel conditions. Here, with the larger leading edge, there is also a greater differentiation between the three materials throughout the test. Additionally, WRC shares a similar trend with regard to its behavior between both deposition orientations. There is a period after deposition in which the board shares a similar profile to that of Kaowool PM, but then rises above. This change, where the combustible profile overcomes that of the inert substrate, indicates that the board itself has become involved in combustion, assuming that the firebrand pile decomposes similarly no matter the material of deposition. After this initial rise, WRC maintains its position above the inert profile. This occurs in both phases of testing, yet the transition occurs sooner after deposition in the larger firebrand pile leading edge length condition. In contrast, the average profile of OSB has a more drastic change due to the pile orientation. This is best explained through the board contribution to HRR, shown in Figure 29.

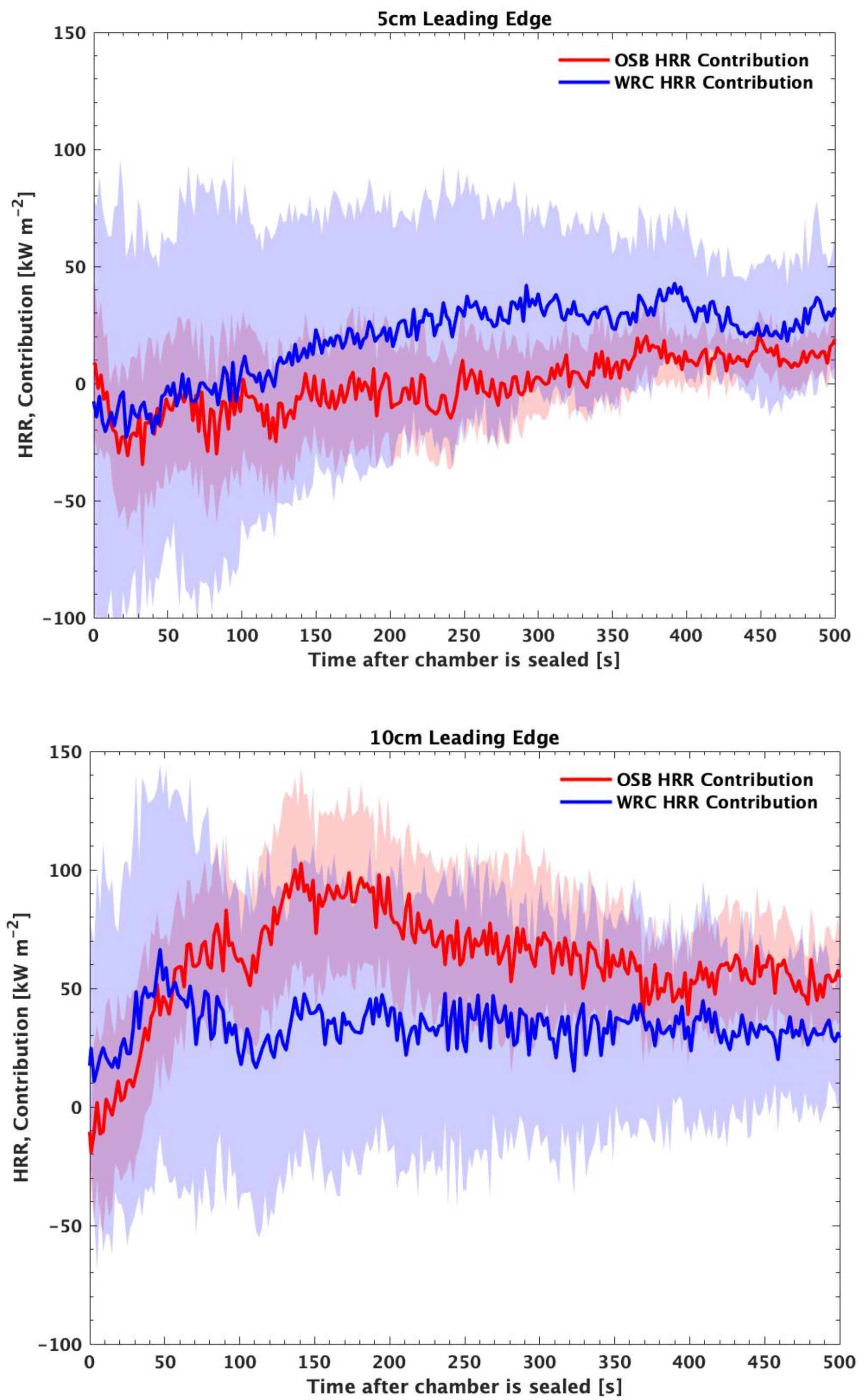

Fig. 29. A comparison of the average board contribution to HRR profiles for WRC and OSB between Phases 1 and 2. Each profile is the average of 9 tests. The variation shown in the shaded regions are two standard deviations.

With the shorter leading edge, the OSB board does not contribute greatly to the overall HRR of combustion, shown by its total HRR profile closely following that of Kaowool PM, even initially falling below. Even when it does have a positive contribution, it is on the order of 20 kW m^{-2}; when considering the total HRR profile, it is the firebrand pile decomposition that dominates the combustion process. The same cannot be said for the 10 cm leading edge condition. At about 20 s, the OSB contribution to HRR crosses into positive values, showing that this is the point in which the board itself becomes involved in combustion. For both combustibles, this transition occurs sooner after deposition than in the Phase 1 tests. Additionally, WRC and OSB maintain this positive contribution for longer. For the 5 cm leading edge, there is a gradual rise to achieve a semi-steady positive value in the first 500 s, while for the longer edge, there is a rapid rise and gradual decrease to a larger, semi-steady positive value in the same range. Similar to Phase 1, there is a large variation due to the number of surface ignitions present during this condition for both woods. Additionally, the flames present in the 10 cm leading edge scenarios were observed to be larger and often wrapped along the width of the firebrand pile. In regard to contribution to HRR, there is a great overlap between the profiles, and it cannot be said that either wood has a systematically greater value.

Lastly for Phase 2, the MCE profiles between the pile orientations were compared. The 10 cm profiles confirm what was observed from the properties of the observed surface ignitions as well as the HRR profiles. Seen in Figure 30, the 10 cm profile is systematically higher than that of the 5 cm leading edge. Of note is that the Kaowool PM profile, indicative of the burning of the isolated firebrand pile, is lower under the same wind tunnel conditions. This change in orientation affected the method of burn for the firebrands, though remained in the same in-between range of smoldering and flaming combustion and cannot decidedly confirm a preference for either. The combustibles are similarly in the same range, yet show a more extreme difference between the two deposition orientations. The upward trend towards the flaming regime is supported by the increased number of surface ignitions of both materials as well as a visual observation that the flames present in the 10 cm leading edge condition were larger than that of the 5 cm scenarios. The surface ignitions for either wood generally occurred, with variation as shown in Figure 25, within the first 50 s after deposition. This is shown with the rise in MCE in this timeframe. In short, with a larger leading edge, both boards become more involved in combustion.

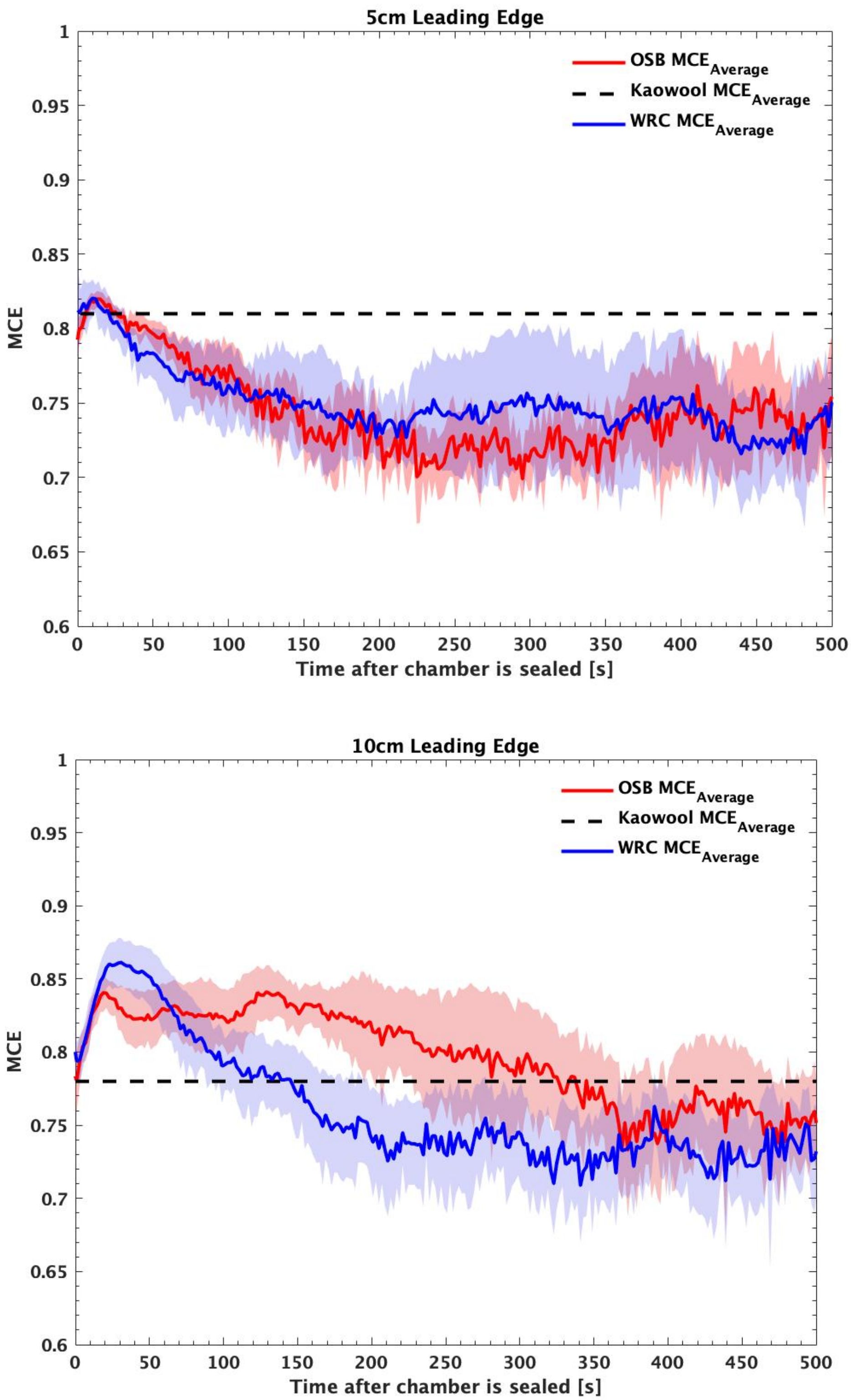

Fig. 30. A comparison of the average MCE profiles for all three materials between Phases 1 and 2. Each profile is the average of 9 tests. The variation shown in the shaded regions are two standard deviations.

Section 4.3: Phase 3

Subsection 4.1.1: Surface Ignition Characterization

While Phases 1 and 2 resulted in only a single surface ignition when ignitions occurred, Phase 3 saw a remarkable increase in the number of ignitions per test on both WRC and OSB. Though the 2.4 m s^{-1} air flow velocity resulted in the most ignitions for both woods during the continuous airflow conditions, during preliminary testing, the maximum wind velocity of 2.7 m s^{-1} resulted in the most surface ignitions on both materials when the wind was introduced intermittently. As more ignitions events occurred with the larger firebrand pile coverage density during the continuous wind tests, 0.16 g cm^{-2} was used for Phase 3 as well. The orientation of the pile is the same as Phase 1 in order to compare only the effects of the intermittent forced flow on combustion behavior. Airflow was introduced continuously for the first 60 s of the test in order to sufficiently oxidize the firebrand pile, and then was turned off for 10 s and back on again for 20 s intervals in order to observe the effects of intermittent flow. The 30 s cycles of turning off and reintroducing the forced airflow occurred for 420 s, resulting in a 480 s test duration (including the first 60 s of initial exposure). The timelines of representative tests for each wood are shown in Figures 31 and 32.

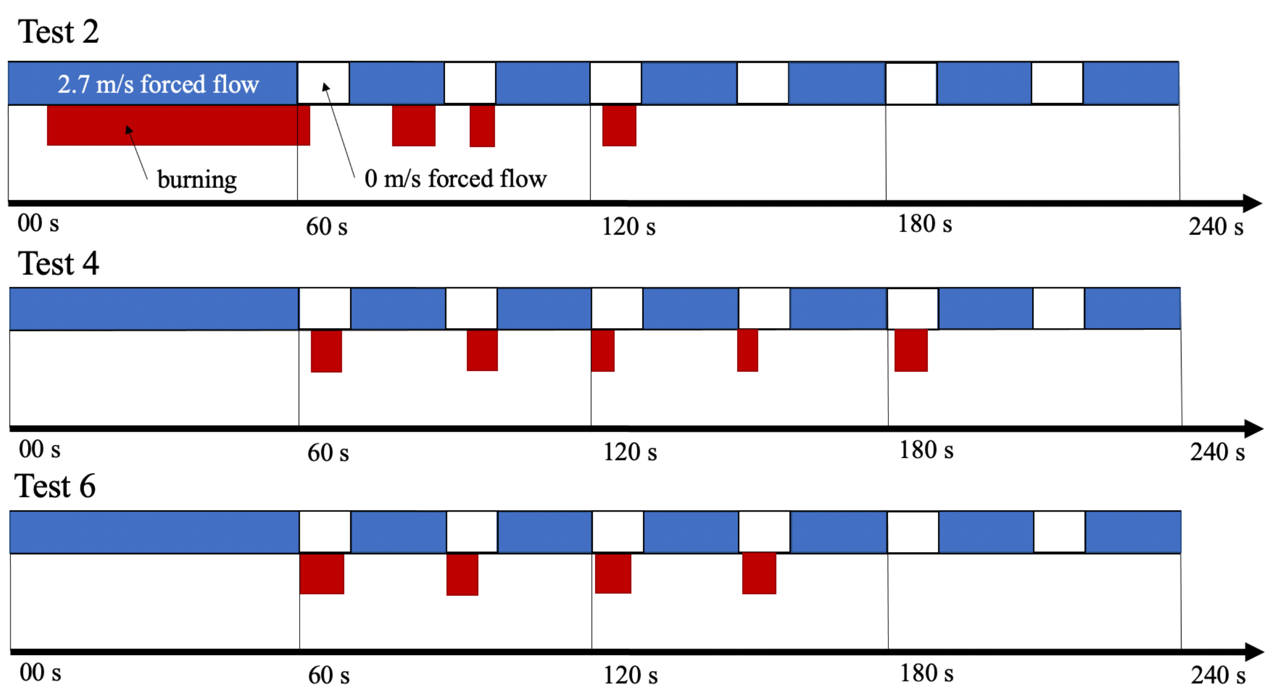

Fig. 31. A timeline of 3 tests on WRC during Phase 3. The blue indicates when the forced flow through the tunnel was turned on, and the blank areas indicate the times that the forced flow was turned off. Durations of flaming surface ignitions are shown in red.

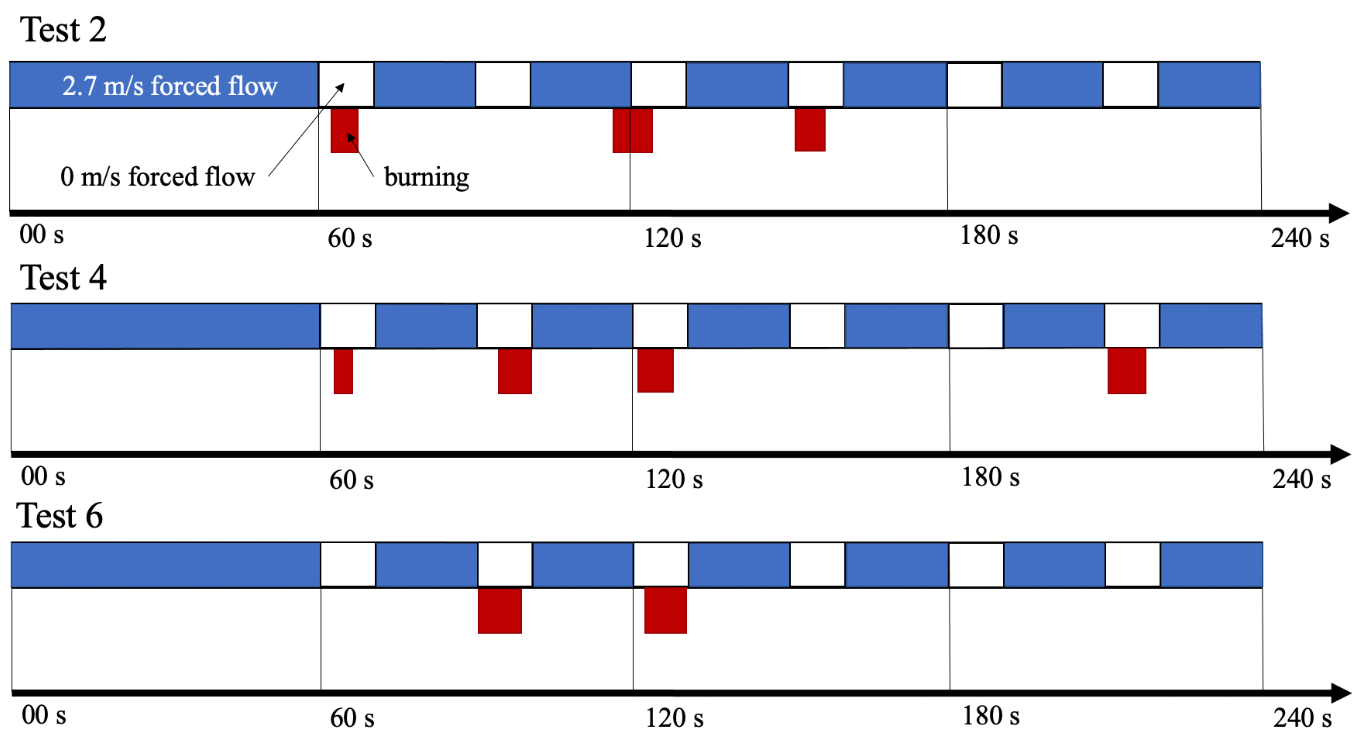

Fig. 32. A timeline of 3 tests on OSB during Phase 3. The blue indicates when the forced flow through the tunnel was turned on, and the blank areas indicate the times that the forced flow was turned off. Durations of flaming surface ignitions are shown in red.

For both materials, it was observed that the majority of ignitions originated when the forced airflow was 0 m s^{-1}. which occurred for only 10 s at a time. With the exception of ignitions events that occurred within the first 60 s of a test, flames were present for only brief periods at a time, often extinguishing before the forced airflow was reintroduced. Additionally, in the continuous airflow condition, referred to as Phase 1 and detailed in Section 4.1, all of the surface ignitions occurred within 75 s after firebrand pile deposition, after which no subsequent ignitions were observed due to cooling of the pile and board. In Phase 3, when flow is intermittent, though each test duration was 480 s, the majority of ignitions for either wood occurred by 240 s into the test duration, the timeframe shown in Figures 31 and 32. 74% of the surface ignitions on WRC had occurred the 240 s mark, and this was 100% for OSB. That is to say that WRC had more overall ignitions per test than OSB, and these ignitions continued to originate later into the test duration.

For WRC, 100% of ignitions occurred within 450 s. Afterwards, it appears that the firebrand pile has decomposed and cooled to the point where the heat feedback cannot pyrolyze the substrate. All tests were concluded at 480 s. Further results from each of the nine tests are summarized in Table 4.

Table 4. Intermittent Wind Testing Quantities

	Average Number of Ignitions per Test	Average Number of Ignitions per Test, excluding those that occurred during the first 60 s	Ignitions when forced flow is OFF (%)	Extinctions when forced flow is OFF (%)
WRC	4.7 ± 1.6	4.3 ± 1.5	83	86
OSB[a]	2.1 ± 1.2	2.1 ± 1.2	74	100

[a] *Note that for OSB, the first two columns refer to the average number of ignitions per test when at least one ignition occurred. Out of the nine tests conducted on OSB, three resulted in no surface ignitions at all. At least one ignition event was observed for all nine tests on WRC.*

As was observed under all previous testing, when exposed to the same conditions as OSB, WRC results in a greater number of surface ignitions during the Phase 3 intermittent airflow tests as well. As a reminder, in the continuous airflow condition, only one ignition event occurred per test if ignition occurred at all. When exposed to the maximum wind velocity of 2.7 m s^{-1}, this resulted in three out of nine tests with flames present on WRC, and only one on OSB. There is a clear increase in the mean number of surface ignitions per test associated with the intermittent wind, seen in Table 4; This corresponded to 14 times more surface ignition events on WRC, and 19 times more on OSB, when the same airflow is intermittent as opposed to continuous. To compare between each material, in the continuous exposure to forced flow condition, WRC had 3 times more ignition events than OSB. In the intermittent condition, WRC had 2.2 times more ignition events than OSB. The locations of ignitions overwhelmingly occurred again in the preleading zone for the same reasons outlined in previous sections and are shown in Figure 33

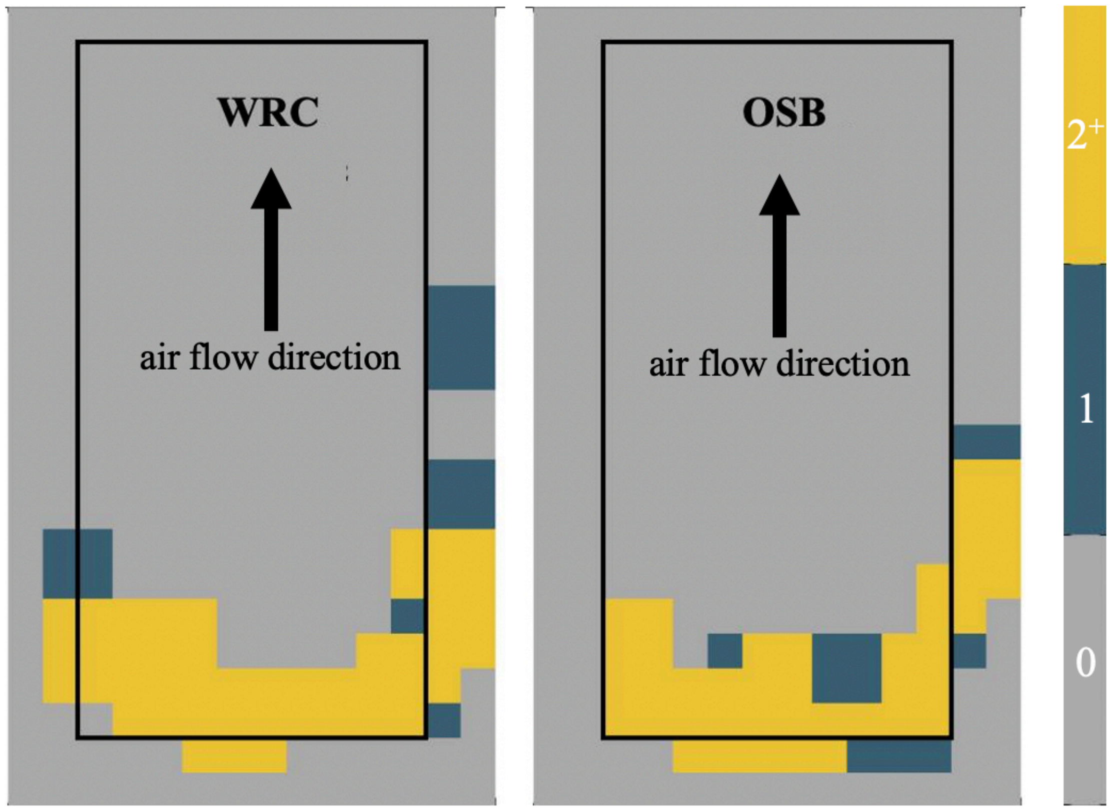

Fig. 33. Surface ignition locations on WRC and OSB for Phase 3, the intermittent wind condition of 2.7 m s^{-1} and a firebrand pile coverage density of 0.16 g cm^{-2}. Grey indicates that no surface ignitions were observed in that location, blue shading indicates that exactly one ignition event was located in that area, and yellow shading indicates that two or more surface ignitions were located in that area. The solid line indicates the location of the firebrand deposition area. Note the direction of airflow through the wind tunnel.

Additional comparisons between substrate behavior in the continuous and intermittent air flow velocities are summarized in Table 5. Due to the short durations the air flow was turned off, only 10 s at a time, and the fact that the majority of ignitions originated during these periods, it was observed that this resulted in shorter burn durations because the reintroduced forced air flow often blew off the flames. As stated above, the probability of observing at least one surface ignition on either substrate per test significantly increased when the flow was intermittent.

Table 5. Comparison of Surface Ignition Behavior at 2.7 m s^{-1} (maximum) Air Flow Speed and 0.16 g cm^{-2} Firebrand Coverage Density between Continuous and Intermittent Forced Air Flow Exposure.

		Probability of at Least One Ignition (%)	Average Burn Duration (s)
WRC	Continuous	33	32 ± 16
	Intermittent	100	5.1 ± 1.0
OSB	Continuous	11	32
	Intermittent	67	6.8 ± 1.7

Subsection 4.1.2: Back Surface Temperature Measurements

Back surface temperature measurements were again only collected for the 2.7 m s^{-1} intermittent air flow tests conducted on Kaowool PM for the purpose of comparison against the Phase 1 tests in which the airflow was continuously at the same velocity. Because the first 60 s after firebrand pile deposition of each phase were the same, 60 s of uninterrupted exposure to 2.7 m s^{-1} of wind, the resulting profiles were anticipated to be the same as well. This is confirmed in Figure 34, in which the peak temperatures reached and the initial heating rate of the average profile across 9 tests of each pile are well within one another's variation, taken as two standard deviations in either case. Over the test duration, the intermittent profile trends higher. Though the intermittent profile trends slightly higher than the continuous case after about 200 s into the test duration, it does not do so in a way that indicates that it is an increased temperature of the firebrand pile and subsequent radiative feedback that controls the increased number of surface ignitions seen under this condition. Instead, these results coupled with the observation that the majority of ignitions occurred when the forced flow was off, shown in Table 4, suggests that the increased ignitions in the intermittent case are due to an allowed buildup of the gaseous combustible board during these off periods. When the wind is continuous, the pyrolyzate is blown away from the preleading zone before ignition is possible. Here, the gas has the time to collect before an increased exposure to oxygen is reintroduced, creating a more favorable environment for flaming ignition. Notably, most ignitions occurred within seconds after the forced flow was turned off while the firebrands were still near their peak temperature. Eventually, the firebrand piles as a whole decompose and cool to a point at which the board does not receive enough heat to sustain ignition as seen with all tests.

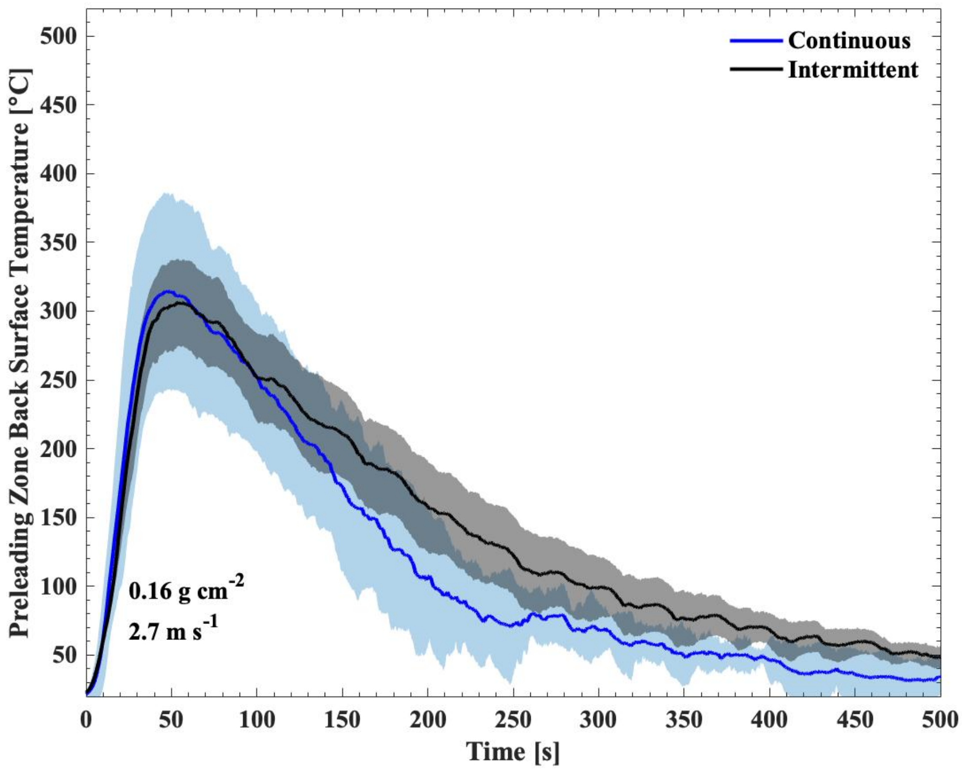

Fig. 34. A comparison of the back surface temperature measurement profiles in the preleading zone, identified in Fig. 6, for the Phase 1 and Phase 3 Kaowool PM tests. The shaded area represents variation, or two standard deviations.

Chapter 5: Conclusions and Future Work

Section 5.1: Conclusions

A bench-scale experimental protocol was developed to study the ignition vulnerability of WRC and OSB, two common WUI decking materials, when exposed to glowing firebrand piles. Each test used the same type and preparation of firebrands. Three phases were introduced in order to study these materials: 135 tests with variable constant airflows and firebrand pile sizes, 27 tests to change the orientation of the firebrand pile, and 27 tests that used pulsed intermittent airflow through the wind tunnel. The ignition and combustion characteristics for all were determined by video analysis, IR back surface temperature profiles, total HRR profiles, board contribution to HRR profiles, and MCE profiles all with respect to time after the wind tunnel was sealed.

In Phase 1, both WRC and OSB were subject to a wind velocity of either 1.4 m s^{-1}, 2.4 m s^{-1}, or 2.7 m s^{-1} and firebrand pile coverage density of either 0.06 g cm^{-2} or 0.16 g cm^{-2}. After analyzing all conditions, it was clear that WRC has a higher propensity towards flaming ignition. WRC saw ignitions in all conditions, while OSB only had ignitions at the 2.4 m s^{-1} and 2.7 m s^{-1} airflows with a firebrand pile coverage density of 0.16 g cm^{-2}. Under the conditions in which both materials had surface ignition events, WRC had a greater number of total ignitions than OSB across 9 tests. Additionally, WRC had shorter times to ignition after firebrand pile deposition as well as an increased amount of surface ignitions present, no matter the condition. Though, the location of the surface ignitions being predominantly directly in front of the firebrand pile, closest to the inflow of air, was constant between the two woods. Next, it was seen that the firebrand pile thermal exposure and burning intensity increased as the air flow increased up to 2.4 m s^{-1}, but decreased upon further air flow velocity increases. In all cases except the 0.16 g cm^{-2} pile at 2.7 m s^{-1}, WRC had a greater contribution to HRR than OSB. When either WRC or OSB had a positive contribution to HRR, there was a decrease in the MCE.

From Phase 2, was shown that a change in the firebrand pile deposition orientation had a significant effect on the ignition and combustion behavior of both WRC and OSB. A constant airflow of 2.4 m s^{-1} and firebrand pile coverage density of 0.16 g cm^{-2} were used for all tests in this condition. Between firebrand pile leading edge lengths, the 10 cm edge had a stark increase of the number of surface ignitions compared to that of the 5 cm leading edge per material for every condition. The leading edge length was effectively doubled, leading to double the ignition probability on both woods, from 55% to 100% on WRC and from 33% to 66% on OSB. The location of these ignitions stayed the same, in the preleading zone, or the area directly in front of the firebrand pile as also seen in the Phase 1 tests. The back surface temperature profile on Kaowool PM achieved a similar peak temperature, within uncertainty, and the shape of the profile with respect to time was the same as the analogous condition with the shorter leading edge firebrand pile length in Phase 1. The total transient heat release rate profile and the MCE profile per material were each greater with this 90-degree orientation change. Between WRC and OSB, there was a greater number of surface ignitions on WRC, the same trend as the 5 cm leading edge conditions. The relationship between WRC and OSB with respect to their HRR profiles changed with the new orientation; in the 5 cm leading edge tests, WRC had a systemically higher HRR and with the 10 cm, WRC was systemically lower. Additionally, there was a greater distinction between the two material's MCE profiles, with OSB trending above WRC.

For Phase 3, there was a large increase in the number of surface ignitions for both WRC and OSB as the intermittent wind condition was introduced. For WRC, there were 14 times the number of surface ignitions observed compared to the continuous wind case, and for OSB, this number was 19 times greater. Additionally, multiple ignitions over the duration of a single test were observed under this condition, when only a single surface ignition event was observed under the continuous wind condition for either material. For both, the burn duration decreased considerably from an average 32 s to an average of between 5 and 7 s on either WRC or OSB. The back surface temperature profile was consistent with its Phase 1 counterpart for the first 100 s, but deviates as the test duration continues.

Section 5.2: Future Work

Part of the motivation for this study includes using this data to be able to conduct an inverse heat transfer analysis to determine temperature and heat flux values underneath the firebrand pile. This would utilize the measurements at the back surface of each material and the known thermophysical properties of each substrate to be able to model the same characteristics at the top surface, directly underneath the deposition area.

WRC and OSB are not the only wooden materials used for decking structures in the WUI, and so additional substrates could be used under the same conditions to determine their combustion and ignition characteristics. Additional materials could include Douglas Fir, Japanese Cedar, and pressure-treated wood. The insight gained by furthering the materials tested could also provide context for inverse modelling as well as inform about the spread of ignition during wildfire events. All new information gathered could potentially lead to safer conditions in the wildfire-prone areas.

The method of analysis used in this study to identify surface ignitions relied on intensive visual observations of the videos taken during each test duration, each location, time to ignition, and burn duration manually documented. This process could be streamlined using image processing tools.

Finally, these tests only considered firebrands deposited onto the top surface of the board in two orientations. Even when the firebrand pile shape was altered, it was still a rectangle. Various ratios between the leading edge length and the width of the pile should be investigated, and could include additional pile shapes, such as a circle. Further orientations, including introducing firebrand piles into the crevices of a material or even firebrand piles collected into a corner of the combustible material, could provide additional context into how firebrand piles cause subsequent ignitions during wildfires. These deposition orientations may more accurately reflect the tendency of firebrands to gather in piles in reality.

Appendix: MATLAB Code used to determine HRR, contribution to HRR, and MCE profiles for each condition. Shown is representative of a 2.4 m s^{-1} test on OSB, though unique codes were used for each material and testing condition.

```
% Gas Analyzer script
% Emily Dietz and Jacques De Beer, 2022


% Material = Western Red Cedar or Kaewool
close all;
clear all;

%ASSIGN THE NUMBER AND LENGTH OF TABLES
numFiles = 9; %Number of STA tests being analyzed
% xlength = 30024
datalines = [24, 8500]; %Lines of data excluding the headers
Gasdata = cell(1,numFiles); %Table in which data from each test is stored

%###########################################################################
%Import Kaowool PM data
opts = delimitedTextImportOptions("NumVariables", 6);

% Specify range and delimiter
opts.DataLines = [2, Inf];
opts.Delimiter = "\t";

% Specify column names and types
opts.VariableNames = ["Time", "CO2", "CO", "CO2std", "COstd", "HRRstd"];
opts.VariableTypes = ["double", "double", "double", "double", "double",
"double"];
opts.ExtraColumnsRule = "ignore";
opts.EmptyLineRule = "read";

% Import the data
Kaodata =
readtable("/Users/emilydietz/Documents/OSB_8g_2_4ms/Average_Kaowool_data.txt"
, opts);

Time_Kao = Kaodata.Time;
CO2_Kao_avg = Kaodata.CO2;
CO_Kao_avg = Kaodata.CO;
CO2_Kao_std = Kaodata.CO2std;
CO_Kao_std = Kaodata.COstd;
HRR_Kao_std = Kaodata.HRRstd;
% HRR_use_Kao = (13.3*CO2_Kao_avg+11.1*CO2_Kao_avg)/0.005;

%Import WRC data
opts1 = delimitedTextImportOptions("NumVariables", 10);

% Specify range and delimiter
opts1.DataLines = [2, Inf];
opts1.Delimiter = "\t";
```

```
% Specify column names and types
opts1.VariableNames = ["Time", "CO2", "CO", "CO2std", "COstd", "MCEavg",
"MCEstd", "HRR", "HRRstd", "HRRCon","HRRstdprop"];
opts1.VariableTypes =
["double","double","double","double","double","double","double","double","dou
ble","double","double"];
opts1.ExtraColumnsRule = "ignore";
opts1.EmptyLineRule = "read";


WRCdata =
readtable("/Users/emilydietz/Documents/OSB_8g_2_4ms/Average_WRC.txt", opts1);
Time_WRC = WRCdata.Time;
CO2_WRC_avg = WRCdata.CO2;
CO_WRC_avg = WRCdata.CO;
CO2_WRC_std = WRCdata.CO2std;
MCE_WRC_avg = WRCdata.MCEavg;
MCE_WRC_std = WRCdata.MCEstd;
HRR_WRC_avg = WRCdata.HRR;
HRR_WRC_std = WRCdata.HRRstd;
HRR_WRC_con = WRCdata.HRRCon;
HRR_WRC_std_prop = WRCdata.HRRstdprop;

%ASSIGN A TABLE WITH LENGTH EQUAL TO THE NUMBER OF TESTS FOR EACH CONDITION
% Timetab = cell(1,numFiles);
% CO2tab = cell(1,numFiles);
% COtab = cell(1,numFiles);
% O2tab = cell(1,numFiles);

%Loop processing script over all tests
for fileNum = 1:numFiles
    %IMPORT DATA INTO A SINGLE TABLE
    fileName = sprintf('OSB_2_4ms_8g_%02d.lvm',fileNum);
    flowrate = 2.4; %[m/s]
    Gasdata{fileNum} = importfile(fileName,datalines);
    itabledata = Gasdata{fileNum};
   %#######################################################################
    %IMPORT DATA FROM EACH PARAMETER INTO SEPERATE ARRAY
    for j = 1:height(itabledata)
        Timedata(j,fileNum) = itabledata.X_Value(j);
        CO2_volt_data(j,fileNum) = itabledata.CO2(j);
        CO_volt_data(j,fileNum) = itabledata.CO(j);
        O2data(j,fileNum) = itabledata.O2(j);
%         CO2_volt_data(j,fileNum) = itabledata.CO2Voltage(j);
%         CO_volt_data(j,fileNum) = itabledata.COVoltage(j);

        if CO2_volt_data(j,fileNum) <= 0.002938
%             CO2_data_mod(j,fileNum) = CO2data_use(k,fileNum);
%             CO2_data_mod(k,fileNum) = 27.367*CO2volts_use(k,fileNum)-
0.0825;
            CO2_data_unmod(j,fileNum) = CO2_volt_data(j,fileNum);
%             CO2_data_mod(k,fileNum) = 0;
        elseif CO2_volt_data(j,fileNum) > 0.002938 &&
CO2_volt_data(j,fileNum) <= 0.003432
            CO2_data_unmod(j,fileNum) = 20.24*CO2_volt_data(j,fileNum)-
0.0595;
```

```
        elseif CO2_volt_data(j,fileNum) > 0.003432 &&
CO2_volt_data(j,fileNum) <= 0.004704
            CO2_data_unmod(j,fileNum) = 7.8647*CO2_volt_data(j,fileNum)-
0.017;
        elseif CO2_volt_data(j,fileNum) > 0.004704 &&
CO2_volt_data(j,fileNum) <= 0.005722
            CO2_data_unmod(j,fileNum) = 9.8184*CO2_volt_data(j,fileNum)-
0.0262;
        elseif CO2_volt_data(j,fileNum) > 0.005722 &&
CO2_volt_data(j,fileNum) <= 0.006995
            CO2_data_unmod(j,fileNum) = 7.8555*CO2_volt_data(j,fileNum)-
0.0149;
        elseif CO2_volt_data(j,fileNum) > 0.006995 &&
CO2_volt_data(j,fileNum) <= 0.008191
            CO2_data_unmod(j,fileNum) = 8.3647*CO2_volt_data(j,fileNum)-
0.0185;
        elseif CO2_volt_data(j,fileNum) > 0.008191 &&
CO2_volt_data(j,fileNum) <= 0.00939
            CO2_data_unmod(j,fileNum) = 8.3368*CO2_volt_data(j,fileNum)-
0.0183;
        elseif CO2_volt_data(j,fileNum) > 0.00939 && CO2_volt_data(j,fileNum)
<= 0.011077
            CO2_data_unmod(j,fileNum) =
5.9277*CO2_volt_data(j,fileNum)+0.0043;
        elseif CO2_volt_data(j,fileNum) > 0.011077 &&
CO2_volt_data(j,fileNum) <= 0.01429
            CO2_data_unmod(j,fileNum) =
3.1095*CO2_volt_data(j,fileNum)+0.0356;
        elseif CO2_volt_data(j,fileNum) > 0.01429 && CO2_volt_data(j,fileNum)
<= 0.017818
            CO2_data_unmod(j,fileNum) =
1.8219*CO2_volt_data(j,fileNum)+0.0468;
        elseif CO2_volt_data(j,fileNum) > 0.017818 &&
CO2_volt_data(j,fileNum) <= 0.025449
            CO2_data_unmod(j,fileNum) =
1.3104*CO2_volt_data(j,fileNum)+0.0667;
        else
            CO2_data_unmod(j,fileNum) =
1.0437*CO2_volt_data(j,fileNum)+0.0734;
        end

        if CO_volt_data(j,fileNum) <= -0.00088
%             CO2_data_mod(j,fileNum) = CO2data_use(k,fileNum);
%             CO2_data_mod(k,fileNum) = 27.367*CO2volts_use(k,fileNum)-
0.0825;
            CO_data_unmod(j,fileNum) = CO_volt_data(j,fileNum);
%             CO_data_mod(k,fileNum) = 0;
        elseif CO_volt_data(j,fileNum) > -0.00088 &&
CO_volt_data(j,fileNum)<= 0.00209
            CO_data_unmod(j,fileNum) = 0.3371*CO_volt_data(j,fileNum)+0.0003;
        elseif CO_volt_data(j,fileNum) > 0.00209 && CO_volt_data(j,fileNum)
<= 0.00457
            CO_data_unmod(j,fileNum) = 0.4023*CO_volt_data(j,fileNum)+0.0002;
        elseif CO_volt_data(j,fileNum) > 0.00457 && CO_volt_data(j,fileNum)
<= 0.00867
            CO_data_unmod(j,fileNum) = 0.2443*CO_volt_data(j,fileNum)+0.0009;
        elseif CO_volt_data(j,fileNum) > 0.00867 && CO_volt_data(j,fileNum)
<= 0.01229
```

```
            CO_data_unmod(j,fileNum) = 0.2764*CO_volt_data(j,fileNum)+0.0006;
        elseif CO_volt_data(j,fileNum) > 0.01229 && CO_volt_data(j,fileNum)
<= 0.01664
            CO_data_unmod(j,fileNum) = 0.2299*CO_volt_data(j,fileNum)+0.0012;
        elseif CO_volt_data(j,fileNum) > 0.01664 && CO_volt_data(j,fileNum)
<= 0.02527
            CO_data_unmod(j,fileNum) = 0.1158*CO_volt_data(j,fileNum)+0.0031;
        elseif CO_volt_data(j,fileNum) > 0.02527 && CO_volt_data(j,fileNum)
<= 0.03264
            CO_data_unmod(j,fileNum) = 0.1357*CO_volt_data(j,fileNum)+0.0026;
        elseif CO_volt_data(j,fileNum) > 0.03264 && CO_volt_data(j,fileNum)
<= 0.04114
            CO_data_unmod(j,fileNum) = 0.1176*CO_volt_data(j,fileNum)+0.0032;
        elseif CO_volt_data(j,fileNum) > 0.04114 && CO_volt_data(j,fileNum)
<= 0.04641
            CO_data_unmod(j,fileNum) = 0.1896*CO_volt_data(j,fileNum)+0.0002;
        elseif CO_volt_data(j,fileNum) > 0.04641 && CO_volt_data(j,fileNum)
<= 0.05589
            CO_data_unmod(j,fileNum) = 0.1055*CO_volt_data(j,fileNum)+0.0041;
        else
            CO_data_unmod(j,fileNum) = 0.0958*CO_volt_data(j,fileNum)+0.0046;
        end


    end

    order = 3;
    framelen = 31;
    CO2_data_unmod_sgol(:,fileNum) =
sgolayfilt(CO2_data_unmod(:,fileNum),order,framelen);
    CO_data_unmod_sgol(:,fileNum) =
sgolayfilt(CO_data_unmod(:,fileNum),order,framelen);

    %######################################################################
    %SUBTRACT BASELINES
    Time_49 = find(Timedata(1:end,fileNum) == 49);
    Time_50 = find(Timedata(1:end,fileNum) == 50);
    Time_51 = find(Timedata(1:end,fileNum) == 51);

    Time_149 = find(Timedata(1:end,fileNum) == 149);
    Time_150 = find(Timedata(1:end,fileNum) == 150);
    Time_151 = find(Timedata(1:end,fileNum) == 151);

    Timeind_50 = (Time_49+Time_50+Time_51)/3;
    Timeind_150 = (Time_149+Time_150+Time_151)/3;

    CO2_data_unmod_base(fileNum) =
sum(CO2_data_unmod_sgol(Timeind_50:Timeind_150,fileNum))/(Timeind_150-
Timeind_50);
    CO_data_unmod_base(fileNum) =
sum(CO_data_unmod_sgol(Timeind_50:Timeind_150,fileNum))/(Timeind_150-
Timeind_50);
    O2_base(fileNum) =
sum(O2data(Timeind_50:Timeind_150,fileNum))/(Timeind_150-Timeind_50);

%   %######################################################################
```

```
%   % HRR Calculations
%
    %Chamber area [m2]
    area = 0.25*0.1; %[m2]
    air_density = 1.184; %[kg/m3]
    %Volumetric flowrate [m3/s]
    V_flowrate = flowrate*area;
    %Component densities [kg/m3]
    CO2_density = 1.784;
    CO_density = 1.13;
    ECO2 = 13.3; %[kJ/g]
    ECO = 11.1; %[kJ/g]
%
%     %###################################################################
    for n = 1:length(Time_Kao)
        HRR_Kao(n,1) = (ECO2*CO2_Kao_avg(n,1)+ECO*CO_Kao_avg(n,1))/0.005;
    end


    for k = 1:height(itabledata)
        CO2_data_use(k,fileNum) = abs(CO2_data_unmod_sgol(k,fileNum)-
CO2_data_unmod_base(fileNum));
        CO_data_use(k,fileNum) = abs(CO_data_unmod_sgol(k,fileNum)-
CO_data_unmod_base(fileNum));

        O2data_use(k,fileNum) = (O2data(k,fileNum)-
O2_base(fileNum))+O2data(k,fileNum);
        CO2_mass_flow_use(k,fileNum) =
V_flowrate*CO2_density*CO2_data_use(k,fileNum)*1000/100; %[g/s]
        CO_mass_flow_use(k,fileNum) =
V_flowrate*CO_density*CO_data_use(k,fileNum)*1000/100; %[g/s]

        %###################################################################
        %HRR calculation normalized by firebrand pile deposition area
        HRR_use(k,fileNum) =
(ECO2*CO2_mass_flow_use(k,fileNum)+ECO*CO_mass_flow_use(k,fileNum))/0.005;
%[kW/m2]
%         HRR_use_Kao = (ECO2*CO2_Kao_avg+ECO*CO2_Kao_avg)/0.005; %[kW/m2]
        %###################################################################
        %MCE Calculation
        CO2_ratio_data_use(k,fileNum) =
(CO2_data_use(k,fileNum))/(CO2_data_use(k,fileNum)+CO_data_use(k,fileNum));
        %###################################################################
        %Calculate Averages for TOTAL CO2 and CO formation
        CO2data_avg1(k,1) = sum(CO2_data_use(k,1:fileNum))/numFiles;
        COdata_avg1(k,1) = sum(CO_data_use(k,1:fileNum))/numFiles;
        O2data_avg1(k,1) = sum(O2data_use(k,1:fileNum))/numFiles;
        CO2_ratio_avg1(k,1) = sum(CO2_ratio_data_use(k,1:fileNum))/numFiles;
        HRR_avg1(k,1) = sum(HRR_use(k,1:fileNum))/numFiles;
        Time_bin1(k,1) = Timedata(k,1);
        CO2_mass_flow_use_avg1(k,1) =
sum(CO2_mass_flow_use(k,1:fileNum))/numFiles;
        CO_mass_flow_use_avg1(k,1) =
sum(CO_mass_flow_use(k,1:fileNum))/numFiles;

        %###################################################################
        %WRC Contribution for CO2 and CO
```

```
        OSB_contribute_CO2(k,fileNum) = CO2_mass_flow_use(k,fileNum) -
CO2_Kao_avg(k,1);
        OSB_contribute_CO(k,fileNum) = CO_mass_flow_use(k,fileNum) -
CO_Kao_avg(k,1);
        OSB_contribute_CO2_avg1(k,1) =
sum(OSB_contribute_CO2(k,1:fileNum))/numFiles;
        OSB_contribute_CO_avg1(k,1) =
sum(OSB_contribute_CO(k,1:fileNum))/numFiles;
        OSB_contribute_HRR(k,fileNum) =
(ECO2*OSB_contribute_CO2(k,fileNum)+ECO*OSB_contribute_CO(k,fileNum))/0.005;
%[kW/m2]
        OSB_contribute_HRR_avg1(k,1) =
sum(OSB_contribute_HRR(k,1:fileNum))/numFiles;

        OSB_HRR_contribute_avg1(k,1) = HRR_avg1(k,1)-HRR_Kao(k,1);

    end

    for j = 1:height(itabledata)
        CO2_std(j,1) = std(CO2_mass_flow_use(j,1:fileNum))/sqrt(numFiles);
        CO_std(j,1) = std(CO_mass_flow_use(j,1:fileNum))/sqrt(numFiles);

        CO2_std_sqr(j,1) = (CO2_std(j,1)).^2;
        CO_std_sqr(j,1) = (CO_std(j,1)).^2;
        CO2_std_sqr_Kao(j,1) = (CO2_Kao_std(j,1)).^2;
        CO_std_sqr_Kao(j,1) = (CO_Kao_std(j,1)).^2;

        CO2_std_propogate(j,1) = sqrt(CO2_std_sqr(j,1) +
CO2_std_sqr_Kao(j,1));
        CO_std_propogate(j,1) = sqrt(CO_std_sqr(j,1) + CO_std_sqr_Kao(j,1));

        CO2_ratio_std(j,1) =
std(CO2_ratio_data_use(j,1:fileNum))/sqrt(numFiles);

        HRR_std(j,1) = std(HRR_use(j,1:fileNum))/sqrt(numFiles);
        HRR_std_sqr(j,1) = (HRR_std(j,1)).^2;
        HRR_std_sqr_Kao(j,1) = (HRR_Kao_std(j,1)).^2;
        HRR_std_propogate(j,1) =
2*sqrt(HRR_std_sqr(j,1)+HRR_std_sqr_Kao(j,1));

    end




%   %####################################################################
    %AVERAGE and BINNED signals for the different gases analyzed
    nbin = 20;
    isave = 1;

      for i = 1:height(WRCdata)
        if (mod(i,nbin)==0)
            MCE_WRC_avg_bin(isave,1) = MCE_WRC_avg(i,1);
            Time_WRC_bin(isave,1) = Time_WRC(i,1);
            MCE_WRC_std_bin(isave,1) = MCE_WRC_std(i,1);
```

```
            HRR_WRC_avg_bin(isave,1) = HRR_WRC_avg(i,1);
            HRR_WRC_std_bin(isave,1) = HRR_WRC_std(i,1);
            HRR_WRC_con_bin(isave,1) = HRR_WRC_con(i,1);
            HRR_WRC_std_prop_bin(isave,1) = HRR_WRC_std_prop(i,1);
            isave = isave+1;
        end
    end

    isave = 1;

    for i = 1:height(itabledata)
        if (mod(i,nbin)==0)
            %Bin data for each test
            CO2_data_use_bin(isave,fileNum) = CO2_data_use(i,fileNum);
            CO_data_use_bin(isave,fileNum) = CO_data_use(i,fileNum);
            O2data_use_bin(isave,fileNum) = O2data_use(i,fileNum);
            CO2_ratio_bin(isave,fileNum) = CO2_ratio_data_use(i,fileNum);
            HRR_use_bin(isave,fileNum) = HRR_use(i,fileNum);
            CO2_mass_flow_bin(isave,fileNum) = CO2_mass_flow_use(i,fileNum);
            CO_mass_flow_bin(isave,fileNum) = CO_mass_flow_use(i,fileNum);
            OSB_contribute_CO2_bin(isave,fileNum) =
OSB_contribute_CO2(i,fileNum);
            OSB_contribute_CO_bin(isave,fileNum) =
OSB_contribute_CO(i,fileNum);
            OSB_contribute_HRR_bin(isave,fileNum) =
OSB_contribute_HRR(i,fileNum);
            OSB_std_propogate(isave,1) = HRR_std_propogate(i,1);

            %Calculate and bin averaged data
            CO2data_avg_bin(isave,1) =
sum(CO2_data_use(i,1:fileNum))/numFiles;
            COdata_avg_bin(isave,1) = sum(CO_data_use(i,1:fileNum))/numFiles;
            O2data_avg_bin(isave,1) = sum(O2data_use(i,1:fileNum))/numFiles;
            CO2_ratio_avg_bin(isave,1) =
sum(CO2_ratio_data_use(i,1:fileNum))/numFiles;
            HRR_avg_bin(isave,1) = sum(HRR_use(i,1:fileNum))/numFiles;
            CO2_mass_flow_use_avg_bin(isave,1) =
sum(CO2_mass_flow_use(i,1:fileNum))/numFiles;
            CO_mass_flow_use_avg_bin(isave,1) =
sum(CO_mass_flow_use(i,1:fileNum))/numFiles;
            Time_bin(isave,1) = Timedata(i,1);

            OSB_contribute_CO2_avg_bin(isave,1) =
sum(OSB_contribute_CO2(i,1:fileNum))/numFiles;
            OSB_contribute_CO_avg_bin(isave,1) =
sum(OSB_contribute_CO(i,1:fileNum))/numFiles;
            OSB_contribute_HRR_avg_bin(isave,1) =
sum(OSB_contribute_HRR(i,1:fileNum))/numFiles;
            HRR_std_propogate_bin(isave,1) = sum(HRR_std_propogate(i,1));
            MCE_Kao(isave,1) = 0.81;

            CO2_ratio_std(isave,1) = CO2_ratio_std(i,1);

            isave = isave+1;
        end
    end
```

```
%   %##################################################################
%   %PLOT ALL DATA ONTO ONE FIGURE

    %Time when glass was slide over tunnel
    t = 265;
    tWRC = 240;

     %
%##################################################################
     % Determine peak values
     % MCE
     MCErange = CO2_ratio_avg1(t*10:t*10+5000,1);
     [MCE_min_value, time_MCE_min] = min(MCErange);
     time_MCE_min1 = time_MCE_min/10; %seconds after deposition
     MCErange_min = MCErange(time_MCE_min-10:time_MCE_min+10);
     MCE_min_value_avg = mean(MCErange_min);

     MCErange_WRC = MCE_WRC_avg(tWRC*10:tWRC*10+5000,1);
     [MCE_min_value_WRC, time_MCE_min_WRC] = min(MCErange_WRC);
     time_MCE_min_WRC1 = time_MCE_min_WRC/10; %seconds after deposition
     MCErange_min_WRC = MCErange_WRC(time_MCE_min_WRC-
10:time_MCE_min_WRC+10);
     MCE_min_value_avg_WRC = mean(MCErange_min_WRC);

     % tHRR
     HRRrange = HRR_avg1(t*10:t*10+5000,1);
     [HRR_max_value, time_HRR_max] = max(HRRrange);
     time_HRR_max1 = time_HRR_max/10; %seconds after deposition
     HRRrange_max = HRRrange(time_HRR_max-10:time_HRR_max+10);
     HRR_max_value_avg = mean(HRRrange_max);

     HRRrange_WRC = HRR_WRC_avg(tWRC*10:tWRC*10+5000,1);
     [HRR_max_value_WRC, time_HRR_max_WRC] = max(HRRrange_WRC);
     time_HRR_max1_WRC = time_HRR_max_WRC/10; %seconds after deposition
     HRRrange_max_WRC = HRRrange_WRC(time_HRR_max_WRC-
10:time_HRR_max_WRC+10);
     HRR_max_value_avg_WRC = mean(HRRrange_max_WRC);

     HRRrange_Kao = HRR_Kao(t*10:t*10+5000,1);
     [HRR_max_value_Kao, time_HRR_max_Kao] = max(HRRrange_Kao);
     time_HRR_max1_Kao = time_HRR_max_Kao/10; %seconds after deposition
     HRRrange_max_Kao = HRRrange_Kao(time_HRR_max_Kao-
10:time_HRR_max_Kao+10);
     HRR_max_value_avg_Kao = mean(HRRrange_max_Kao);


%   %##################################################################
     % FIGURES

    figure(1)
    hold on
    box on;
    plot(Time_bin(1:end,1)-
t,CO2_mass_flow_bin(1:end,fileNum),'DisplayName',num2str(fileNum),'LineWidth'
,0.5);
```

```
%     plot(Time_bin(1:end,1)-
t,CO2_mass_flow_bin(1:end,8),'DisplayName',num2str(fileNum),'LineWidth',0.5);
    legend('boxoff');

    figure(2)
    hold on
    box on;
    plot(Time_bin(1:end,1)-
t,CO_mass_flow_bin(1:end,fileNum),'DisplayName',num2str(fileNum),'LineWidth',
0.5);
    legend('boxoff');

    figure(3)
    hold on
    box on;
%     plot(Time_bin(1:end,1)-
t,WRC_contribute_HRR_bin(1:end,fileNum),'DisplayName',num2str(fileNum),'LineW
idth',0.5);
    legend('boxoff');
end

nmean = 20;

CO2_ratio_mov = movmean(CO2_ratio_avg1,nmean);
OSB_contribute_CO2_mov = movmean(CO2_mass_flow_use_avg1,nmean);
OSB_contribute_CO_mov = movmean(CO_mass_flow_use_avg1,nmean);
OSB_HRR_mov = movmean(HRR_avg1,nmean);

for m = 1:length(Time_bin1)
    HRR_min_OSB(m) = HRR_avg1(m)-2*HRR_std(m);
    HRR_min_OSB(isnan(HRR_min_OSB)) = 0;
    HRR_max_OSB(m) = HRR_avg1(m)+2*HRR_std(m);
    HRR_max_OSB(isnan(HRR_max_OSB)) = 0;
    time_error_OSB(m) = Time_bin1(m);
end

for m = 1:length(Time_bin)-40

    HRR_min_OSB_contribute(m) = OSB_contribute_HRR_avg_bin(m)-
OSB_std_propogate(m);
    HRR_max_OSB_contribute(m) =
OSB_contribute_HRR_avg_bin(m)+OSB_std_propogate(m);
    time_error_hrr(m) = Time_bin(m);
    MCE_min(m) = CO2_ratio_avg_bin(m) - 2*CO2_ratio_std(m);
    MCE_max(m) = CO2_ratio_avg_bin(m) + 2*CO2_ratio_std(m);
end

for l = 1:length(Time_Kao)-3000
    HRR_min_Kao(l) = HRR_Kao(l)-2*HRR_Kao_std(l);

    HRR_max_Kao(l) = HRR_Kao(l)+2*HRR_Kao_std(l);

    time_error_Kao(l) = Time_Kao(l);
end

for l = 1:length(MCE_WRC_avg_bin)-20
```

```
    MCE_min_WRC(l) = MCE_WRC_avg_bin(l)-2*MCE_WRC_std_bin(l);
    MCE_max_WRC(l) = MCE_WRC_avg_bin(l)+2*MCE_WRC_std_bin(l);

    HRR_min_WRC(l) = HRR_WRC_avg_bin(l)-2*HRR_WRC_std_bin(l);
    HRR_max_WRC(l) = HRR_WRC_avg_bin(l)+2*HRR_WRC_std_bin(l);

    HRR_min_WRC_contribute(l) = HRR_WRC_con_bin(l)-2*HRR_WRC_std_prop_bin(l);
    HRR_max_WRC_contribute(l) = HRR_WRC_con_bin(l)+2*HRR_WRC_std_prop_bin(l);

    time_error_WRC(l) = Time_WRC_bin(l);
end

%Plot averaged data and end hold on figures
figure(1)
set(gca,'FontName','times','FontWeight','bold');
% x2 = [Time_bin,fliplr(Time_bin)];
% y2 = [min_middle,fliplr(max_middle)];
% fill(x2,y2,[0.9 0.9 0.9],'LineStyle','None','DisplayName','Variation');
plot(Time_bin1(1:end,1)-t,CO2_mass_flow_use_avg1(1:end,1),'k.-
','DisplayName','Avg','LineWidth',0.5);
plot(Time_Kao(1:end,1)-t,CO2_Kao_avg(1:end,1),'r.-
','DisplayName','Avg','LineWidth',1.5);
% CO2_std_plot = errorbar(Time_bin(1:end,1)-
t,CO2_mass_flow_use_avg_bin(1:end,1),2*CO2_std_bin(1:end,1),2*CO2_std_bin(1:e
nd,1),'k.','markersize',0.1,'linewidth',0.1,'capsize',5,'DisplayName','Variat
ion');
% plot(Time_bin(1:end,1)-t,CO2_mass_flow_bin(1:end,8),'r.-
','DisplayName','8','LineWidth',1);
% plot(Time_bin(1:end,1)-t,CO2_mass_flow_bin(1:end,9),'b.-
','DisplayName','9','LineWidth',1);
xlim([0,800]);
xlabel('Time after chamber is sealed [s]');
ylabel('CO_{2} production rate [g s^{-1}]');
hold off
legend show

figure(2)
set(gca,'FontName','times','FontWeight','bold');
plot(Time_bin1(1:end,1)-t,CO_mass_flow_use_avg1(1:end,1),'k.-
','DisplayName','Avg','LineWidth',0.5);
plot(Time_Kao(1:end,1)-t,CO_Kao_avg(1:end,1),'r.-
','DisplayName','Avg','LineWidth',1.5);
% CO_std_plot = errorbar(Time_bin(1:end,1)-
t,CO_mass_flow_use_avg_bin(1:end,1),CO_std_bin(1:end,1),CO_std_bin(1:end,1),'
k.','markersize',0.1,'linewidth',0.1,'capsize',5,'DisplayName','Variation');
% plot(Time_bin(1:end,1)-t,CO_mass_flow_bin(1:end,8),'r.-
','DisplayName','8','LineWidth',1);
% plot(Time_bin(1:end,1)-t,CO_mass_flow_bin(1:end,9),'b.-
','DisplayName','9','LineWidth',1);
xlim([0,800]);
xlabel('Time after chamber is sealed [s]');
ylabel('CO production rate [g s^{-1}]');
hold off
legend show

figure(3)
```

```
set(gca,'FontName','SansSerif','FontWeight','bold','XMinorTick','on','YMinorT
ick','on');
x1 = [time_error_hrr-t,fliplr(time_error_hrr)-t];
y1 = [HRR_min_OSB_contribute,fliplr(HRR_max_OSB_contribute)];
x2 = [time_error_WRC-tWRC,fliplr(time_error_WRC)-tWRC];
y2 = [HRR_min_WRC_contribute,fliplr(HRR_max_WRC_contribute)];
h1 = fill(x1,y1,[1 0 0],'LineStyle','None','DisplayName','Variation');
set(h1,'facealpha',0.2);
h2 = fill(x2,y2,[0 0 1],'LineStyle','None','DisplayName','Variation');
set(h2,'facealpha',0.2);
% HRR_std_plot = errorbar(Time_bin1(1:end,1)-
t,WRC_contribute_HRR_avg1(1:end,1),HRR_std_propogate(1:end,1),HRR_std_propoga
te(1:end,1),'k.','markersize',0.1,'linewidth',0.1,'capsize',5,'DisplayName','
Variation');
p1 = plot(Time_bin(1:end,1)-t,OSB_contribute_HRR_avg_bin(1:end,1),'r-
','DisplayName','OSB HRR Contribution','LineWidth',2);
p2 = plot(Time_WRC_bin-tWRC,HRR_WRC_con_bin,'b-','DisplayName','WRC HRR
Contribution','LineWidth',2);
% plot(Time_bin(1:end,1)-t,HRR_use_bin(1:end,8),'r.-
','DisplayName','8','LineWidth',1);
% plot(Time_bin(1:end,1)-t,HRR_use_bin(1:end,9),'b.-
','DisplayName','9','LineWidth',1);
xlim([0,500]);
ylim([-100,100]);
legend([p1 p2],{'OSB HRR Contribution','WRC HRR
Contribution'},'FontSize',10);
xlabel('Time after chamber is sealed [s]');
ylabel('HRR, Contribution [kW m^{-2}]')
title('5cm Leading Edge');
hold off
legend show

figure(4)
hold on
box on;
set(gca,'FontName','SansSerif','FontWeight','bold','XMinorTick','on','YMinorT
ick','on');
xtest = [0 50 50 0];
ytest = [0 0 400 400];
%rec1 = patch(xtest,ytest,[0.9,0.9,0.9],'FaceAlpha',0.75,'EdgeColor','none');
x1 = [time_error_OSB-t,fliplr(time_error_OSB)-t];
y1 = [HRR_min_OSB,fliplr(HRR_max_OSB)];
 x2 = [time_error_Kao-t,fliplr(time_error_Kao)-t];
 y2 = [HRR_min_Kao,fliplr(HRR_max_Kao)];
x3 = [time_error_WRC-tWRC,fliplr(time_error_WRC)-tWRC];
y3 = [HRR_min_WRC,fliplr(HRR_max_WRC)];
h1 = fill(x1,y1,[1 0 0],'LineStyle','None','DisplayName','Variation');
set(h1,'facealpha',0.2);
 h2 = fill(x2,y2,[0.222 0.377
0.448],'LineStyle','None','DisplayName','Variation');
 set(h2,'facealpha',0.2);
h3 = fill(x3,y3,[0 0 1],'LineStyle','None','DisplayName','Variation');
set(h3,'facealpha',0.2);
% HRR_std_plot = errorbar(Time_bin1(1:end,1)-
t,WRC_contribute_HRR_avg1(1:end,1),HRR_std_propogate(1:end,1),HRR_std_propoga
te(1:end,1),'k.','markersize',0.1,'linewidth',0.1,'capsize',5,'DisplayName','
Variation');
```

```
p1 = plot(Time_bin1(1:end,1)-t,HRR_avg1(1:end,1),'r-','DisplayName','OSB
HRR_{Average}','LineWidth',2);
p2 = plot(Time_Kao-t,HRR_Kao(1:end,1),'k-','DisplayName','Kaowool PM
HRR_{Average}','LineWidth',2);
p3 = plot(Time_WRC-tWRC,HRR_WRC_avg(1:end,1),'b-','DisplayName','WRC
HRR_{Average}','LineWidth',2);
% plot(Time_bin(1:end,1)-t,HRR_use_bin(1:end,8),'r.-
','DisplayName','8','LineWidth',1);
% plot(Time_bin(1:end,1)-t,HRR_use_bin(1:end,9),'b.-
','DisplayName','9','LineWidth',1);
xlim([0,500]);
ylim([0,400]);
xlabel('Time after chamber is sealed [s]');
ylabel('Total HRR [kW m^{-2}]');
legend boxoff;
legend([p1 p2 p3],{'OSB HRR_{Average}','Kaowool PM HRR_{Average}','WRC
HRR_{Average}'},'FontSize',10);
title('5cm Leading Edge');
hold off
legend show

figure(5)
hold on
box on;
set(gca,'FontName','SansSerif','FontWeight','bold','XMinorTick','on','YMinorT
ick','on');
xtest = [0 50 50 0];
ytest = [0 0 1 1];
%rec1 = patch(xtest,ytest,[0.9,0.9,0.9],'FaceAlpha',0.75,'EdgeColor','none');
x1 = [time_error_hrr-t,fliplr(time_error_hrr)-t];
y1 = [MCE_min,fliplr(MCE_max)];
x2 = [time_error_WRC-tWRC,fliplr(time_error_WRC)-tWRC];
y2 = [MCE_min_WRC,fliplr(MCE_max_WRC)];
h1 = fill(x1,y1,[1 0 0],'LineStyle','None','DisplayName','Variation');
set(h1,'facealpha',0.3);
h2 = fill(x2,y2,[0 0 0.9],'LineStyle','None','DisplayName','Variation');
set(h2,'facealpha',0.2);
p1 = plot(Time_bin(1:end,1)-t,CO2_ratio_avg_bin(1:end,1),'r-
','DisplayName','WRC OSB_{Average}','LineWidth',2);
p2 = plot(Time_bin,MCE_Kao,'k--','LineWidth',2,'DisplayName','Kaowool PM
MCE_{Average}');
p3 = plot(Time_WRC_bin-tWRC, MCE_WRC_avg_bin,'b-
','LineWidth',2,'DisplayName','WRC MCE_{Average}');
xlim([0,500]);
ylim([0.6 1]);
xlabel('Time after chamber is sealed [s]');
ylabel('MCE');
legend boxoff;
legend([p1 p2 p3],{'OSB MCE_{Average}','Kaowool PM MCE_{Average}','WRC
MCE_{Average}'},'FontSize',10);
%legend([p1 p3 rec1],{'OSB MCE_{Average}','WRC MCE_{Average}','Surface
Ignition Time Frame'},'FontSize',10);
title('5cm Leading Edge');
hold off
legend show
```

Bibliography

[1] Radeloff V.C. et al. (2018) "Rapid Growth of the Us Wildland-Urban Interface Raises Wildfire Risk," Proceedings of the National Academy of Sciences of the United States of America, 115(13), pp. 3314–3319

[2] Boer, M. M., Nolan, R. H., Dios, V. R. D., Clarke, H., Price, O. F., & Bradstock, R. A. (2017). Changing weather extremes call for early warning of potential for catastrophic fire. Earth's Future, 5(12), 1196–1202. https://doi.org/10.1002/2017EF000657

[3] Shi, G., Yan, H., Zhang, W., Dodson, J., Heijnis, H., & Burrows, M. (2021). Rapid warming has resulted in more wildfires in northeastern Australia. Science of the Total Environment, 771, 144888. https://doi.org/10.1016/j.scitotenv.2020.14488

[4] Coogan, S. C. P., Robinne, F.-N., Jain, P., & Flannigan, M. D. (2019). Scientists' warning on wildfire—A Canadian perspective. Canadian Journal of Forest Research, 49(9), 1015–1023. https://doi.org/10.1139/cjfr- 2019- 009

[5] Kharuk, V. I., Ponomarev, E. I., Ivanova, G. A., Dvinskaya, M. L., Coogan, S. C. P., & Flannigan, M. D. (2021). Wildfires in the Siberian taiga. Ambio, 50(11), 1953–1974. https://doi.org/10.1007/s1328 0-020-01490 -x

[6] Federal Emergency Management Agency (2022). Wildland Urban Interface: A Look at Issues and Resolutions. United States. Web. https://www.usfa.fema.gov/

[7] Congressional Research Service. Wildfire Statistics (2021). url: https://crsreports.congress.gov/product/pdf/IF/IF10244.

[8] Tineke Kraaij et al. "An assessment of climate, weather, and fuel factors influencing a large, destructive wildfire in the Knysna region, South Africa". In: Fire Ecology 14.2 (2018). doi: 10.1186/s42408-018-0001-0.

[9] Coop, J. D., Parks, S. A., Stevens-Rumann, C. S., Ritter, S. M., & Hoffman, C. M. (2022). Extreme fire spread events and area burned under recent and future climate in the western USA. *Global Ecology and Biogeography*.

[10] Mietkiewicz, N., Balch, J. K., Schoennagel, T., Leyk, S., St. Denis, L. A., & Bradley, B. A. (2020). In the line of fire: Consequences of human-ignited wildfires to homes in the U.S. (1992–2015). Fire, 3(3), 50. https://doi.org/10.3390/fire3 030050

[11] Pickrell, J., & Pennisi, E. (2020). Record US and Australian fires raise fears for many species. American Association for the Advancement of Science.

[12] National Interagency Coordination Center. Wildland Fire Summary and Statistics Annual Report (2022). National Interagency Coordination Center, Boise, Idaho, 2022.

[13] Joan L. Pellegrino, Nelson P. Bryner, and Erik L. Johnsson. “Wildland-Urban Interface Fire Research Needs: Workshop Summary Report”. In: NIST (2013). doi: 10.6028/nist.sp.1150.

[14] Caton, S.E., R.S.P. Hakes, D.J. Gorham, A. Zhou, and M.J. Gollner. Review of Pathways for Building Fire Spread in the Wildland Urban Interface Part I: Exposure Conditions. Fire Technology, 53(2):429-473, 2016. DOI: 10.1007/s10694-016-0589-z.

[15] Vladimir Fateev et al. “Determination of smoldering time and thermal characteristics of firebrands under laboratory conditions”. In: Fire Safety Journal 91 (2017), pp. 791–799. doi: 10.1016/j.firesaf.2017.03.080.

[16] Cheng et al. “The Diagnostic Methods for Resurgences of Smoldering Fire in the Forests by Infrared Thermal Imaging”. In: Spectroscopy and Spectral Analysis 38.1 (2018), Cheng. H., L. Ke–zhen., S. Li–fu, H. Xia–fang, and Z. Si–yu. url: https://www.researching.cn/articles/OJ509ad5c03143763b.

[17] Anne Ganteaume et al. “Laboratory characterization of firebrands involved in spot fires”. In: Annals of Forest Science 68.3 (2011), pp. 531–541. doi: 10.1007/s13595-011-0056-4.

[18] Ali Tohidi, Nigel Kaye, and William Bridges. “Statistical description of firebrand size and shape distribution from coniferous trees for use in Metropolis Monte Carlo simulations of firebrand flight distance”. In: Fire Safety Journal 77 (2015), pp. 21–35. doi: 10.1016/j.firesaf.2015.07.008.

[19] Sayaka Suzuki and Samuel L. Manzello. “Garnering understanding into complex firebrand generation processes from large outdoor fires using simplistic laboratory-scale experimental methodologies”. In: Fuel 267 (2020), p. 117154. doi: 10.1016/j.fuel.2020.117154.

[20] Raquel S.P. Hakes et al. “Thermal characterization of firebrand piles”. In: Fire Safety Journal 104 (2019), pp. 34–42. doi: 10.1016/j.firesaf.2018.10.002.

[21] William E. Mell et al. (2010). “The wildland-urban interface fire problem - current approaches and research needs”. In: International Journal of Wildland Fire 19.2, p. 238. doi: 10.1071/wf07131.

[22] Manzello, S. L. et al. (2020). “Role of Firebrand Combustion in Large Outdoor Fire Spread,” Progress in Energy and Combustion Science, 76. doi: 10.1016/j.pecs.2019.100801.

[23] Maranghides, A., D. McNamara, W. Mell, J. Trook, and B. Toman. (2013). A case study of a community affected by the Witch and Guejito fires: Report 2 - evaluating the effects

of hazard mitigation actions on structure ignitions. Technical Note (TN 1796) National Institute of Standards and Technology.

[24] www.nwcg.gov. (n.d.). Spotting Fire Behavior | NWCG. [online] Available at: https://www.nwcg.gov/publications/pms437/crown-fire/spotting-fire-behavior.

[25] Hadden, R. M. et al. (2011). "Ignition of Combustible Fuel Beds by Hot Particles: An Experimental and Theoretical Study," Fire Technology, 47(2), pp. 341–355. doi: 10.1007/s10694–010–0181–x.

[26] Gollner, M. J. and Hakes, Raquel, Sara Pilar. (2017). Thermal characterization of firebrand piles. Dissertation. University of Maryland (College Park, Md.). doi: 10.13016/M2H70814D.

[27] Santamaria, S., K. Kempn´a, J.C. Thomas, M. El Houssami, E. Mueller, D. Kasimov, A. Filkov, M.R. Gallagher, N. Skowronski, R. Hadden, and A. Simeoni. Investigation of structural wood ignition by firebrand accumulation. In: Proceedings of the First International Conference on Structures Safety under Fire Blast, 2015.

[28] Dowling, V.P. Ignition of Timber Bridges in Bushfires. Fire Safety Journal, 22:145-168, 1994.

[29] Viegas, D.X., M. Almeida, J. Raposo, R. Oliveria, and C.X. Viegas. Ignition of Mediterranean Fuels Beds by Several Types of Firebrands. Fire Technology, 50(1):60-77, 2014. DOI: 10.1007/s10694-012-0267-8.

[30] Tao, Z., Bathras, B., Kwon, B., Biallas, B., Gollner, M. J., & Yang, R. (2021). Effect of firebrand size and geometry on heating from a smoldering pile under wind. *Fire Safety Journal*, *120*, 103031.

[31] Manzello, S. L. et al. (2017) "Experimental Investigation of Wood Decking Assemblies Exposed to Firebrand Showers," Fire Safety Journal, 92, pp. 122–131.

[32] Manzello, S. L. et al. (2014) "Exposing Decking Assemblies to Continuous Wind–Driven Firebrand Showers," Fire Safety Science, vol. 11, pp. 1339–1352.

[33] Manzello, S. L. et al. (2009) "Investigation on the Ability of Glowing Firebrands Deposited Within Crevices to Ignite Common Building Materials," Fire Safety Journal, 44(6), pp. 894–900.

[34] Manzello, S.L., T.G. Cleary, J.R. Shields, and J.C. Yang. Ignition of mulch and grasses by firebrands in wildland-urban interface fires. International Journal of Wildland Fire, 15:427-431, 2006. DOI: 10.1071/WF06031.

[35] Quarles, S.L., L.G. Cool, and F.C. Beall. Performance of Deck Board Materials Under Simulated Wildfire Exposures. In: Proceedings of the Seventh International Conference on Woodfiber-Plastic Composites, pp. 89-93, 2003.

[36] Waterman, T.E. and A.N. Takata. Laboratory Study of Ignition of Host Materials by Firebrands. IIT Research Institute, 1969

[37] Alascio. (2021). “ACCUMULATED FIREBRAND PILE THERMAL CHARACTERIZATION AND IGNTION STUDIES OF FIREBRAND EXPOSED DECKING MATERIALS INTHE WILDLAND–URBAN INTERFACE”. Master’s Thesis. University of Maryland (College Park, MD).

[38] Stoliarov, S. I. and McKinnon, Mark (2016). *A generalized methodology to characterize composite materials for pyrolysis models.* Dissertation. University of Maryland (College Park, MD). doi: 10.13016/M2CB6S.

[39] WESTERN RED CEDAR QUICK FACTS (2013). Real Cedar [online]. Available at: https://www.jwlumber.com

[40] Forest Products Laboratory (U.S.) (2010). Wood handbook: Wood as an Engineering Material. Centennial ed. Madison, Wis.: U.S. Dept. of Agriculture, Forest Service, Forest Products Laboratory (General technical report FPL, GTR-190). https://www.fpl.fs.fed.us.

[41] Gollner, M. J. and Babetta Duarte, Julia. (2020). *Characterization of ignition conditions of decking assembly materials to smoldering firebrands*. Dissertation. University of Maryland (College Park, MD).

[42] American Society for Testing and Materials. ASTM D4442: Standard Test Methods for Direct Moisture Content Measurement of Wood and Wood–Based Materials, 2020.

[43] Chen, L. W. et al. (2007) “Emissions from Laboratory Combustion of Wildland Fuels: Emission Factors and Source Profiles,” Environmental Science & Technology, 41(12), pp. 4317–25

[44] Kruse, K., Dai, C., & Pielasch, A. (2000). An analysis of strand and horizontal density distributions in oriented strand board (OSB). *European Journal of Wood and Wood Products*, *58*(4), 270-277.

[45] Igaz, R., Krišťák, L., Ružiak, I., Gajtanska, M., & Kučerka, M. (2017). Thermophysical properties of OSB boards versus equilibrium moisture content. *BioResources*, *12*(4), 8106-8118.

[46] “What is Oriented Strand Board (OSB)?” (2022). NaturallyWood [online]. Available at: https://www.naturallywood.com/products/oriented-strand-board/

[47] Biteau H, Steinhaus T, Schemel C, et al. Calculation methods for the Heat Release Rate of Materials of unknown Composition. In: *Fire Safety Science*. ; 2008:1165-1176. doi:10.3801/IAFSS.FSS.9-1165